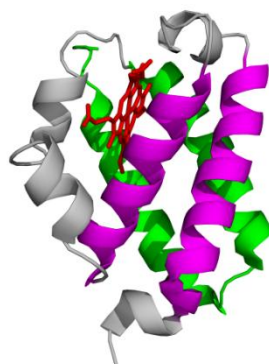


DOTTORATO DI RICERCA IN BIOCHIMICA

XXVI CICLO (A. A. 2010-2013)

**LIGAND BINDING DYNAMICS AND SPECTROSCOPY IN
TRUNCATED HEMOGLOBINS**



Dottoranda

Natascia Sciamanna

Docente guida

Prof. Alberto Boffi

Docente coordinatore

Prof. Francesco Malatesta

Dicembre 2013

TABLE OF CONTENTS

INTRODUCTION.....	1
1.1 THE GLOBIN SUPERFAMILY.....	1
1.2 GLOBINS IN VERTEBRATES.....	4
1.3 GLOBINS IN PLANTS.....	10
1.5 MICROBIAL GLOBINS	11
1.6 TRUNCATED HEMOGLOBINS	12
1.7 SPECTROSCOPIC PROBES FOR THE STUDY OF LIGAND RECOGNITION AND STABILIZATION IN HEMOGLOBINS.	16
STATE OF ART	30
MATERIALS AND METHODS.....	43
3.1 CLONING, EXPRESSION, AND PURIFICATION OF RECOMBINANT <i>B.</i> <i>SUBTILIS TRHB</i>	43
3.2 CLONING, EXPRESSION, AND PURIFICATION OF RECOMBINANT TRHB FROM THERMOBIFIDA FUSCA AND ITS DISTAL MUTANTS.	44
3.3 ELECTRONIC ABSORPTION SPECTROSCOPY	46
3.4 RESONANCE RAMAN SPECTROSCOPY	47

3.5 KINETIC MEASUREMENTS	48
3.6 VISIBLE-PUMP/MIDIR-PROBE SPECTROSCOPY.	48
3.7 ANISOTROPY MEASUREMENTS	50
RESULTS AND DISCUSSION	51
4.1 ELECTRONIC ABSORPTION SPECTRA AND RESONANCE RAMAN SPECTRA OF FLUORIDE COMPLEXES OF <i>TF-TRHB</i> AND ITS DISTAL MUTANTS.....	51
4.2 FLUORIDE BINDING AND RELEASE KINETICS IN <i>TF-TRHB</i>	55
4.3 STUDY OF CO REBINDING IN <i>TF-TRHB</i>	59
4.4 STUDY OF CO REBINDING IN <i>BS-TRHB</i>	68
4.5 STUDY OF CO REBINDING IN <i>3F-TF-TRHB</i>	73
4.6 RECOMBINATION DYNAMICS COMPARISONS BETWEEN <i>TF-TRHB</i> AND <i>BS-TRHB</i>	77
CONCLUSIONS	84
BIBLIOGRAPHY	89
ACKNOWLEDGEMENTS.....	98
APPENDIX.....	100

INTRODUCTION

1.1 The Globin superfamily

The discovery of genes coding for globins among bacteria, yeast, protozoa, algae, fungi and plants has challenged the traditional view that envisaged these proteins as hallmarks of oxygen transport and storage in mammals and pushed forward novel hypotheses on their biological roles. Although the sequence homology within the globin family is low, in some cases less than 20%, all globins share a common overall three-dimensional structure conform to α -helices rich assembly (globin fold) harbouring a heme prosthetic group. A typical globin fold is characterized by two groups of three α -helices assembled in a 3-over-3 α -helical sandwich motif that embed the non covalently bonded heme prosthetic group. The three-dimensional structure was described for the first time by the Nobel prize Kendrew and his co-workers fifty years ago(1). They solved the structure of Whale Myoglobin by X-ray crystallography and observed a 150 amino acids long motif characterized by 8 helices designated A through H from the N to the C terminal. Helices A, B, C and E are on the distal site of the heme and helices F, G and H on the proximal site[Fig.1.1]. Although the amino acid sequence alignments of globins from various sources reveals a high variability, two key residues are conserved among all globins encountered so far: Phe at position CD1 and His at position F8(2). PheCD1 is located in the distal heme

pocket and HisF8 is responsible of heme iron coordination to the proximal side of the heme pocket. Moreover hydrophobic interactions between the tetrapyrrole ring and hydrophobic amino acid side chains in the protein pocket, strongly stabilize the heme protein conjugate. Heme is a chemically highly reactive group that is involved in many biological processes due to its ability to bind oxygen reversibly to the ferrous iron atom (Fe^{2+}). In the deoxygenated protein, Fe^{2+} forms four coordination bonds with four nitrogen atoms of the tetrapyrrolic ring while the fifth coordination position is occupied by HisF8 (proximal) and the sixth one is left free for ligand binding. When the oxygen binds to the sixth coordination position of the ferrous iron, the distal histidine interacts with the ligand by an hydrogen bond thus providing additional stabilization besides the coordination bond [fig.1.2](1). Heme also participates to the binding and transport of other gaseous ligands (NO, CO), to the scavenging of free oxidant species, to oxido-reduction and oxygen-sensing reactions. This diversity in biochemical reactivities reflects the variety of the physico chemical properties of the aminoacid side chains that harbor the heme moiety.

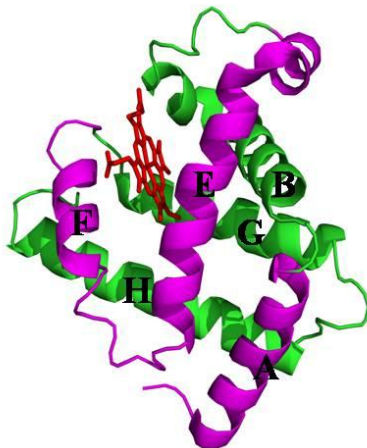


Figure 1. 1. Three-dimensional structure of Sperm Whale Myoglobin(1). The 3/3 α -helical fold is highlighted in purple and green color. The heme group is surrounded by 3 helices on its proximal site (F, G, and H) and 3 helices on its distal site (A, B and E).

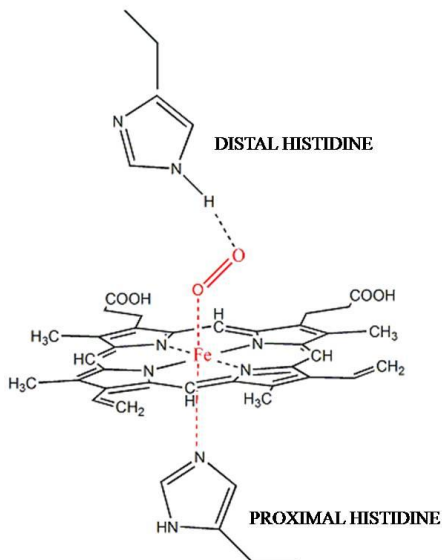


Figure 1. 2. Active site structure of Sperm Whale oxymyoglobin.

1.2 Globins in vertebrates

A large variety of hemoglobins (Hbs) with different structures and oxygen binding properties have been reported among vertebrates. The amino acid sequence by itself is not sufficient to classify the protein as a globin; the large heterogeneity in the continuously expanding database, in fact, includes globins with differences over 90%(3). Myoglobins (Mb) and hemoglobins (Hb) are hemoproteins whose physiological importance is mainly related to their ability to bind molecular oxygen. Myoglobins are monomeric heme proteins that serve as intracellular storage sites for oxygen; hemoglobins are the iron-containing oxygen-transport proteins in the red blood cells of all vertebrates as well as the tissues of some invertebrates. Fig. 1.3 displays the three dimensional structure of both human Myoglobin (A) and human Hemoglobin (B). In the first a typical globin fold, as described for Whale Myoglobin in the previous chapter, is highlighted. The second image shows human Hemoglobin tetrameric structure in which each subunit has a prosthetic group identical to that described for Myoglobin(4). The common peptide subunits are designated α_1 , β_1 , α_2 , β_2 and are arranged into the most commonly occurring functional hemoglobins. Although the secondary and tertiary structure of various hemoglobin subunits are similar, reflecting extensive homology in amino acid composition, the latter impart marked differences in hemoglobin's oxygen carrying properties.

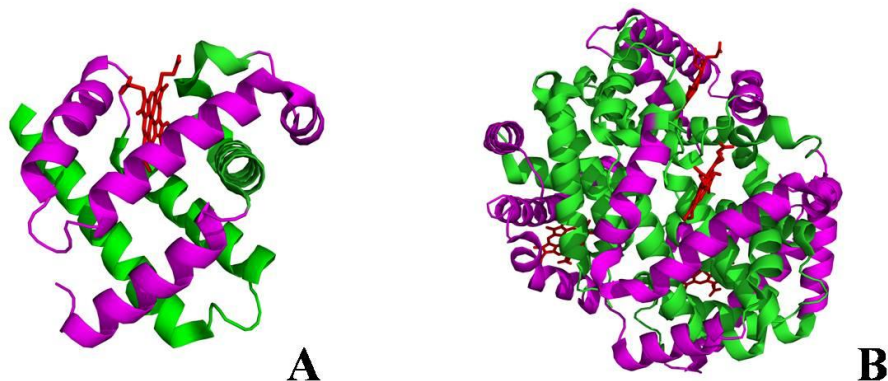


Figure 1. 3. Three-dimensional structure of human Myoglobin (A) and human Hemoglobin (B).

Actually, comparison of the oxygen binding properties of hMb and hHb illustrates the allosteric properties of Hemoglobin that results from its quaternary structure and differentiate hemoglobin's oxygen binding properties from that of Myoglobin. The curve of oxygen binding to hemoglobin is sigmoidal typical of allosteric proteins in which the substrate, in this case oxygen, is a positive homotropic effector [Fig. 1.4]. When oxygen binds to the first subunit of deoxyhemoglobin it increases the affinity of the remaining subunits for oxygen. As additional oxygen is bound to the second and third subunits oxygen binding is further favoured, so that, at the oxygen tension in lung alveoli, hemoglobin is fully saturated with oxygen. As oxyhemoglobin circulates to deoxygenated tissue, oxygen is incrementally unloaded and the affinity of hemoglobin for oxygen is reduced. Thus at the lowest oxygen tensions found in very active tissues the binding affinity of hemoglobin for oxygen is very low allowing

maximal delivery of oxygen to the tissue. In contrast the oxygen binding curve for Myoglobin is hyperbolic in character indicating the absence of allosteric interactions in this process. The allosteric oxygen binding properties of hemoglobin arise directly from the interaction of oxygen with the iron atom of the heme prosthetic groups and the resultant effects of these interactions are reflected on the quaternary structure of the protein. When oxygen binds to an iron atom of deoxyhemoglobin it pulls the iron atom into the plane of the heme. Since the iron is also bound to HisF8, this residue is also pulled toward the plane of the heme ring. The conformational change at HisF8 is transmitted throughout the peptide backbone resulting in a significant change in tertiary structure of the entire subunit.

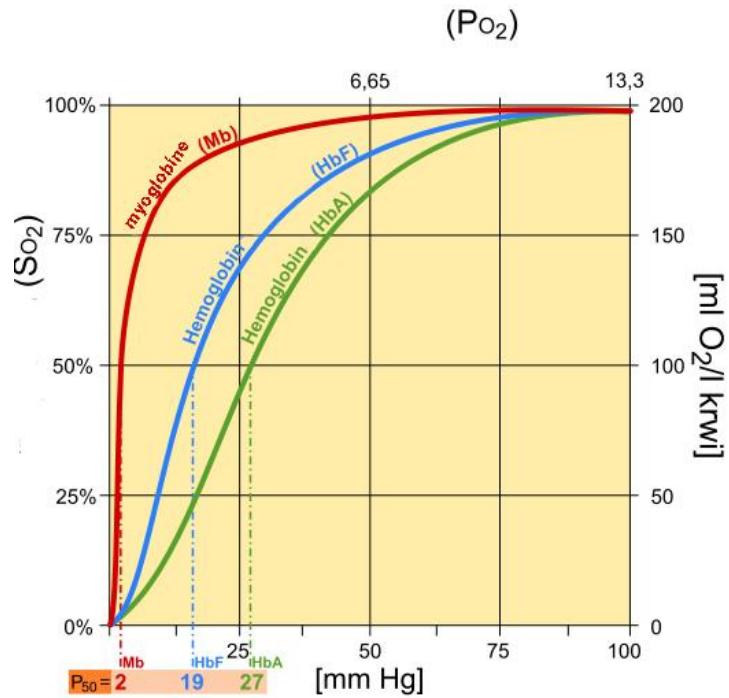


Figure 1. 4. Oxygen saturation curves for myoglobin and hemoglobin. The saturation curve for myoglobin (red) shows the typical rapid oxygen concentration-dependent saturation of this monomeric oxygen-binding protein. The other two curves show the typical sigmoidal saturation curves for cooperative oxygen binding exhibited by fetal hemoglobin HbF (blue) and adult hemoglobin HbA (green).

Conformational changes at the subunit surface lead to a new set of binding interactions between adjacent subunits. The latter changes include disruption of salt bridges and formation of new hydrogen bonds and new hydrophobic interactions, all of which contribute to the new quaternary structure. The latter changes in subunit interaction are transmitted, from the surface, to the heme binding pocket of a second deoxy subunit and result in easier access of oxygen to the iron atom of the second heme and thus a greater affinity of the hemoglobin molecule for a second oxygen molecule. The tertiary configuration of low affinity, deoxygenated Hb is known as the taut (T) state. Conversely, the quaternary structure of the fully oxygenated high affinity form of hemoglobin (HbO₂) is known as the relaxed (R) state. In the high O₂ environment (high pO₂) of the lungs there is sufficient O₂ to overcome the inhibitory nature of the T state but when the oxyhemoglobin reaches the tissues the pO₂ is sufficiently low, the T state is favored and the O₂ is released. Moreover, ligand binding to the heme influences the association state between subunits because $\alpha_1\beta_2$ interface, where the transition T→R happens, is involved in tetramer dissociation to dimers $\alpha\beta$. At the contrary, both $\alpha_1\beta_1$ and $\alpha_2\beta_2$ don't undergo to significant variations. Correlation between bond and association state has been very studied in hHb (5) highlighting its ability to dissociate in dimers after ligand-protein bond formation or after Fe²⁺ oxidation to Fe³⁺.

Further association phenomena in order to obtain tetramer-tetramer complexes has been discovered in some birds where hemoglobins have low affinity for oxygen, leading to an interestingly super cooperation event. Reptile hemoglobins display heterotetrameric $\alpha_2\beta_2$ form, but $\alpha_1\beta_1$ interface is not stable as the

mammals one so that oxygenated protein has only $\alpha\beta$ dimers or in some cases only monomers (6). Amphibians hemoglobins are generally monomeric when bind oxygen and can be found as tetramers or polymers when oxygen is released (7) (8).

Although myoglobins and hemoglobins are the most studied globins, other recently discovered respiratory proteins of vertebrates are neuroglobins and cytoglobins (9). Cytoglobin and neuroglobin are the first examples of hexa-coordinated globins in which the His residue at the sixth position of the heme iron is an endogenous ligand in both the ferric and ferrous forms. Actually, in the non-oxygenated form, the iron 6th coordination position is occupied by distal histidine.

Neuroglobin, has been found in peripheral and central nervous system thus suggesting to be involved against hypoxic/ischemic-induced cell injury in brain that is associated with accumulation of reactive oxygen species (ROS) and/or reactive nitrogen species (RNS)(10). On the other hand, Cytoglobin is expressed in splanchnic fibroblasts of various organs and details of its function remain unknown. Using both transgenic rats and cultured kidney fibroblasts, it was demonstrated that gene expressing cytoglobin confers cellular protection via an antioxidant mechanism (11).

1.3 Globins in plants

Three types of globins have been identified in land plants: symbiotic hemoglobins, non-symbiotic hemoglobins, and truncated hemoglobins (12). Among them, the most abundant hemoglobins are the symbiotic leghemoglobins (Lbs) discovered in leguminous root nodules. These nodules are a symbiosis between rhizobial bacteria and the plant to allow fixation (reduction) of atmospheric nitrogen(13) into an usable form, eventually appearing in amino acids and other building blocks for the cells: NO accumulates during the early stages of the rhizobia–legume symbiosis and in mature nodules. Legume nodules are an interesting model to study Hb function and regulation as they express the three types of plant globins(14). Specifically, Lbs are present at concentrations of 2–3 mM and maintain a free O₂ concentration of 20–40 nM in the cytosol of host cells. This range of O₂ concentration permits an adequate supply of ATP for N₂ fixation but avoids nitrogenase inactivation. Actually, reduction of nitrogen consumes large amounts of energy, and the nodules have an abundant plant-encoded Leghemoglobin that facilitates the diffusion of oxygen to the respiring bacteroids in the root nodule.

The discovery of a hemoglobin in a non-nodulating relative of *Parasponia*, *Trema tomentosa*, suggested that hemoglobins are in fact widespread in plants and can carry out more generalized roles besides those in nodulation(15). Indeed, hemoglobins have now been found in many plants, not only in the dicots just mentioned but also in the monocot cereals *Hordeum* (barley), *Triticum* (wheat), and *Zea* (corn)(16)(17).

1.5 Microbial globins

Microbial globins include three subfamilies: coupled globin sensors (CGS), flavohemoglobins and truncated hemoglobins. CGS are chimeric globins constituted by a globin domain fused with a transducer domain that can be a kinase, phosphodiesterase, nucleotide cyclase and chemotax receptors. The GCS superfamily is composed of two major subfamilies: the aerotactic and gene regulators. Flavohemoglobins, are made of a globin domain fused with a ferredoxin reductase-like FAD and NAD-binding modules. [fig. 1.5](18). The flavoHb family is formed by a very homogeneous group of proteins that share highly conserved active sites in both the heme- and flavin-binding domains. The conserved amino acids within the heme domain include the residues lining the heme pocket on both the proximal and distal sites, thus indicating that there must be a strong region and stereochemical requirement for ligand binding and/or for gaseous ligand diffusion. In parallel, also the amino acid residues responsible for flavin binding are strictly conserved and conform to the typical architecture of flavodoxin-reductase proteins, indicating clearly that the flavin moiety serves as an electron-transfer module from the NADH to the heme. The flavoHb from *E.coli* has been the first flavohemoglobin discovered in 1991(19) and many studies on it demonstrated that its expression play an important role in nitrosative stress pointing out its ability to convert nitrogen oxide to nitrate consuming oxygen and NADH(20)(21). The functional annotations of flavoHbs are still controversial but at now the overall picture that emerges from more than a decade of biochemical and microbiological investigations on flavoHbs indicates

that these proteins are key enzymes in maintaining the cell redox homeostasis at the aerobic/anaerobic interface when bacterial cells are exposed to oxidative/nitrosative stress.

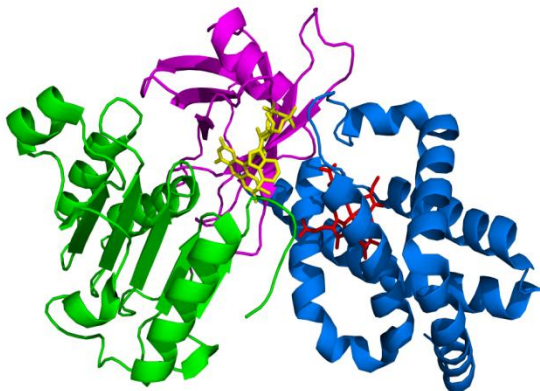


Figure 1. 5. Three-dimensional structure of flavohemoglobin from *Escherichia coli* characterized by a globin domain (blue) fused with ferredoxin reductase like FAD-domain (green) and NAD-binding domain (pink).

1.6 Truncated hemoglobins

Truncated hemoglobins (trHbs) belong to a family of single domain small oxygen-binding Myoglobin-like proteins distributed in *eubacteria*, *cyanobacteria*, *protozoa*, and *plants* forming a distinct group within the Hemoglobin Superfamily. They are nearly ubiquitous in the plant kingdom, occur in many aggressively pathogenic bacteria, and are held to be of very ancient origin. Many trHbs display amino acid sequences 20–40 residues shorter than non-vertebrate hemoglobins to which they are scarcely related by sequence

similarity. Although their low sequence similarity, trHbs have been distinguished into three groups that have in common the secondary structure: a two-over-two α -helical sandwich motif. In trHbs the antiparallel helix pairs B/E and G/H are the main secondary structure elements arranged in a 2-on-2 α -helical sandwich [Fig. 1.6](22). Within the trHb fold, the N-terminal A helix is almost completely deleted, and the whole CD-D region is trimmed to about 3 residues, possibly the minimum polypeptide stretch to bridge between C and E-helices. Moreover, most of the heme proximal F-helix is substituted by a polypeptide segment (pre-F) in extended conformation, followed by the one-turn F-helix that properly supports the HisF8 residue, allowing heme iron coordination (23). Very few amino acids are strictly conserved throughout the known trHb sequences but the proximal HisF8 is the only invariant residue. A Phe-Tyr pair is strongly conserved at the B9-B10 sites, where TyrB10 participates in heme ligand stabilization. Site CD1, invariably Phe in non-vertebrate Hbs, hosts Phe, Tyr, or His, whereas at least six different residue types occupy the distal E7 position. Moreover, the almost invariant Phe-E14, located along the heme distal face, may be related to a heme/solvent shielding role together with apolar residues of the pre-F segment [fig.1.7].

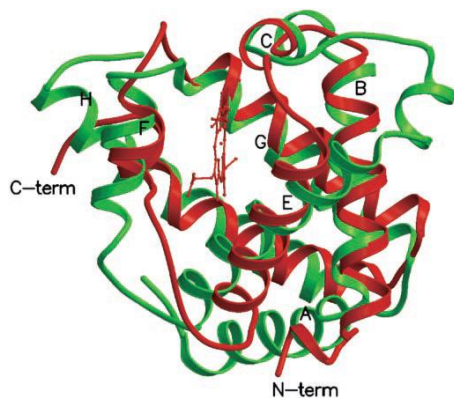


Figure 1. 6. A structural overlay of *C. eugametos* trHb (red ribbons) on sperm whale Mb (green), the latter taken as the prototype of the (non)-vertebrate globin fold. *Reproduced from(23).*

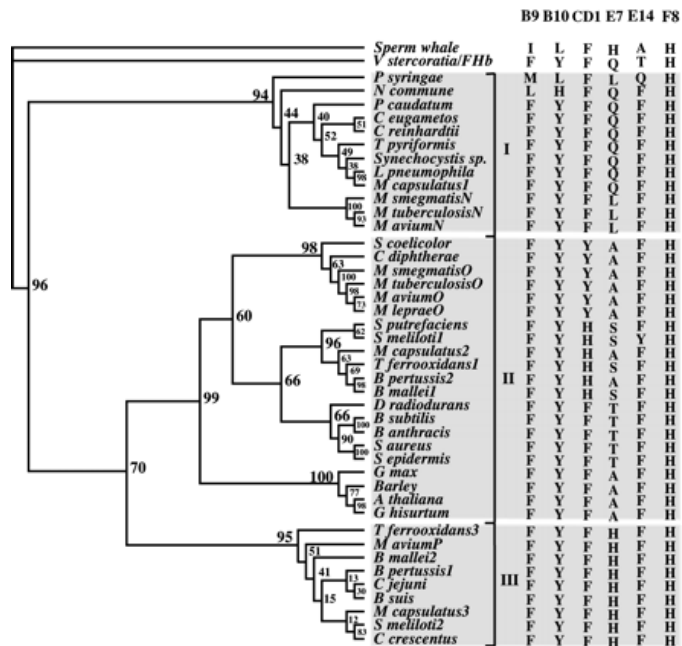


Figure 1. 7. Phylogenetic tree showing the relationships among trHbs. *Reproduced from(23)*

The functional roles of trHbs are virtually unknown and may be various. When the green unicellular alga *Chlamydomonas eugametos* is grown under light/dark regimes, nuclear genes are periodically activated in response to the changes in light conditions. These genetic responses are dependent upon the activation of genes associated with photosynthesis (LI616 and LI637), nonphotosynthetic photoreceptors (LI410 and LI818) and the biological clock (LI818). Couture and co-workers(24) have demonstrated that the LI410 and LI637 genes are part of a small gene family encoding hemoglobins (Hbs). Moreover, investigations of the intracellular localization of *C. eugametos* Hbs by means of immunogold electron microscopy indicate that these proteins are predominantly located in the chloroplast, particularly in the pyrenoid and the thylakoid region. The soluble trHb of the cyanobacterium *Nostoc commune* is localized on the cytoplasmic face of the cell membrane and is expressed only under anaerobic conditions. It is a component of a membrane-associated microaerobically induced terminal cytochrome oxidase and has been associated to the scavenging of oxygen(25). At the same time, the success of *Mycobacterium tuberculosis*, the causative agent of most cases of tuberculosis, depends on its ability to withstand and survive the hazardous environment inside macrophages that are created by reactive oxygen intermediates (ROI), reactive nitrogen intermediates (RNI), severe hypoxia, low pH, and high CO₂ levels. So, an effective detoxification system is required for the pathogen to persist in vivo. The genome of *M. tuberculosis* contains glbO and glbN genes, encoding truncated hemoglobin O (trHbO) and truncated hemoglobin N (trHbN), respectively. Analysis of these gene demonstrated that whereas glbN shows an early response to the oxidative and nitrosative stresses

tested, glbO gives a lasting response to lower concentrations of both stresses(26). Other trHbs are involved in NO-detoxification, in redox reactions, in O₂ and NO sensing or in metabolic steps of cysteine biosynthesis and in mediated thiol redox homeostasis(27).

1.7 Spectroscopic Probes for the study of ligand recognition and stabilization in hemoglobins.

The recognition of diatomic ligands in heme proteins is a complex phenomenon, its description requires a full understanding of the environment experienced by ligands in heme binding pockets. In the last three decades a large number of investigations have been carried out by means of spectroscopic methods to analyze the physicochemical properties of the active site using iron ligands with different chemical properties. Ligand recognition in heme proteins is mediated by a network of interactions that contributes to modulate the functional properties of the macromolecule around the metal binding site. The environment experienced by ligands in heme pockets is thus a reflection of the electrostatic fields and hydrogen-bonding interactions exerted by amino acid side chains close to the iron-bound molecule. Specific short-range hydrogen-bonding interactions with ligand adjacent amino acid side chains as well as longer range interactions from internal fields give rise to the amazing diversity in the functional behavior of heme based proteins. One of the key objectives of current research in heme proteins is to assign the observed functional behaviors to chemical properties of the active site. To this end, static and time-resolved spectroscopic methods have

been employed both with physiological and non-physiological ligands both in the ferrous and ferric states. Carbon monoxide is the most widely studied Fe(II) ligand due to the high thermodynamic stability of the iron adduct, to the photolability of the iron carbon bond and to the abundance of diverse spectroscopic marker bands that virtually cover the whole range of visible, near and mid infrared radiation. On these basis, both steady-state(28) and time-resolved spectroscopic(29) studies have been extensively carried out. Carbon monoxide is a useful vibrational probe of heme binding sites in proteins, because Fe-CO backbonding is modulated by polar interactions with protein residues, and by variations in the donor strength of the trans ligand. This modulation is sensitively monitored by the C-O and Fe-C stretching frequencies, which are readily detectable in infrared and resonance Raman spectra. In this context, CO-adducts of globins are spectroscopically rich of signals that can be appropriately defined as “marker bands” of specific structural configurations and have been assigned to equilibrium or transient states of the globin. Moreover the photodissociation quantum yield of the CO adduct is equal to 1(30), a feature that brings out great advantages over O₂ or NO ligands. Analysis of protein CO-complexes provides many informations about the distal cavity structure of hemoproteins. Within the protein matrix, the $\nu(\text{CO})$ stretching frequency of both heme-bound and free CO are shifted by the internal electric field acting on the CO dipole; it diminishes for heme-bound CO by $\approx 200 \text{ cm}^{-1}$ from its gas phase value of 2143 cm^{-1} and falls in a region of the vibrational spectrum free from other molecular vibrations. The reason of these changes is that CO stretching frequency for CO bound to the heme iron is a sensitive and anisotropic local

detector of changes in the electrostatic field(31). Polar interactions, in particular the hydrogen bond between CO and distal cavity residues, modulate the back-bond donation from iron d_{π} orbital to CO π^* orbital. Actually, the electrostatic field generated by polar amino acid residues in the distal pocket affects the electronic distribution of the Fe-C=O system and the bond order of CO: when CO is near a positively charged group, the $\text{Fe}^+=\text{C}=\text{O}^-$ tautomer in which the Fe-CO and C-O bonds have a double bond character and the ligand oxygen has a partial negative charge is stabilized. In contrast, when CO is near a negatively charged group, the $\text{Fe}-\text{C}\equiv\text{O}^+$ tautomer is stabilized, in which the Fe-CO bond leans toward a single bond character, and the C-O tends toward a triple bond character, whereas the ligand oxygen has a partial positive charge. In the first case, the following event is the increasing of stretching frequency of Fe-C bond and the decreasing of stretching frequency of C=O bond; in the second case an inverse event happens(28). C=O stretching frequency is an indicator of hemoproteins functional properties: in hemoglobins and myoglobins, in which the integrity of ligand is needed, $\nu\text{C}=\text{O}$ ($1950\text{-}1960\text{ cm}^{-1}$) is major than $\nu\text{C}=\text{O}$ in peroxidases and cytochromes p450 ($1920\text{-}1950\text{ cm}^{-1}$) that carry out the heterolytic splitting of diatomic distal ligand.

However, experimental data have been reported that CO-derivative of Sperm Whale Myoglobin is characterized by three different stretching frequencies at 1930 cm^{-1} , 1945 cm^{-1} and 1966 cm^{-1} assigned to three different conformers of CO-complex A1, A2, A3 through infrared low temperature photolysis and polarized light experiments(32). Figure 1.8 reports a model proposed by Hong and coworkers for Myoglobin in which three conformers differs each other for

different CO dipole moment angulations respect to the normal to heme plane. Intensity of each conformer is proportional to its population and its frequency is proportional to the energy of the conformer.

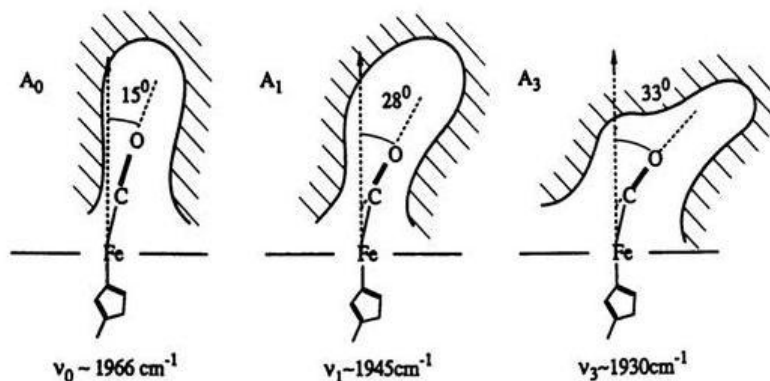


Figure 1. 8. Model of CO-derivate of Sperm Whale Myoglobin proposed by Hong. Mb can assume three different overall structures. Each substate permits only a small range of CO orientations centered around a mean angle between CO dipole and heme normal. The shapes of the heme pocket do not correspond to the reality, but are drawn only to illustrate the concepts. *Reproduced from*(32).

Actually, the situation is more complex: rebinding experiments after photolysis pointed out many different conformers diverging each other by an angle between CO moment dipole and the normal to heme plane. These conformers are named “conformational states” due to the fact that interconversion phenomena do not happen between 4K and 193K although they are separated by few cm^{-1} . In other words, a high kinetic energy barrier exists on the interconversion between

conformers; this barrier cannot be only due to the orientation of diatomic ligand in the protein distal cavity [Fig 1.9].

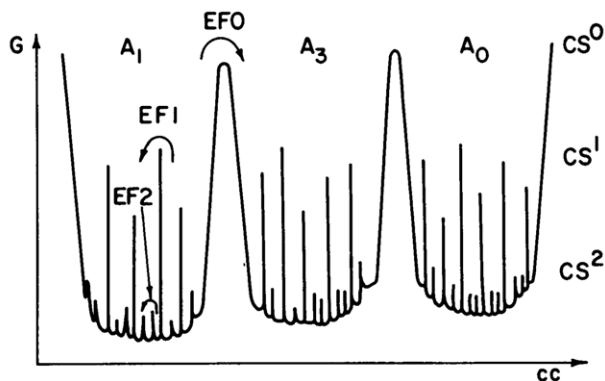


Figure 1. 9. The arrangement of conformational substates in MbCO. The figure shows the Gibbs energy of MbCO as a function of a representative conformational coordinate cc . *Reproduced from(32)*.

Probably, different protein conformations are at the origin of diverse CO stretching frequencies. To obtain more informations about structural features of the different conformational states, crystallographic data are not adequate but investigation of the IR spectrum can provide information on the direction of the transition moment via polarization measurements. Moore and coworkers studied iron-carbonyl geometries in carboxymyoglobin (MbCO) and carboxyhemoglobin (HbCO) using picosecond time-resolved infrared spectroscopy(33). Monitoring the change in infrared absorbance of the bound CO stretch bands through

polarized infrared and visible beams, the authors found an angle of 18 degrees for the 1951 cm^{-1} band of HbCO against 20 degrees and 35 degrees, respectively, for the 1944 cm^{-1} and 1933 cm^{-1} bands of MbCO.

In this background another important aspect is that vibrational transitions of free CO are sensitive to the chemical environment. Since heme-CO system is characterized by an intense and typical absorption spectrum, it is generally a well suited model system for investigations of photodissociation initiated relaxation processes. Although the photodissociation of the heme-ligand bond is not a physiologically relevant event, it can be used to mimic the actual dynamics of the protein. In particular, the ultrafast processes triggered by the optical pulses are strongly related to the structure of the protein and to the protein-cofactor interactions. Photodissociated CO trapped inside the protein matrix displays multiple IR bands around 2130 cm^{-1} called B states and arise from different locations and/or orientations of CO within the protein. In MbCO complex, within picoseconds after photolysis the ligand settles into an initial docking site B on top of the heme group, parallel to pyrrole C, where it resides for several nanoseconds before either rebinding or escaping to the solvent. It is well known(34) that the photodissociated ligand can either recombine rapidly with the metal or diffuse out into the solvent through the protein matrix. If the amino acids residues constituting the heme pocket confine the ligand near the metal, the *geminate recombination* (this expression refers to the reaction between two transient species produced from a common precursor before any separation by diffusion has occurred) takes place. If the ligand can easily diffuse away, and then comes back to the heme pocket, the *bimolecular recombination* takes place.

In Mb and Hb, CO geminate recombination contributes only for a few percent to the total recombination at room temperature and occurs on the microsecond timescale and a few tens of percents on the tens of nanoseconds timescale(35) respectively. The dissociation of the ligand bound at the heme iron has been investigated for MbCO complex by means of femtosecond time-resolved infrared spectroscopy by Lim et al.(36) and two trajectories (state B1 and state B2) have been identified within few hundreds femtoseconds that lead to CO located with opposite orientations.

Both rotamers are characterized by the CO axis ligand parallel to the heme plane but whereas the B1 state high frequency (2130 cm^{-1}) has been assigned to the conformer with the O atom pointing back toward the heme iron atom, low frequency (2120 cm^{-1}) B2 state is established to have another orientation on the basis of the kinetics of the appearance of the $\nu(\text{CO})$ bands after photolysis and the effect of isotopic substitution on the rate of recombination[Fig. 1.10].

The two B states are kinetically and spectroscopically distinguishable due to the vibrational Stark shift that arises from the electrostatic field surrounding the ligand.

Furthermore, because the electrostatic field is inhomogeneous (non uniform in the three-dimensional space) the centre frequency of CO will be positioned depending on the orientation. As reported in Fig. 1.9, the energy barrier against the conversion from B2 to B1 conformer is about 3-4 KJ/mol, very small if compared with the recombination energy of CO ligand to the iron atom (10 KJ/mol); it means that the conversion consists in a simple rotation of the ligand around the centre of C-O bond(37).

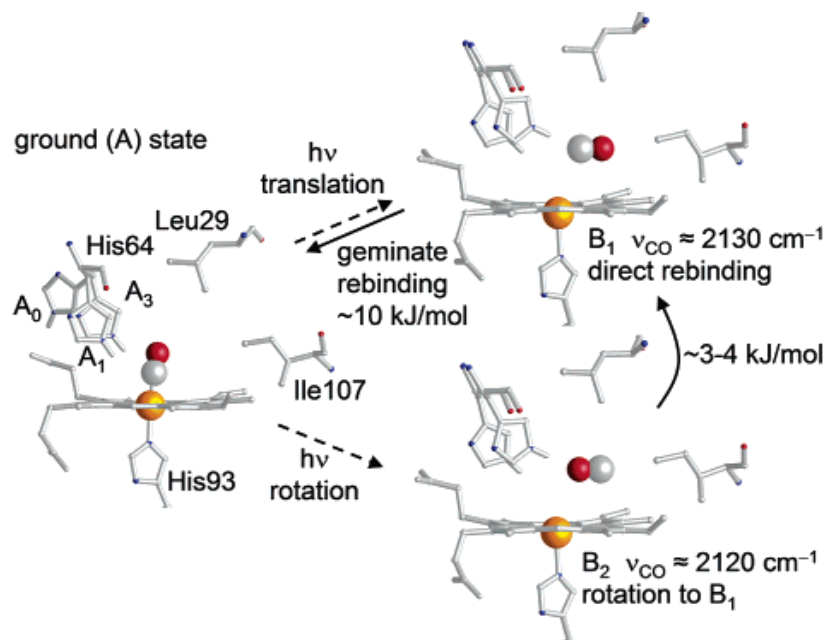


Figure 1. 10. (Left) Schematic representation of heme-bound states A₀, A₁, and A₃ of MbCO. The O and C atoms of the ligand are red and white, respectively. (Right) Photoproduct states B₁ and B₂, with the His64 imidazole farther away from dissociated ligand. *Reproduced from(37).*

The change in absorption strength of the C-O bond to the heme respect to the free ligand inside the docking site of Myoglobin observed by Polack and coworkers(38) through Vis-pump mid-IR-probe experiments, have pointed out the effect of charge displacement from the heme iron to the CO on the absorption strength and underlined that the CO vibrational absorption strength is a suitable probe related to the ligand dissociation and transfer processes.

Moreover, substitution of Leu in B10 position of mammalian Mb with a Phe residue in the docking site, led to a lifetime reduction of the docked CO to 140

ps(39). Other data by dynamic simulation studies have revealed the detailed kinetics of CO migration and binding in crystallized and solvated Myoglobin(40)(41) pointing out that the CO motion and the protein fluctuations were strictly correlated. In other words, ligand do not diffuse randomly but takes preferred directions in moving away from the heme iron, ultimately reaching secondary well-defined sites(42)(43). The interaction of ligand with amino acidic residues located in the distal cavity of globins is responsible of a slow geminate recombination process. The distal barrier clearly depends on the enclosed amino acids residues and the trajectory of the dissociated ligand brings to collisions that vary with the protein motion fluctuations, thus influencing the rebinding kinetics. Time-resolved CO rebinding studies on microperoxidases have performed by Lim and co-workers(44) to investigate the rebinding process on a system that mimics the hemoprotein structure in absence of a distal heme pocket. In this way, the photodissociated CO is exposed to the solvent and not to a closed docking site, as in Mb. They disappointed the previous idea concerning differences about geminate recombination between NO and O₂ adducts of Mb and MbCO: geminate recombination following photolysis of MbCO in solution is minimal and occurs on the few hundred ns time scale; on the other hand, NO and O₂ undergo significant geminate rebinding, with NO rebinding on the sub-ns time scale. It was proposed that these kinetic differences arise from differences in the electronic barrier to the binding, with CO having the highest electronic barrier and NO having the lowest.

Actually the differences in the geminate rebinding rates may be due to steric constraints imposed on the docked ligands. The docking site permits O₂ and NO

to access their transition state for rebinding but strongly inhibits such access by CO, whose transition state for binding is much more upright compared to O₂ and NO. The observed rebinding kinetics in microperoxidases is not exponential, probably because the solvent cage effect influences the process. In this latter paper a model for the CO trapped within the solvent cage surrounding the heme has been formulated and a kinetic time constant of $k = (110 \text{ ps})^{-1}$ has been estimated. It emerges that the rate of CO rebinding in this protein is much faster than in Mb; this suggests the idea that the presence of a docking site is responsible for the slow CO rebinding observed in most heme proteins.

The geminate heme-CO recombination in heme proteins is quite different. Flash photolysis experiments performed on a carboxymethyl cytochrome c have been described the kinetics and spectral transitions that accompany the recombination(45): the recombination of CO is multiphasic with time constant of 16 ps, 120 ps and 1ns corresponding to rebinding of CO from three different locations within the distal cavity. These data, have pointed out that the CO enclosed in the distal heme pocket rebinds to heme efficiently as a consequence of a sterically hindered ‘caged’ nature of the distal heme pocket from which it is difficult for CO to escape. In other words, the protein does not possess a ligand exchange pathway due to the fact that in cytochrome c the heme group is surrounded by a hydrophobic, structurally rigid pocket in which the interactions are weak. This configuration assures the restraint of the reorganization energy of the active heme environment, that guarantees the efficient electron transfer process, and it is necessary for protein whose role is ligand transfer.

The study of the ligand entry/escape dynamics to the active site of hemoglobins yields information useful to clarify their functions: slow geminate recombination of ligand to the heme after photolysis is typical of proteins that show gaseous ligand exchange role; high geminate recombination belongs to proteins where the ligand transfer role is essential. The benefits of these kind of studies are applicable to recently discovered truncated hemoglobins in order to characterize them.

In the distal site of their heme pocket, the ensemble of polar residues are in contact with the iron-bound ligand coordination shell. Spectroscopic properties of CO in different wild-type and mutant adducts have revealed that the oxygen atom of the heme-bound CO could be H-bonded to the indole nitrogen of tryptophan, the hydroxyl of tyrosine or the amine group of glutamine. This common pattern has been defined 'ligand inclusive hydrogen bond network' and may represent a considerable barrier to ligand entrance and escape from/to the distal heme pocket.

In the picture of recently discovered truncated hemoglobins, trHbO, one of two trHbs in *Mycobacterium tuberculosis*, has been shown rate constants for combination ($<1.0\mu\text{M}^{-1}\text{ s}^{-1}$) and dissociation ($<0.006\text{ s}^{-1}$) of O_2 that are among the slowest known(46)(47). Femtosecond spectroscopy experiments, have been displayed that upon photoexcitation, ligands rebind with unusual speed and efficiency. Only 1% O_2 can escape from the heme pocket and less than 1% NO. Most remarkably, CO rebinding occurs for 95%, predominantly in 1.2 ns(48) showing an unusually high barrier for ligand escaping. This situation is ascribable to extremely high reactivity of ligand with the heme combined to the

preventing of ligand access to the heme distal pocket by a network of aromatic residues, in particular by Trp88(G8). On the basis of dynamics simulations, a primary role for the structural water molecule present in the heme pocket has been suggested: this water molecules would retain the CO close to the heme iron at a distance favorable for ligand-heme bond formation by restricting the effective distal pocket volume. Site directed mutagenesis to substitute TrpG8 and TyrCD1 with Phe residues in single and double mutants led to the fact that CO rebinding is not drastically altered; moreover all the mutants have shown an additional decay phase of ≈ 250 ps not present in the wild type protein ($\tau_1 = 37$ ps and $\tau_3 = 1,2$ ns) indicating that changes in the strong hydrogen bonding network at the distal site yields a more flexible heme pocket and a more heterogeneous environment for dissociated CO, but not strongly changing its reactivity. These evidences induce to think that HbO effectively acts as a cage for ligands once they enter in the heme pocket, precluding transport or diffusion of O₂ as a major function.

Although CO probe for heme proteins is the most studied marker to investigate heme pocket structure and dynamics, a captivating contribution is offered by the purpose of fluoride as alternative probe for hemoproteins. Even if it's not a physiological ligand, fluoride has recently revalued for studying heme proteins. The main advantage offered by fluoride ion probe is its ability to yield only 6-coordinate high spin (6c-HS) complexes if bond to the heme(49), as highlighted by electronic absorption spectra of these complexes in which $\pi \rightarrow \pi^*$ transitions give rise to the strong Soret band with maxima between 404–406 nm, and the weaker Q band at 490 nm. Charge transfer transitions occur between 607 and

617 nm [CT1 due to $a_{2u}(\pi) \rightarrow e_g(d\pi)$ transition] and between 450 and 460 nm [CT2 due to $a'_{2u}(\pi) \rightarrow a_{1g}(dz_2)$]. This latter transition gives rise to a very weak band in the electronic absorption spectra.

The analysis of resonance Raman spectra of fluoride complexes and the study of RR frequency of the $\nu(\text{Fe-F})$ stretching mode would provide direct evidence for H-bonding of the fluoride ligand to distal residues via information on the Fe-ligand strength.

Previous studies demonstrated that the specific enhancement of the $\nu(\text{Fe-F})$ stretching vibrational modes occurs when excitation is within the CT1 band(49)(50)(51) so, utilizing a tunable dye laser which can excite within the CT1 bands (600–640 nm) the ligation properties of the complexes of fluoride with *Sperm Whale Mb* (swMb) and *Human Hb* were investigated. The $\nu(\text{Fe-F})$ stretching modes appeared in the region between 380 and 470 cm^{-1} . In particular, in the case of the fluoride complex of swMb, at neutral pH, both bands at 422 and 462 cm^{-1} have been assigned as Fe-F stretching bands. The latter band had also been observed upon excitation at 441.6 nm for the fluoride complex of *Horse Myoglobin* (hhMb)(52), and assigned to the Fe-F stretching mode on the basis of the 2 cm^{-1} up-shift observed upon $^{56}\text{Fe}/^{54}\text{Fe}$ isotopic substitution. In addition, the band at 462 cm^{-1} has been reported to be pH sensitive, as its intensity decreased upon acidification with the concomitant appearance of a band at 399 cm^{-1} . This result was interpreted as an acid-base equilibrium with $\text{pK}=5.5$, being due to protonation of the distal His and formation of a strong H-bond to the fluoride ligand in swMb. Latest studies developed on a series of heme containing peroxidases reported a clear correlation

between the absorption maxima of the CT1 band and the H bonding to the bound fluoride ion: Smulevich and coworkers focused their interest on the RR and electronic absorption spectra of the fluoride adducts of different peroxidases belonging to the three classes of the plant peroxidase superfamily, together with some selected mutants in the distal cavity, and compared them with those of Mb(53)(54). These different three structural classes have less than 20% sequence identity, but they have conserved residues, namely, the distal His and Arg, and the proximal His hydrogen-bonded with an Asp residue. From these studies resulted that in peroxidases, the Arg is determinant in controlling the ligand binding via a strong hydrogen bond between the positively charged guanidinium group and the anion. Mutation of Arg to Leu decreases the stability of the complex by 900-fold, suggesting that this interaction stabilizes the complex by 4 kcal/mol. The distal His also contributes to the stability of the fluoride complex, presumably by accepting a proton from HF and hydrogen-bonding, through a water molecule, to the anion. Mutation of His to Leu decreases the stability of the fluoride complex by 30-fold, suggesting that this interaction is much weaker than the interaction with the distal Arg. For Mb, the distal His is solely responsible for stabilization of the exogenous ligand. They also confirmed that the wavelength of the CT1 band is a sensitive probe of axial ligand polarity and of its interaction with the distal protein residues.

STATE OF ART

Data presented in this work concern two truncated hemoglobins isolated from the thermostable *Actinobacterium Thermobifida fusca* and *gram-positive* bacterium *Bacillus subtilis* respectively. The identification of *T. fusca* together with the crystal structure of its ferric acetate-bound derivative has been recently described by Ilari and coworkers(55). As reported in fig. 2.1, its three-dimensional structure is characterized by a two-over-two α -helical sandwich motif formed by the helices B, E, G and H with F and A helices shorter than in the classical globin fold; helices C and D are absent against the presence of an additional phi-helix between helices E and F. Respect to other truncated hemoglobins, *Tf-trHb* is lacking of internal cavities. For example, both truncated hemoglobins from *Mycobacterium tuberculosis* (*Mt-trHbO*) and from *Bacillus subtilis* (*Bs-trHb*) contain internal cavities, although much smaller than those found in group I *trHbs*(56). In *Tf-trHb*, some of these cavities are filled by substitutions with larger residues (e.g.Trp87 and Trp141 replace Leu57 of *Bs-trHb* and Leu113 of *Mt-trHbO*, respectively), others by conformational differences of conserved or similar size residues.

The distal heme pocket architecture [Fig.2.2] shows that the acetate ion ligand is stabilized by interactions with residues Tyr67 (CD1) and Trp119 (G8). The carbonyl oxygen of the acetate ion is hydrogen bonded to the OH group of the former amino acid and to the indole group of tryptophan (distances = 2.86 and 2.52 °A, respectively).

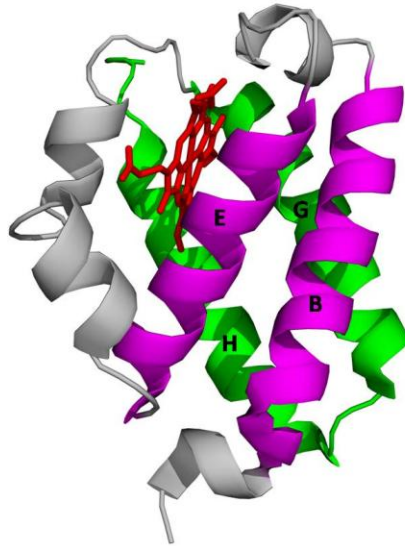


Figure 2. 1. Three-dimensional structure of Tf-trHb.

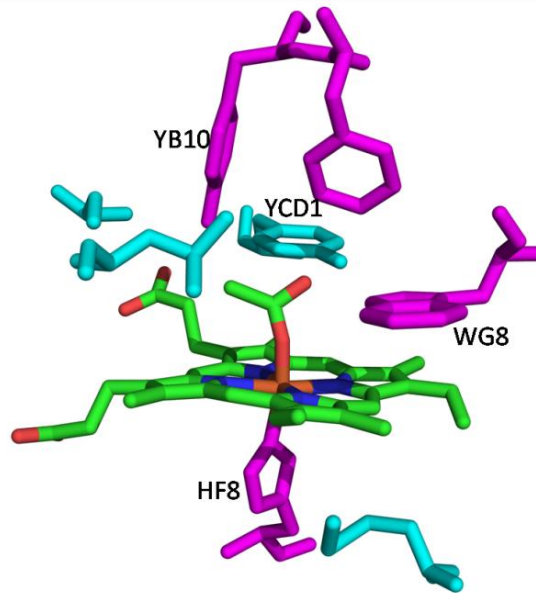


Figure 2. 2. Close up view of *Thermobifida fusca* trHb heme pocket.

The latter amino acid is rigorously conserved, i.e., in *Tf-trHb* and in other group II hemoglobins from *Mycobacterium tuberculosis* (*Mt-trHbO*) and from *Bacillus subtilis* (*Bs-trHb*). The Trp119 (G8) is essentially parallel to the heme plane. In the proximal region the His106(F8) is bonded to the Fe(III) of the heme at a short distance (N-Fe = 1.92 Å).

Droghetti and coworkers, have been studied carbon monoxide complexes of *Tf-trHb*(57) and a series of mutants of distal cavity through infrared and Resonance Raman spectroscopy: the acid surface variant ASV of *Tf-trHb* (that differs from the Wild Type (WT) protein because both Phe107 and Arg91 are mutated to glutamic acid to increase protein solubility, without affecting thermostability or ligand binding, was used in a combinatorial mutagenesis of the distal heme pocket residues in which one, two, or three of the conserved polar residues [Tyr54 (B10), Tyr67 (CD1), and Trp119 (G8)] were substituted with Phe [Fig.2.3]. Similar Fe-proximal His stretching frequencies have suggested that none of the mutations alters the proximal site of the heme cavity. In fig. 2.4 is also reported the crystal structure of the triple mutant of *Tf-trHb* (YCD1F-YB10F-WG8F or *3F-Tf-trHb*). The arrangement of residues in the distal cavity reflects that of the wild type protein, confirming that the same arrangement characterizes the entire set of mutants.

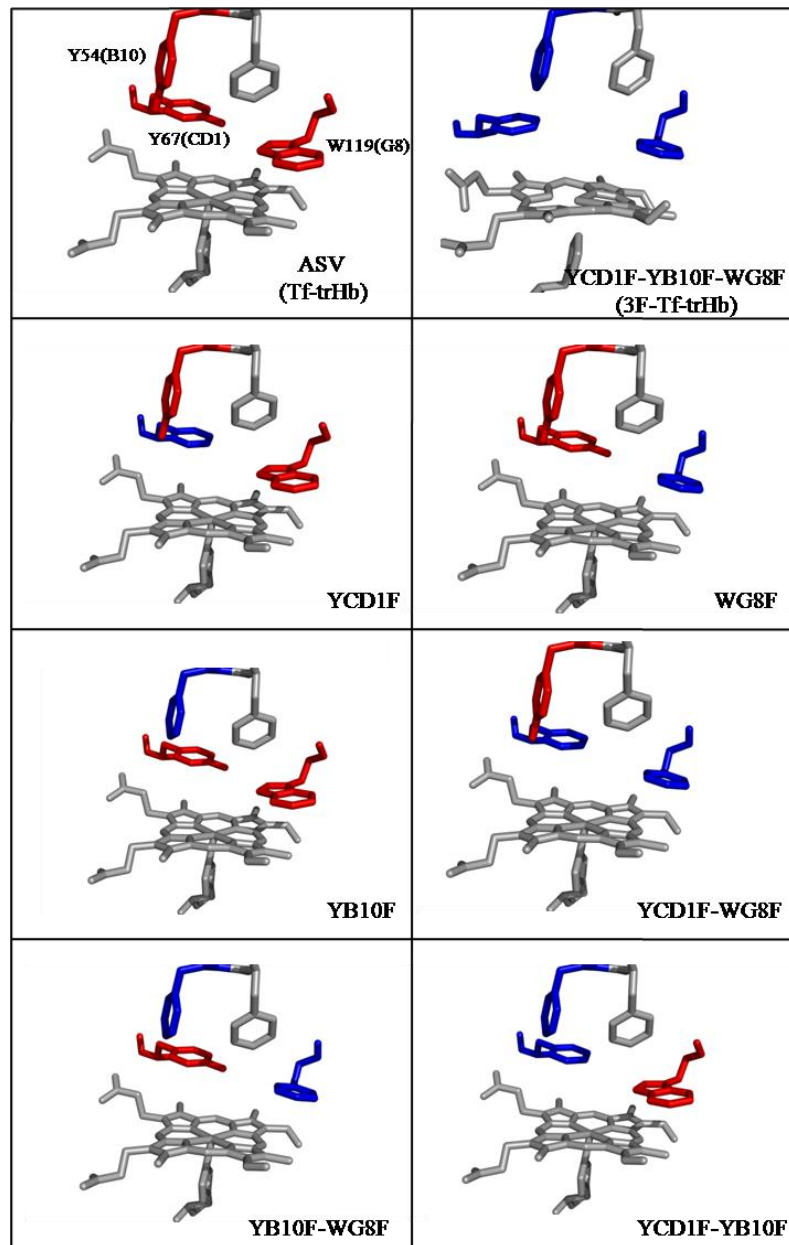


Figure 2. 3. Set of distal mutants of Tf-trHb. Wild type residues are highlighted in red, mutated residues in blue.

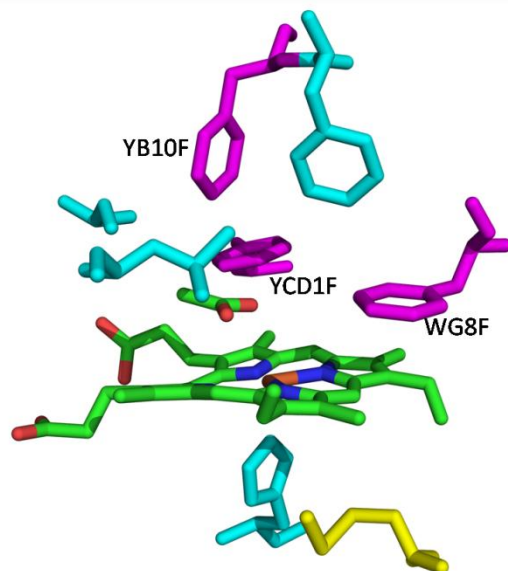


Figure 2. 4. Close up view of YB10F-YCD1F-WG8F mutant of *Thermobifida fusca trHb* heme pocket.

Figure 2.5 reports the IR and Raman resonance spectra of WT protein and its mutants; the existence of two bands allows to think the presence of two conformers for the protein. The single mutation $WG8 \rightarrow F$ led to a drastic change arising in the transfer of absorbance bands to lower frequencies in IR spectra (491 cm^{-1} and 497 cm^{-1}) and to higher frequencies in RR spectra (1942 cm^{-1} e 1965 cm^{-1}). Also $YCD1 \rightarrow F$ mutation produces drastic consequences: RR spectrum shows one only band at 505 cm^{-1} , similarly to IR spectrum (1943 cm^{-1}). On the contrary, single mutant $YB10 \rightarrow F$ shows a similar spectrum to the WT and ASV protein form with a slight shift to higher frequencies. Moreover the substitution of distal Tyrosines in YB10F-YCD1F mutant shows only one band

in RR spectrum as in IR spectrum: a single stretching frequency has been obtained for Fe-C bond (522 cm^{-1}) and C-O bond (1931 cm^{-1}). The presence of two bands in IR and RR spectra for YB10F-WG8F and YCD1F-WG8F mutants, demonstrate that they display two conformers. At the same time, YB10F-YCD1F-WG8F mutant displays only one band in IR and RR spectra, respectively at 494 cm^{-1} and 1955 cm^{-1} ; in this case the hydrogen bonding network is completely removed and CO is not stabilized by the formation of H-bonds. These data led to identify two conformers for CO-derivates of *Tf-trHb*: one with $\nu(\text{FeC})$ and $\nu(\text{CO})$ at 509 and 1938 cm^{-1} respectively, and form 2 with $\nu(\text{FeC})$ and $\nu(\text{CO})$ at 518 and 1920 cm^{-1} respectively. CO interacts with Trp119 (G8) as single H-bond donor in form 1, whereas in form 2 is stabilized by two H-bonds in which both Tyr67 (CD1) and Trp119 (G8) are involved (fig.2.6).

Truncated hemoglobins have been found also in *Bacillus* genus including *Bacillus anthracis*, *Bacillus cereus*, *Bacillus halodurans*, and *Oceanobacillus ihyeiensis*, as well as in *Bacillus subtilis*. *Bs-Hb* belongs to group II truncated hemoglobins and shows with them many common features such as >60% sequence similarity and the same heme pocket setting.

In all *Bacillus* species whose genomes have been sequenced, truncated hemoglobins coexist with true-type heme-containing chemotactic oxygen sensors and flavohemoglobins while, in *B. subtilis*, the globin-like sensor domain of the HemAT oxygen sensor as well as the flavohemoglobin heme domain share little sequence similarity with the *trHb*. Moreover, alignments reveal that key residues within the heme pocket are not conserved, suggesting different functional roles for the three proteins(58).

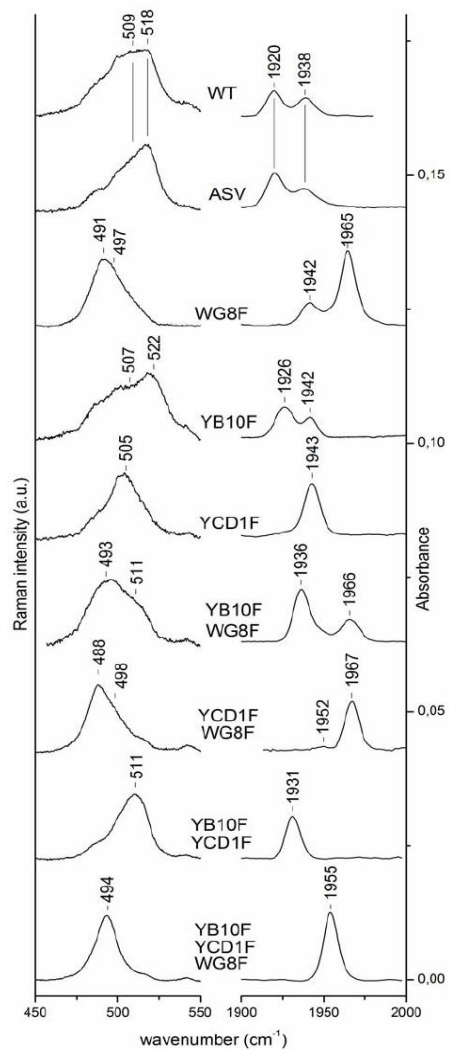


Figure 2. 5. RR spectra (*left*) obtained with 413.1 nm excitation wavelength and IR spectra (*right*) of the carbon monoxide complexes of native and mutated ferrous Tf-trHb variants at pH 7.0. Reproduced from (57).

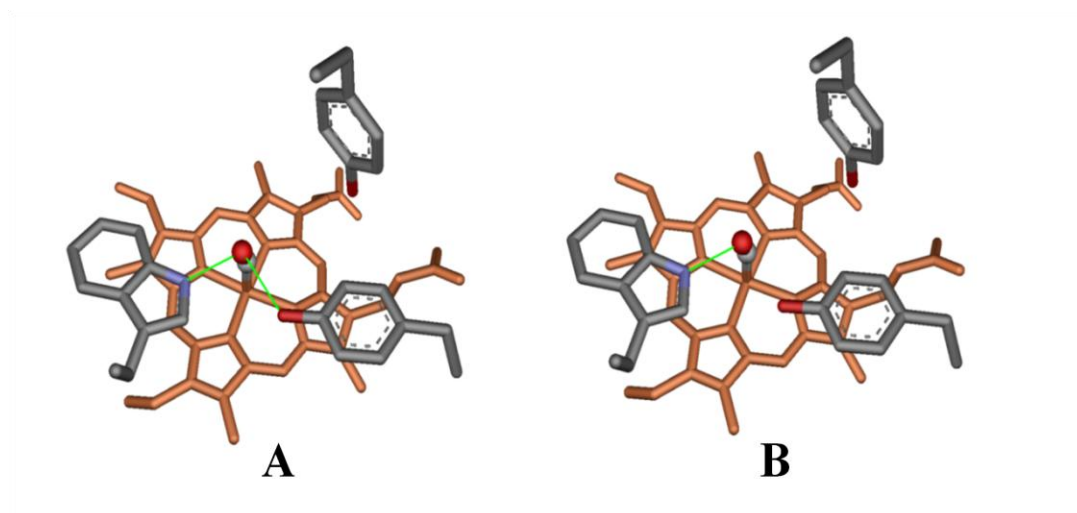


Figure 2. 6. Two different conformers for Tf-trHb-CO. A) CO interacts with Trp119 (G8) and Tyr67. B) CO interacts with Trp119 (G8) as single H-bond donor. *Reproduced from (57).*

As shown in fig. 2.7 the protein is characterized by a two-over-two- α helical sandwich motif very similar to the *Tf-trHb* one. Crystal structure of cyanide-bound derivative of *Bs-trHb* resolved by Giangiacomo and coworkers(59), has been highlighted a distal heme pocket characterized by the presence of polar residues surrounding the bound ligand, namely Tyr25 (B10), Thr45 (E7), and Gln49 (E11) (Fig. 2.8). The cyanide ion is almost perpendicular to the heme plane and stabilized mostly by the Tyr25 (B10) residue, which is hydrogen-bonded through the OH group directly to the cyanide nitrogen atom (distance=2.54Å).

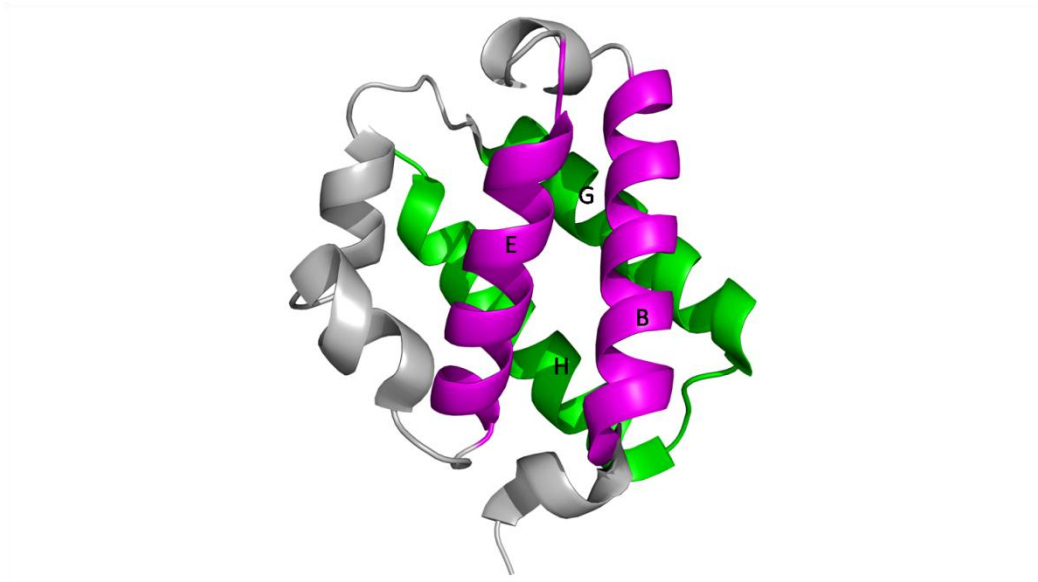


Figure 2. 7. Three-dimensional structure of truncated hemoglobin from *B. subtilis*.

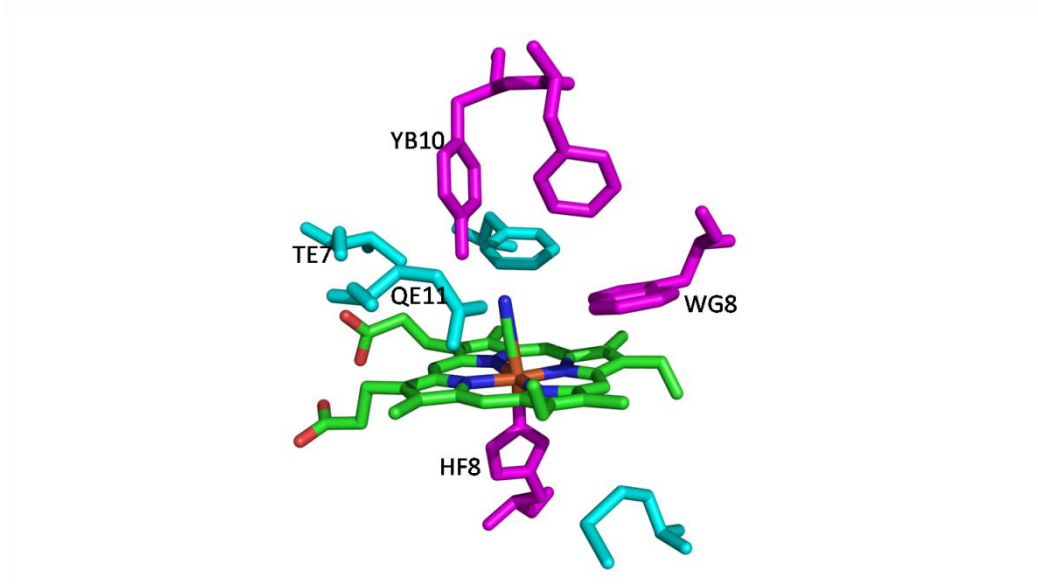


Figure 2. 8. Close up view of *Bacillus subtilis* trHb heme pocket.

The carbon atom is bound to the ferric heme iron at a distance of 1.92 Å. It is of interest that in *Bs-trHb* the proximal pocket appears to be directly exposed to solvent through a 55-Å² aperture situated in a shallow depression delimited by the phenyl ring of Phe79, the carbonyl backbone portion of Arg75(F7), and the heme propionates. Trp89 (G8) is buried in the distal pocket and is roughly parallel to the heme plane with the indole NE1 atom placed at a distance of 3.4 Å from the cyanide nitrogen atom. At the external edge of the distal site, a Lys residue, Lys48 (E10), forms a salt bridge with the heme propionate D. This salt bridge is on the external surface of the protein and may hinder access to the distal pocket. Most interestingly, position E10 is occupied by a positively charged residue in all three groups of *trHbs*. The unconstrained histidine conformation appears to be a common feature of the trHbs investigated to date(60) and the coordination bond formed by His76 (F8) is stronger than in other hemoglobins as indicated by the unusually short iron-histidine distance (N-Fe(III)=1.91 Å). A first characterization of active site of *Bacillus subtilis* truncated hemoglobin has been performed by Feis and co-workers(47) through IR and RR spectroscopy. Actually, carbon monoxide is a sensitive probe for investigating distal environmental effects on ligand binding of heme proteins and in particular, polar interactions since the formation of H-bonds between the bound CO and the distal residues increases the extent of back-donation from the Fe d_{π} to the CO π^* orbitals. As a consequence, the Fe-C bond strengthens while the CO bond weakens, thereby increasing the ν (Fe-C) vibrational frequencies and decreasing the ν (C-O) frequencies. The authors reported for *Bs-trHb* the presence of two Fe-CO stretching bands at 545 and 520 cm⁻¹, respectively.

Accordingly, two C-O stretching bands at 1924 and 1888 cm^{-1} were observed in infrared absorption and resonance Raman measurements. The very low C-O stretching frequency at 1888 cm^{-1} (corresponding to the extremely high RR stretching frequency at 545 cm^{-1}) indicates unusually strong hydrogen bonding between CO and distal residues. On the basis of a comparison with other truncated hemoglobins it is envisaged that the two CO conformers are determined by specific interactions with the TrpG8 and TyrB10 residues. Mutation of TrpG8 to Leu has deeply altered the hydrogen bonding network giving rise mainly to a CO conformer characterized by a Fe-CO stretching band at 489 cm^{-1} and a CO stretching band at 1958 cm^{-1} .

As well as the study of hydrogen bonding network, truncated hemoglobins from *Bacillus subtilis* (*Bs-trHb*) and *Thermobifida fusca* (*Tf-trHb*) has been recently investigated to evaluate the recombination dynamics.

Feis and coworkers have also developed picosecond laser photolysis experiments on the CO bound adduct revealing a geminate recombination with a time constant of 770 ps indicating that even in this case the ligand is confined within the distal pocket with a remote possibility to escape to the solvent or to the adjacent small cavity located at the top of distal pocket. These data induce to think that as *Mt-trHbO*, *Bs-trHb* is not designed to perform gaseous ligand exchange but probably to perform redox processes involving oxygen or hydrogen peroxide.

Similar experiments to investigate the recombination dynamics are conducted on *Tf-trHb* by Marcelli and coworkers(61) through a combination of techniques such as femtosecond transient absorption, nanosecond laser flash photolysis and

optoacoustic spectroscopy, assisted by molecular dynamics simulations. They have shown that photolysis of bound CO is followed by a rapid geminate recombination with a time constant of ≈ 2 ns, representing almost the 60% of the global reaction, and a second recombination around 100 ns. Accordingly to *Bs-trHb* and *Mt-trHbO*, in *Tf-trHb* the barrier for CO escaping is high.

In this background the present work is introduced. The aim of it is the better characterization of truncated hemoglobins from *Bs-trHb* and *Tf-trHb*. In order to complete the study to establish the role of distal residues on the stabilization of ligand in *Tf-trHb*, we propose to reconsider the opportunities yielded by spectroscopic studies on the fluoride complexes of heme proteins. Actually, fluoride coordinates to Fe(III) heme with the formation of 6-coordinate (6c) HS complexes and their electronic absorption spectra display an interesting feature in the 600–620 nm range, where a weak band due to a charge transfer transition (CT1) appears. Since a correlation between the absorption maxima of the CT1 and the H-bonding to the bound anion has been found in a series of mutated heme containing peroxidases(53), thus indicating that fluoride is a sensitive probe of the distal environment in peroxidases, in the present work we would investigate the fluoride binding mode to *Tf-trHb* and a set of distal mutants in which TyrB10, TyrCD1 and TrpG8 are substituted with Phe in single, double and triple mutations, by combining UV-VIS electronic absorption with RR spectroscopy. This choice derived from the fact that RR spectroscopy has been demonstrated to be a very powerful tool for investigate the interaction between exogenous ligands and heme iron due to the selectively enhancing of the metal

ligand stretching modes by tuning the laser frequency within the Soret or charge transfer transition bands(62)(63).

Moreover, in the second part of this work, attention will be given to the study of CO-recombination dynamics in *Tf-trHb* (and its triple mutant *3F-Tf-trHb*) and in *Bs-trHb* by UV-Vis-Pump Mid-IR-probe spectroscopy in order to obtain additional informations about ligand dynamics within the protein structure matrix.

MATERIALS AND METHODS

3.1 Cloning, Expression, and Purification of Recombinant *B. subtilis trHb*

The gene *YjbI* codifying for the truncated hemoglobin of *B. subtilis* has been amplified from *B. subtilis* genomic DNA through polymerase chain reaction (PCR) choosing the primers 5'-GGA GTA GTC ACC ATG GGA CAA TC-3'(forward) and 5'-TCA GGA CAT AAA GGA TCC ACA AAC-3' (reverse). The DNA fragment was purified with the Qiagen GmbH (Hilden, Germany) kit, digested with restriction enzymes *BamHI* and *NcoI* (MBI Fermentas, Vilnius, Lithuania), and inserted into a pET28b(+) plasmid (Novagen, Darmstadt, Germany). The plasmid has been transformed in *Escherichia coli* BL21 (DE3) supercompetent cells (Agilent Technology, USA) and the colonies with the correct DNA insert has been selected through PCR screening(59). Transformed *E. coli* cells were grown in a Luria-Bertani broth in presence of 1mM kanamycin. When the optical density amounted to a value of 0,6 gene expression has been induced with 1mM isopropyl- β -D-thiogalactopyranoside and the culture has been left to grow for sixteen hours. Then it has been centrifuged and pellets have been resuspended in a minimum volume of lysis buffer (20mM sodium phosphate buffer pH 7.0) and sonicated with the addition of proteases inhibitors cocktails (Roche) until the supernatant was reddish and clear. After

centrifugation at 12000 rpm for 20 minutes, the supernatant has been loaded on a DEAE-cellulose column (Whatman International Ltd., Maidstone, UK) equilibrated with 20 mM sodium phosphate buffer, pH 7.0, and eluted with a NaCl step gradient (0–0.2 M). The protein obtained was >98% pure on SDS-PAGE.

3.2 Cloning, Expression, and Purification of recombinant trHb from *Thermobifida fusca* and its distal mutants.

A synthetic gene coding for *T. fusca* truncated hemoglobin has been synthesized by GENEART (Regensburg, Germany) with optimized *E. coli* codons. The gene, designed with NcoI/HindIII restriction sites, has been cloned within puC19 KpnI cloning site by GENEART. The insert has been digested with restriction enzymes NcoI and HindIII (MBI Fermentas, Vilnius, Lithuania), loaded onto an agarose gel and purified with the DNA gel extraction kit (Qiagen, Hilden, Germany). The purified fragment has been inserted into a pET28b(+) expression vector (Novagen, Darmstadt, Germany) cut with the same restriction enzymes. All mutants have been obtained by PCR on plasmid pET28b-Tf-trHb as DNA template. Site-directed mutagenesis has been carried out with the Quick Change mutagenesis kit (Stratagene, La Jolla, CA) according to the manufacturer's instructions, using complementary oligonucleotide pairs introducing the aminoacid substitutions.

A set of single, double, and triple mutants in which the polar distal amino acids [Tyr54 (B10), Tyr67 (CD1), and Trp119(G8)] were replaced with Phe residues

(fig. 2.3). Seven distal mutants of ASV were studied, namely, TrpG8fPhe (hereafter WG8F), TyrCD1fPhe (YCD1F), TyrB10fPhe (YB10F), TyrB10fPhe-TrpG8f Phe (YB10F-WG8F), TyrCD1fPhe-TrpG8fPhe (YCD1F-WG8F), TyrB10fPhe-TyrCD1fPhe (YB10F-YCD1F), and TyrB10fPhe-TyrCD1fPhe-TrpG8fPhe (YB10F-YCD1F-WG8F hereafter 3F-tr-Hb). The mutants have been transformed into *E. coli* XL1 Blue competent cells, selected on kanamycin plates and screened by DNA sequencing. Then, plasmid DNA bearing the gene with the desired mutation has been transformed into *E. coli* BL21 (DE3) supercompetent cells (Agilent Technology, USA) for expression and the colonies with the correct DNA insert have been selected through PCR screening. The WT protein and its mutant have been expressed and purified as follow: transformed *E. coli* cells have been grown in a Luria-Bertani broth until OD=0,6 when the gene expression were induced by adding 1mM isopropyl- β -D-thiogalactopyranoside; after sixteen hours of induction, cells have been centrifuged, pellet resuspended in a minimum volume of lysis buffer (20 mM sodium phosphate buffer) and sonicated with the addition of proteases inhibitors cocktails (Roche) until the supernatant was reddish and clear. After centrifugation at 12000 rpm for 20 minutes the supernatant has been discarded and the pellet resuspended in a buffer containing 6M urea and 20 mM sodium phosphate pH 7 for about 1 hour. After a second centrifugation the supernatant has been loaded on a DEAE-cellulose column (Whatman International Ltd., Maidstone, UK) equilibrated with 20 mM sodium phosphate buffer pH 7.0, washed extensively with the same buffer to eliminate urea and eluted with the same buffer upgraded with 0,2 M NaCl.

The fraction eluted was dialyzed versus 100 mM phosphate pH 7 and titolated with a solution of hemin (Sigma Aldrich) dissolved in 0,2M NaOH; this step has been monitored by UV-VIS spectrophotometer until $A_{400-450\text{ nm}}=2A_{280\text{ nm}}$. Then, the protein were dialyzed versus 20 Mm phosphate pH 7 to eliminate the excess of free heme, and loaded on a second DEAE-cellulose column (Whatman International Ltd., Maidstone, UK) equilibrated with 20 mM sodium phosphate buffer, pH 7.0, washed with the same buffer and eluted in a step gradient of NaCl (0:0,3M). This procedure yielded >600 mg (per liter of culture) of protein with a purity >90% confirmed also in SDS-PAGE with a 17000 Da band. Since their stability, the protein and its mutants were lyophilized.

3.3 Electronic absorption spectroscopy

Electronic absorption spectra, measured with a double-beam spectrophotometer (Varian Cary 5), have been recorded using a 1 cm cuvette and a 600 nm/min scan rate.

Absorption spectra (using a 5-mm NMR tube) have been measured both prior to and after RR measurements, ensuring that no degradation had taken place under the experimental conditions used. The fluoride complexes have been prepared by adding a 0.5 M buffered solution of NaF to the Fe(III) proteins, giving a final concentration of 0.2M. Buffers (0.1M) have been used for experiments at pH 8.5 (TRIS), 7.0 (phosphate), 5.5 (MES).

The samples concentration was in the range of 50-100 μM . The fluoride complexes of the YB10F-WG8F, YCD1F-WG8F, YB10F-YCD1F, YB10F-

YCD1F-WG8F *Tf-trHb* mutants have been obtained after the oxidation of the Fe(II) form (present in a mixture with the Fe(III) form) using excess potassium ferricyanide followed by gel filtration on a Sephadex G-25 column to remove the oxidant.

3.4 Resonance Raman Spectroscopy

RR spectra have been measured with excitation at 406.7 nm (Kr⁺ laser, Coherent, Innova 300C) and 441.6 nm (He-Cd laser, Kimmon IK4121R-G) using a triple spectrometer (consisting of two Acton Research SpectraPro 2300i working in the subtractive mode, and a SpectraPro 2500i in the final stage with a 3600 grooves per millimeter grating), equipped with a liquid-nitrogen cooled CCD detector (Roper Scientific Princeton Instruments). RR spectra have been calibrated with indene, n-pentane, and carbon tetrachloride as standards to an accuracy of 1 cm⁻¹ for intense isolated bands. All RR measurements have been repeated several times under the same conditions to ensure reproducibility. To improve the signal-to-noise ratio, a number of spectra have been accumulated and summed only if no spectral differences were noted. To determine peak bandwidth and positions, a curve-fitting program (Lab Calc; Galactic) was used to simulate the spectra using a mix of (50%) Gaussian and (50%) Lorentzian line shapes.

3.5 Kinetic measurements

Fluoride binding and release have been carried out by stopped flow measurements using an Applied Photophysics apparatus (Leatherhead, UK). Fluoride and azide binding kinetics have been measured by mixing Fe(III) WT or mutated proteins with increasing concentrations of NaF or NaN₃ solutions in 50 mM phosphate buffer at pH 7.0. A range of 4-8 μM protein solutions have been used for experiments and the kinetics have been registered at 404 nm for fluoride and 414 nm for azide. Fluoride release kinetics has been measured according to the ligand displacement methods by mixing fluoride-bound proteins with 0.1 M NaN₃ solutions in 50 mM phosphate buffer at pH 7.0 and monitoring the absorbance decrease at 404 nm. Under these experimental conditions, given the higher affinity and faster binding kinetics of N³⁻ with respect to fluoride, the observed signal decay reflected uniquely the contribution from the fluoride release process. Ligand binding data have been fitted to standard second-order equations, and ligand release to monoexponential decays by using the Matlab program (South Natick, MA).

3.6 Visible-Pump/MidIR-Probe Spectroscopy.

Since many vibrational modes are resolved in prosthetic systems, as heme group, and the stretching frequencies and band widths of these IR bands are very sensitive of the environmental changes, time-resolved-infrared-spectroscopy represents an important technique to study ligand-protein interaction in heme

proteins. In this work, the dissociation of CO ligand has been photo induced by a pump UV-VIS pulse (400 or 550 laser pulse) and the dynamics of the system followed by probing the induced changes of transmission of a sample with femtosecond mid-IR pulses. Measurements have been performed probing both the absorption region of the $\nu(\text{CO})$ stretching vibration of the iron-bound CO (1880–1990 cm^{-1} for *Tf-trHb* and 1825–1975 cm^{-1} for *Bs-trHb*) and the dissociated free CO absorption (2030–2230 cm^{-1}). Protein solution for Vis-pump-Mid-IR-probe measurements were prepared by dissolving the samples in a Tris-HCl buffer 0.2 M in D_2O (pD=8). In case of *Tf-trHb* and its triple mutant *3F-Tf-trHb*, 10-13 mM solutions have been prepared by dissolving the lyophilized protein preparations in the buffer, while *Bs-trHb* solutions with a concentration of 4 mM have been obtained by microcentrifugation with Millipore ultracon filters starting from a liquid preparation. Reduction of proteins was accomplished by adding a freshly prepared anaerobic solution of sodium dithionite in stoichiometric excess to the protein solution, previously degassed with nitrogen. Carbon monoxide (Rivoira), has been gurgled at low flux intensity, and the sealed protein solution saturated with 1 atm CO for 15 minute. In this way CO was homogeneously distributed in spite of the high viscosity of the sample. Samples for transient infrared measurements have been prepared by squeezing about 40 μl of solution between two calcium fluoride windows of 3 mm thickness and separated by a 50 μm teflon spacer for *Tf-trHb* and mutants. In case of *Bs-trHb* a 100 μm spacer has been used. The OD at the excitation wavelength was about 0.8 for all samples. CO dissociation has been induced by pumping the systems either with a 400 nm or a 550 nm laser pulses.

In the case of UV excitation the pulses energy has been ranged from 200 to 500 nJ, in the case of Vis excitation the pulses energy used was 200 nJ. The samples have been moved with a home-built scanner to refresh the solutions and avoid photodegradation. The data have been collected over the two different spectral regions, respectively between 1880 and 1975 cm^{-1} and from 2030 to 2230 cm^{-1} . The signals in every spectral region have been recorded with freshly prepared samples and measured at least three times. To obtain a good signal-to-noise ratio in the case of the free CO signal, which has a small absorption cross section, a number of data sets, corresponding to about 12000 laser shots have been collected and averaged. The integrity of the samples has been checked by FT-IR (Bruker Alpha-T) and visible absorption (Perkin-Elmer LAMBDA 950) spectra collected before and after the time-resolved measurements.

3.7 Anisotropy measurements

In order to determine the equilibrium orientation of carbon monoxide respect to the heme plane, time-resolved polarized mid-IR spectroscopy has been performed. Experiments have been repeated by setting the pump pulse polarization either to 0 or 90 degrees with respect to the probe pulse, and the time dependent anisotropy of the transition was calculated assuming that the heme behaves like a circular absorber (the heme possesses a two-fold degenerate transition dipole in its plane) when excited at 400 nm(64).

RESULTS AND DISCUSSION

4.1 Electronic absorption spectra and Resonance Raman spectra of fluoride complexes of *Tf-trHb* and its distal mutants.

In order to exploit the high sensitivity of fluoride complexes to probe H-bonding in the distal cavity of *Tf-trHb*, a set of mutants of this protein have been obtained through site directed mutagenesis as described previously. Mutations were performed on ASV variant of *Tf-trHb* and consisted in the substitution of TyrB10, TyrCD1 and TrpG8 with Phe in single, double and triple combinations. The investigation of electronic absorption spectra and Resonance Raman spectra of the fluoride complexes of *Tf-trHb* and its mutants has been recorded with both 406.7 and 441.6 nm excitation wavelengths. As shown in fig. 4.1, UV-Vis absorption spectra of fluoride complexes of *Tf-trHb* and its distal mutants display typical features of six-coordinate (6c) HS forms, with fluoride coordinated as the sixth ligand of the iron ion: Soret bands at 406-403 nm and Q bands at 485-491 nm. The RR spectra have been recorded with excitation in resonance with the Soret (406.7 nm, black line) and with the CT2 band (441.6 nm, blue line).

WT and ASV have displayed almost identical spectra with a CT1 maximum at 612 nm, the $\nu(\text{Fe-F})$ stretch at 381 cm^{-1} and have the same propionyl bending mode pick; moreover a second band at 420 cm^{-1} has been highlighted in RR

The spectra of the YCD1F and WG8F mutants have given rise to spectra which are similar to each other but different from those of WT and ASV: CT1 band is blue shifted (609 nm), and a single $\nu(\text{Fe-F})$ band at 421 cm^{-1} has been observed. Similar results have been obtained for YB10F-YCD1F (CT1 at 609 nm and $\nu(\text{Fe-F})$ band at 419 cm^{-1}) and YB10F-WG8F (CT1 at 610 nm and $\nu(\text{Fe-F})$ band at 415 cm^{-1}) mutants. Actually, important differences has been registered for YCD1F-WG8F mutant in which both TyrCD1 and TrpG8 has been replaced by Phe: the blue-shifted of CT1 band to 605 nm and the moving up of $\nu(\text{Fe-F})$ band to 432 cm^{-1} suggest the presence of a weak interaction between the TyrB10 and the bound fluoride. Finally, the YB10F-YCD1F-WG8F triply mutant has been proved to be not fully bound with fluoride being a mixture of two 6cHS forms, an aquo 6cHS heme (CT1 at 632 nm) and a 6cHS fluoride complex. This latter form has showed a CT1 band at 602 nm and a Raman band at 471 cm^{-1} which, being enhanced upon 441.6 nm excitation, is assigned to the $\nu(\text{Fe-F})$ stretch. Moreover, in absence of TrpG8 and TyrCD1, the increasing stretching frequency $\nu(\text{Fe-F})$ and the concomitant blue shifting of the CT1 band demonstrate that the $\nu(\text{Fe-F})$ band at 381 cm^{-1} together with the CT1 at 612 nm correspond to a conformer where the bound fluoride is stabilized by H-bond interactions donated by both TrpG8 and TyrCD1. The role of TyrB10 is quite different because it can't interact with fluoride ligand and curiously it promotes a better stabilization of ligand when replaced with Phe, as highlighted in YB10F, YB10F-WG8F and YB10F-YCD1F. On the other hand, Tyr B10 is able to interact weakly with fluoride in absence of TyrCD1 and TrpG8. All these data has been confirmed by classical molecular dynamics (MD) simulations of Fe(III) *Tf-trHb* with

coordinated fluoride (data not shown). First of all, MD simulations verify that Phe107 and Arg91 mutations, in order to obtain more soluble protein (ASV), do not affect the ligand binding properties. Moreover, in both the WT and ASV proteins, the coordinated fluoride is stabilized by a H-bond with the indole N proton of the TrpG8 and the hydroxylic hydrogen of the TyrCD1. Although MD simulations have revealed only one conformer for fluoride derivative, RR spectra has shown a second $\nu(\text{Fe-F})$ band at 420 cm^{-1} for WT and ASV proteins. It can be assigned to a second conformer, whose bound fluoride is stabilized by a single strong H-bond. Only this form, in fact, is observed in the mutants where either the TrpG8 or TyrCD1 residues have been replaced by Phe. However, within the time scale of the simulation, only one conformation has been sampled by MD simulations in WT, ASV, and YB10F mutant, exhibiting stable H-bonds with both TrpG8 and TyrCD1. The absence of the second conformation detected in the RR experiments is probably due to limitations of the classical MD approach employed.

Finally, an interesting result is provided by the hydrophobic triple mutant YB10F-YCD1F-WG8F: its spectra have displayed the highest energy CT1 band in the *Tf-trHb* mutant series (*i.e.*, at 603 nm) together with the highest $\nu(\text{Fe-F})$ stretch at 471 cm^{-1} . This behavior can be explained considering that in the triple mutant, the heme environment, where fluoride is surrounded by three Phe residues, does not appear to be apolar as would be expected. Actually MD simulations has clearly indicated that two water molecules interacting with the coordinated fluoride ion are accommodated into the active site.

4.2 Fluoride Binding and Release Kinetics in *Tf-trHb*

Fluoride and azide binding kinetics have been measured by mixing Fe(III) WT or mutated proteins with increasing concentrations of NaF or NaN₃ solutions at 404 nm for fluoride and 414 nm for azide. Fluoride release kinetics have been measured according to the ligand displacement methods by mixing fluoride-bound proteins NaN₃ solutions and monitoring the absorbance decrease at 404 nm. Under these experimental conditions, given the higher affinity and faster binding kinetics of N³⁻ with respect to fluoride (80-fold higher), the observed signal decay reflected uniquely the contribution from the fluoride release process. In table 4.1 kinetic constants of fluoride binding (K_{on}) and releasing (K_{off}) in WT protein and distal mutants are reported. Although fluoride binding proceeds at rates between 4-8 mM⁻¹s⁻¹, many differences have been found between the WT or ASV proteins and the single distant mutants: fluoride k_{off} increases from a value of 1,2-1,7 s⁻¹ for not mutated proteins to 242 s⁻¹ for the triple mutant. In particular the rate of ligand dissociation in stopped-flow kinetic measurements progressively increases upon substitution of the H-bonding amino acids. The Fe-F stretching frequencies and the MD simulations are consistent with the dissociation kinetic rate constants, because the fluoride complexes of the mutants with multiple H-bonding interactions have exhibited lower dissociation rate constants. In agreement with the spectroscopic results, the progressive removal of distal H-bonding contributions to the bound fluoride brings about an increase in the observed rate of ligand release.

Protein	$k_{\text{on}}(\text{F}^-)$, $\text{mM}^{-1} \text{s}^{-1}$	$k_{\text{off}}(\text{F}^-)$, s^{-1}
ASV	$6,4 \pm 0,6$	$1,2 \pm 0,08$
WT	$6,5 \pm 0,4$	$1,7 \pm 0,07$
YB10F	$5,5 \pm 0,3$	$29 \pm 0,11$
YCD1F	$4,2 \pm 0,6$	$9 \pm 0,12$
WG8F	$4,5 \pm 0,5$	$30,2 \pm 0,26$
YB10F-YCD1F	$6,0 \pm 0,5$	$49 \pm 0,09$
YB10F-WG8F	$5,4 \pm 0,3$	$106 \pm 0,35$
YCD1F-WG8F	$6,6 \pm 0,4$	$117 \pm 1,25$
YB10F-YCD1F-WG8F	$7,6 \pm 0,4$	$242 \pm 12,75$

Table 4. 1. Fluoride Binding and Dissociation Kinetics for Tf-trHb and Its Distal Side Mutants. All experiments were carried out in 50 mM phosphate buffer at pH 7.0 at 25 °C. Ligand dissociation rates were obtained by fluoride displacement with 0.1 M sodium azide.

In fig. 4.2 is shown the plot of fluoride ion k_{off} versus $\nu(\text{Fe-F})$ for WT and mutants. Analysis of these data indicate that there is a clear correspondence between the Fe-F stretching frequencies and the rates of ligand release. The singly, doubly or triply mutated species appear to gather into separate groups within the “stretching frequency/kinetic rate” correlation plot. Moreover all

mutants lacking of YB10 highlight a consistent increase in the kinetics of ligand release with respect to the YB10-containing mutants indicating that this residue, though not preeminently involved in fluoride ligand hydrogen bonding, is still capable of influencing the ligand release process.

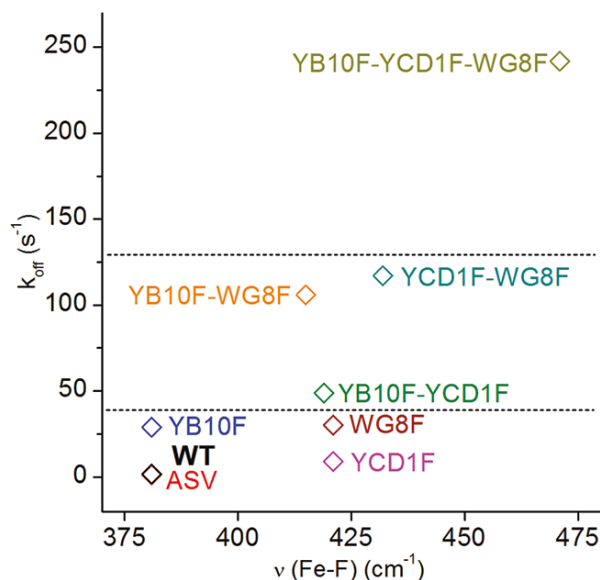


Figure 4. 2. Correlation between the $\nu(\text{Fe-F})$ wavenumbers and the dissociation kinetics constant. The dashed lines separate groupings of triple, double, and single mutants.

Another empirical correlation can be highlighted by plotting $\nu(\text{Fe-F})$ wavenumber and the CT1 energy [fig. 4.3]. In the plot has been included literature data belonging to other hemoglobins to comparison(57)(65)(28)(66). The data are fitted well by a straight line with positive slope. The $(\text{CT1})/\nu(\text{Fe-F})$

position along the correlation line appears to reflect the extent of distal H-bonding interactions. Fluoride complexes which are stabilized by multiple, strong H-bond interactions, like those of the WT, ASV *Tf-trHb*, and YB10F conformer ($\nu(\text{Fe-F})$ at 381 cm^{-1}), are located at the extreme left side. In fact, H-bonding decreases both the $\nu(\text{Fe-F})$ stretching frequency and the energy of the $e_g(d\pi)$ orbitals, thereby lowering the energy of the $a_{2u}(\pi) \rightarrow e_g(d\pi)$ CT1 transition. At the other extreme of the line, fluoride complexes with very weak H-bond interactions are found, like that of the YB10F-YCD1F-WG8F mutant. Unlike the points for the 381 cm^{-1} conformer, those for the second conformer of WT, ASV *Tf-trHb*, and YB10F ($\nu(\text{Fe-F})$ at $420\text{-}421\text{ cm}^{-1}$) fall off the line. In fact, the presence of two conformers should give rise to two CT1 absorption bands. Based on the CT1 energy measured for WG8F, YCD1F, and YCD1F-YB10F mutants which show only the second conformer, the expected energy difference between the two conformers is about 200 cm^{-1} . Because the CT1 band is relatively weak and broad, in practice we observe a single maximum. Therefore, given the impossibility to single out two different CT1 bands for WT, ASV, and YB10F, we correlate the two different Raman Fe-F with the same energy value. As a consequence for the proteins with multiple conformers, some points are off the line.

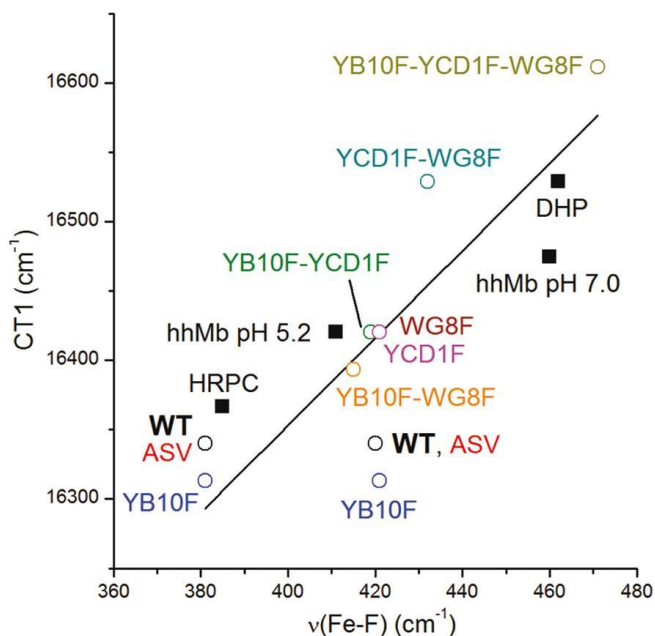


Figure 4. 3. Empirical correlation plot between the $\nu(\text{Fe-F})$ wavenumbers and the CT1 energy. The frequencies of the CT1 are plotted as a function of the frequencies of the Fe-F stretching modes for the following proteins: WT, ASV, YB10F, YCD1F, WG8F, YB10F-WG8F, YB10F-YCD1F, YCD1FWG8F, YB10F-YCD1F-WG8F, HRPC, DHP, hhMb pH 7.0, hhMb pH 5.2.

4.3 Study of CO rebinding in *Tf-trHb*

The UV-Vis spectrum and the FT-IR spectrum of *Tf-trHb-CO* complex are reported in fig. 4.4. In the first, a Soret band at 420 nm and two Q bands at 540 and 570 nm respectively are shown, while in the second, an intense band at 1940 cm^{-1} and a shoulder at 1920 cm^{-1} have confirmed the presence of two conformers

as already demonstrated(57). The lower frequency band, located at 1920 cm^{-1} corresponds to the conformer in which CO is H-bonded to both TrpG8 and TyrCD1, while the 1940 cm^{-1} stretching band correspond to CO singly H-bonded to TrpG8. The high capacity of TrpG8 to stabilize the coordinated CO and the flexibility of TyrCD1, combined to the high polarity of the distal pocket residues, allowing that the bonding network is responsible of an efficient stabilization of the exogenous ligand and also of the dynamics of rebinding process. In order to investigate the CO recombination dynamics in *Tf-trHb-CO* complex with UV-Vis pump mid-IR-probe spectroscopy, ligand dissociation has been induced either with 400 nm UV or 550 nm Visible pump pulses and the CO rebinding has been monitored in both region of the $\nu(\text{CO})$ stretching vibration of the iron-bound CO (1880-1990 cm^{-1}) and the dissociated free CO absorption region (2030-2230 cm^{-1}). In fig.4.5 time resolved spectra recorded at different time delays for CO-derivate of *Tf-trHb* is reported. The spectrum recorded immediately after excitation have displayed the appearance of a bleaching signal in the spectral region where the bound CO stretching vibration is expected, indicating photolysis of the ligand. A main bleaching band and a small shoulder are visible, respectively at 1920 and 1940 cm^{-1} , in good correspondence with the absorption bands measured in the FT-IR spectrum of the CO adduct for this protein.

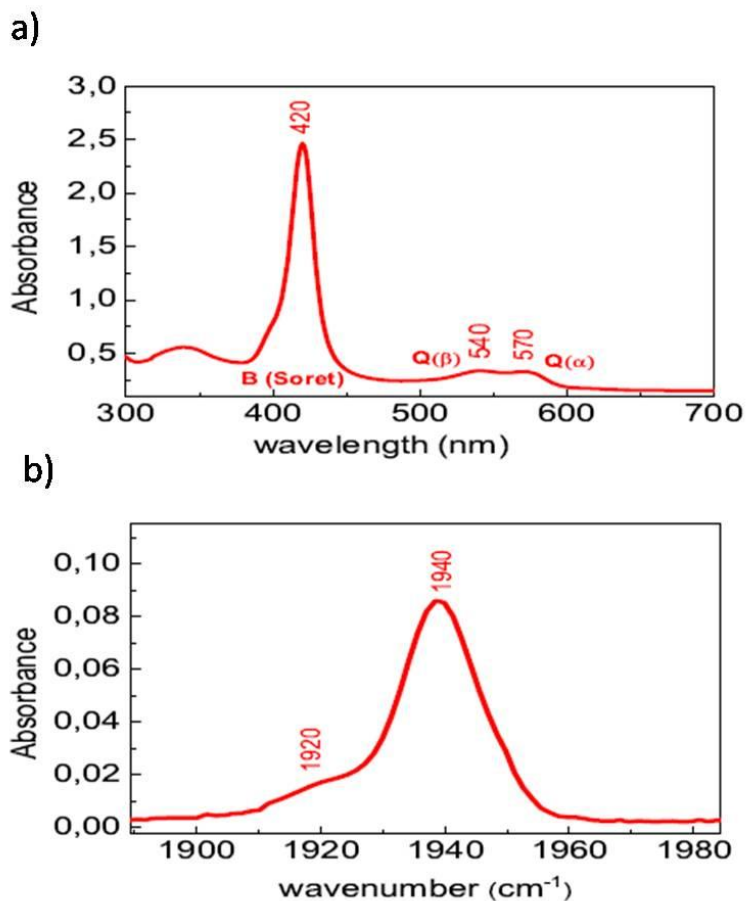


Figure 4. 4: a) UV-Visible spectrum of Tf -trHb-CO complex. b) FT-IR spectrum of Tf -trHb-CO complex. In both cases, protein solution was prepared by dissolving the lyophilized protein in a TRIS-HCl buffer 0.2 M in D₂O (pD=8). The concentration of Tf -trHb was 10 mM, the cell pathlength 50 μm. CO was added after protein reduction with sodium dithionite.

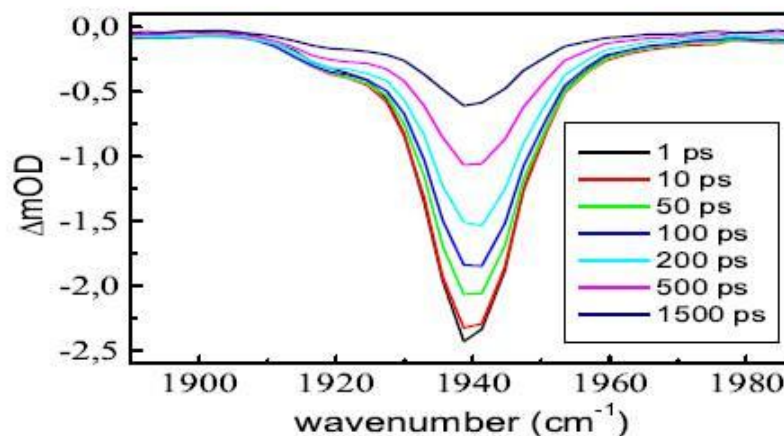


Figure 4. 5: Time resolved spectra recorded at different time delays, showing the bleaching induced by the excitation at 400 nm in the $\nu(\text{CO})$ stretching region for the coordinated CO.

In order to study the kinetic of recombination of CO in the protein, kinetics traces have been recorded at the maxima of bleaching bands; data analyzed and fitted are reported in fig. 4.6. Recovery kinetics measured at 1940 cm⁻¹ band are shown in black scattered points while kinetics measured at 1920 cm⁻¹ in red points. As clear in the figure, the bleaching band at 1940 cm⁻¹ recovers faster than the band at 1920 cm⁻¹. The analysis of kinetic traces revealed a bi-phasic recovery, occurring within sub-nanosecond timescale. An exhaustive analysis of the kinetics has revealed that the kinetic traces can be satisfactorily fitted with two components, whose time constants are 250 ps and 1.5 ns, respectively. The relative weight of the fast component is quite different between the two bands

and in particular the fast one accounts for almost 40% of the recombination dynamics at 1940 cm^{-1} (fig. 4.7).

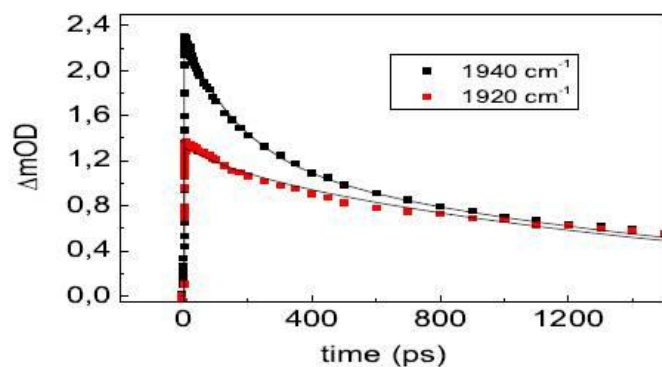


Figure 4. 6: Kinetic traces (scattered points) at selected frequencies together with the fit (solid line) obtained by global analysis. The trace at 1920 cm^{-1} has been scaled to overlap the trace at 1940 cm^{-1} on the long time scale.

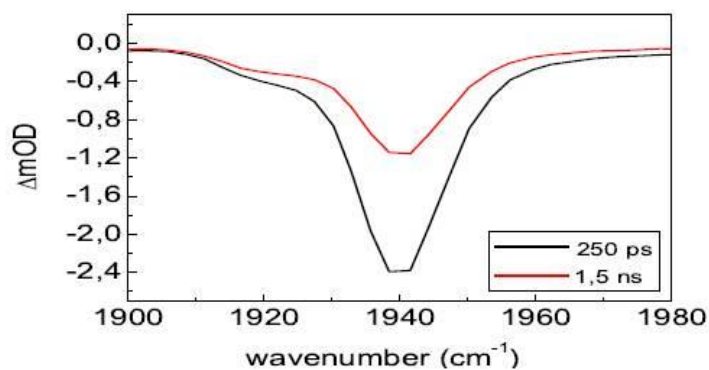


Figure 4. 7: EADS (Evolution Associated Difference Spectra) obtained by globally analyzing all the kinetic traces recorded in the $1850\text{-}1950\text{ cm}^{-1}$ spectral range after excitation at 400 nm .

In order to equate this measurement with geminate recombination, it must be assumed that geminately recombined CO and CO in unphotolysed subunits have the same spectrum as that of equilibrium-ligated CO(67). Actually, through anisotropy measurements, the position of CO at equilibrium has been established: time-resolved polarized mid-IR spectra of *Tf-trHb-CO* complex recorded where the pump pulses polarization was set either to 0 or 90 degrees with respect to the probe pulse, have revealed that the ligand is coordinated to heme with an angle next to the normal to the heme plane, minor than 15 degrees. These results are in agreement with that found for other globins(68)(64). At the same time, CO recombination has been studied also investigating spectroscopic changes around 2100-2150 cm^{-1} where free CO signal should have appeared. The first attempt performed with 400 nm pump pulse has revealed a significant baseline problem, heating, and excess energy dissipation in the system. Furthermore, the fact that free CO is characterized by a low cross section and that its signal is smoothed by high water absorbance, led to the experiment very difficult. To solve these problems, CO photolysis has been triggered by exciting the heme in the Q-band absorption region (550-600 nm) instead of the B-band region. Measurements have been carried out by setting the excitation pulse at 550 nm and probing both the $\nu(\text{CO})$ stretching region for the coordinated CO and the free CO absorption region. The dynamic evolution in the bleaching region resulted substantially identical to what previously observed by exciting the sample at 400 nm. Instead, significant improvements have been obtained in the free CO region. In fig.4.8 time resolved spectra in the free CO region recorded with a 550 nm laser pulse is shown.

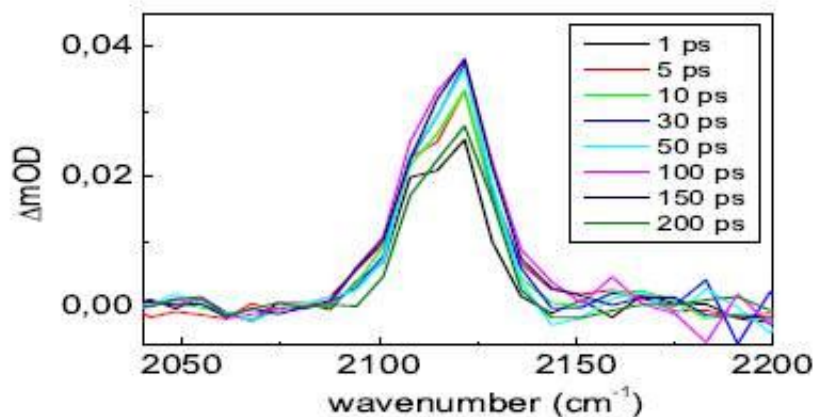


Figure 4. 8: Time resolved spectra in the free CO region recorded at different time delays after excitation of the sample with a 550 nm laser pulse. The baseline, which still contributes in this region although with a minor extent than in the previous measurements with 400 nm excitation, is removed by subtracting a third order polynomial fit with the following procedure: the region between 2080 and 2150 cm^{-1} , where the signal is observed, was removed and a polynomial fit of the remaining signal was performed; then, the polynomial line was subtracted to the entire signal achieving much cleaner spectra.

The measured CO absorption peak is quite asymmetrical and has a rather large bandwidth ($\text{FWHM} \approx 30 \text{ cm}^{-1}$), which suggests the presence of an inhomogeneous distribution of two unresolved bands behind the measured line shape. The signal dynamically evolves by slightly shifting to the blue, but no substantial line shape variations are observed. Although it has been shown that in similar systems a certain percentage (reported values between 3.6 and 13%) of the photolysed CO is initially in a vibrationally hot state(36)(38)(68)(69)(70)(71)

no vibrational hot band could be resolved in the present case. Since the CO anharmonicity has been estimated to be 27-30 cm^{-1} (69)(71) hot bands are probably not resolved due baseline fluctuation problems. Comparing time resolved spectrum of free CO (fig 4.8) with that of bound CO (fig. 4.5) it is easy to observe that the ratio between their absorptions is about 50. This result well fit with previous findings(67). In fig. 4.9 is shown the comparison between kinetics traces measured at the absorption maximum of free CO and that of the 1940 cm^{-1} bleaching band of bound CO, which has been scaled to match the intensity of the free CO signal.

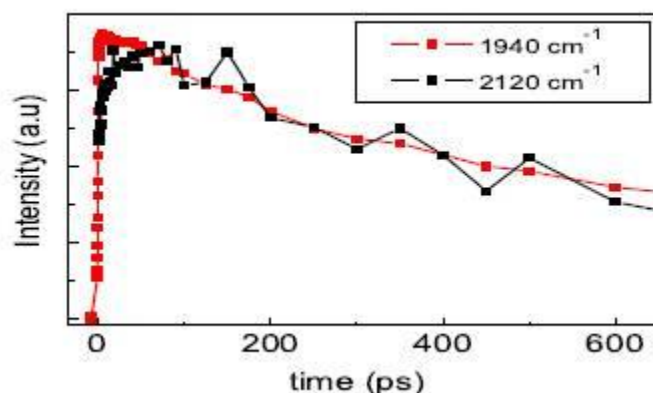


Figure 4. 9: comparison of kinetic traces at 2120 cm^{-1} (black line), corresponding to the maximum absorption in the free CO region in *Tf-trHb* with the trace at 1940 cm^{-1} (red line), corresponding to the maximum absorption of the coordinated CO.

The two traces are in agreement except for the short time scale, where the signal corresponding to the free CO absorption (2120 cm^{-1}) shows an initial rise component. An accurate analysis of kinetic traces has revealed that this rise

component fits well with a time constant of 30 ps. Moreover, a global fit of the kinetic traces collected in the free CO region (2050-2200 cm^{-1}) results in two additional decay components, with time constants of 300 ps and 1.2 ns, respectively. In the case of bleaching band of bound CO the global fit have produced two time constants of 250 ps and 1,5 ns. The good agreement between the two results confirmed that the process of dynamic evolution of the system deduced from these data is the geminate recombination of the photolysed CO. As a consequence, the time constant of 30 ps is not ascribable to a geminate recombination process. The presence of an initial rise component for free CO signal after photolysis was found also in Myoglobin(36) and the authors assigned it to protein relaxation processes around the photolysed CO. Also thermal relaxation processes was registered for *Mb-CO* excited at 597 nm(72). Interestingly, in these two latter cases, time constants for relaxation process are 1,6 ps and 6,2 ps, a very small value if compared to the rise component of 30 ps found in *Tf-trHb*. Probably the relaxation process in *Tf-trHb* may involve a more significant mechanism that can include reorientation or rotation of one or more amino acids side chains in the CO docking site. The slow relaxation could be due to the presence of a water molecule which could rearrange by breaking/forming H-bonds with the tyrosine amino acids (TyrB10 and TyrCD1). Actually, previous MD simulation analysis on *Tf-trHb*(57) have reported an interesting interaction with the solvent: a water molecule enters the protein active site via a gate near E7 helice and remains in intimate contact with TyrB10; this water molecule can live the active site and be replaced by another water molecule so that only one water molecule remains in the active site. Accordingly, the crystal

structure of *Tf-trHb* displays the connection of Tyr B10 and the heme propionyls via H-bonding network involving water molecule: the OH group of TyrB10 is H-bonded to the water molecule (W15) which, in turn, is H-bonded to another water molecule (W64); this latter molecule is H-bonded to heme propionyl which is held into place by a salt-bridge with ArgE10(55).

4.4 Study of CO rebinding in *Bs-trHb*

The same analysis conducted on *Tf-trHb* has been realized on *Bs-trHb*. The UV-Vis spectrum and the FT-IR spectrum of *Bs-trHb-CO* complex are reported in fig. 4.10. The UV-Vis spectrum with a Soret band at 421 nm and two Q bands at 545 nm and 569 nm respectively are similar to the *Tf-trHb* one. Anyway the infrared spectrum reflects the presence of two conformers also in this protein even if the populations are different (two clear bands at 1888 and 1925 cm^{-1} are visible). The 1888 cm^{-1} band corresponds to the conformer in which CO is stabilized by hydrogen bond formed with TyrB10 and TrpG8 while, the high stretching frequency band (1925 cm^{-1}) is relative to the conformer in which only TyrB10 stabilizes the CO(47).

In *Bs-trHb* as in *Tf-trHb*, both the absorption regions of the $\nu(\text{CO})$ stretching vibration of the iron-bound CO (1825-1975 cm^{-1}) and of the dissociated free CO absorption (2030-2230 cm^{-1}) has been monitored. No differences have been found in time resolved spectra for bound CO collected by exciting the sample both with a 400 nm laser pulse and that at 550 nm.

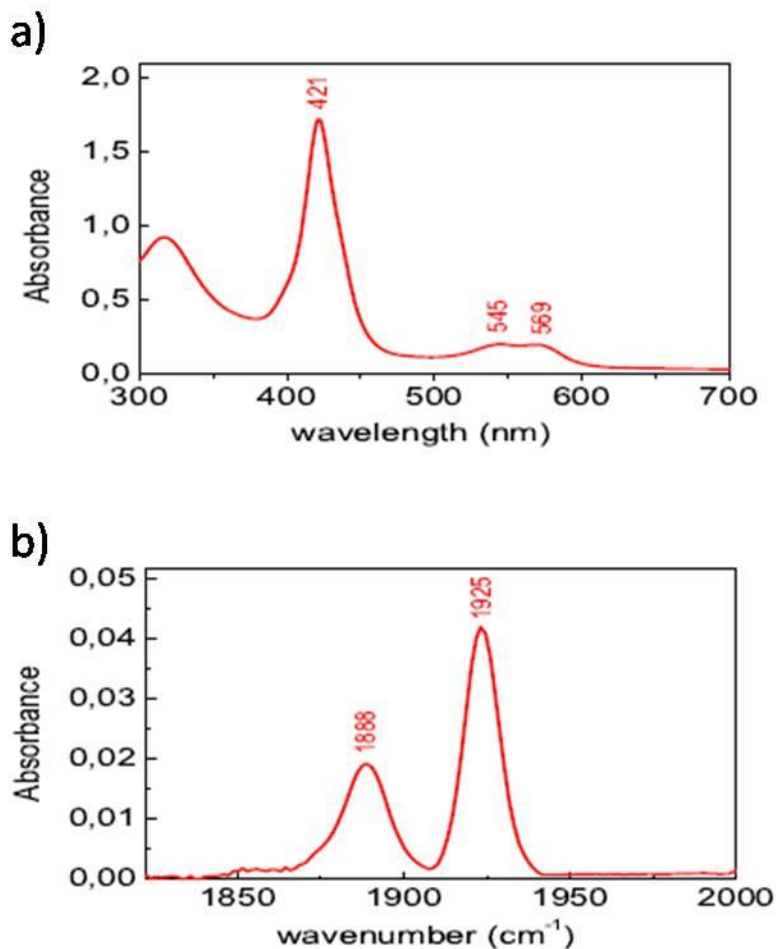


Figure 4. 10: a) UV-Visible spectrum of Bs-trHb-CO complex. b) FT-IR spectrum of Bs-trHb-CO complex. In both cases, Protein solution was prepared by microcentrifugation with Millipore ultracon filters, the final concentration was 4 mM in Tris-HCl buffer 0.2 M in D₂O (pD=8), the cell pathlength 100 μ m. CO was added after protein reduction with sodium dithionite.

The profile of the CO photodissociation reported in fig. 4.11 showed two bleaching bands at 1888 and 1925 cm^{-1} in perfect correlation with the FT-IR spectrum bands.

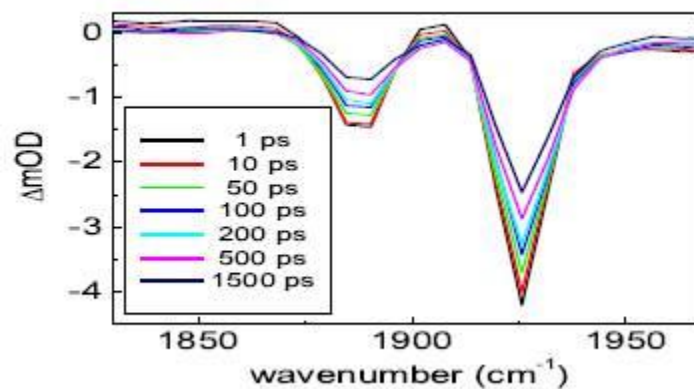


Figure 4. 11: Time resolved spectra recorded at different time delays, recorded at 550 nm, showing the bleaching induced in Bs-trHb-CO complex in the $\nu(\text{CO})$ stretching region for the coordinated CO.

The study of kinetic traces reported in fig. 4.12 shows that the two bleaching bands recover with the same kinetic, in contrast to what observed for *Tf-trHb*. Both curves well fit with two time constant of 120 ps and 2 ns, respectively. In this case the relative weight of the fast component is lower than in *Tf-Hb-CO* for both the bleaching bands: it accounts only for 10% of the recombination dynamics implying that the fraction of picosecond geminate recombination is smaller than that observed in *Tf-trHb*.

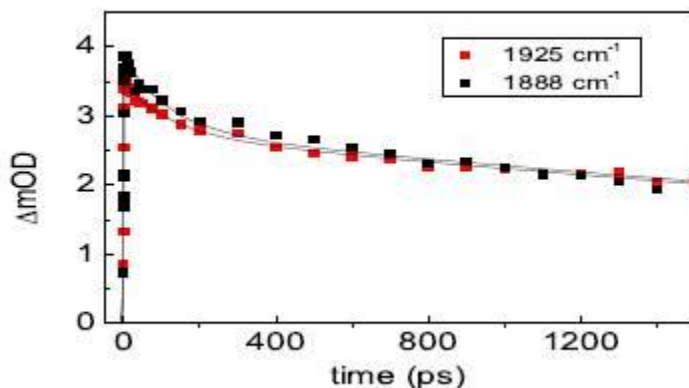


Figure 4. 12: Kinetic traces (scattered points) together with the fit (solid lines) taken at the maxima of the two bleaching bands for Bs-trHb-CO complex. The trace at 1925 cm^{-1} (red dots) overlaps the trace at 1888 cm^{-1} (black dots).

The figure 4.13 shows the time resolved spectra in the free CO region recorded with a 550 nm laser pulse. Time resolved spectra in this region is characterized by an absorption band at 2130 cm^{-1} . The peak shape of the docked CO is not completely symmetrical, the FWHM is about 30 cm^{-1} and a blue shift on a 10 ps time scale, which could be an indication of vibrational cooling, is visible. The large bandwidth could be due to the possible presence of two bands hidden under the observed lineshape, with a population exchange occurring on this timescale. The comparison between kinetic trace recorded at 1925 cm^{-1} for bound CO with that recorded at 2130 cm^{-1} for free CO is shown in fig. 4.13. Differently for what happens in the case of *Tf-trHb*, the two traces well fit.

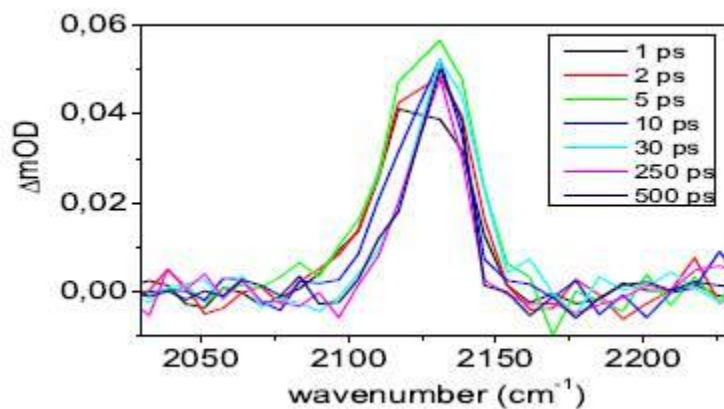


Figure 4. 13: Time resolved spectra in the free CO region recorded at different time delays after excitation of the sample with 550 nm laser pulse.

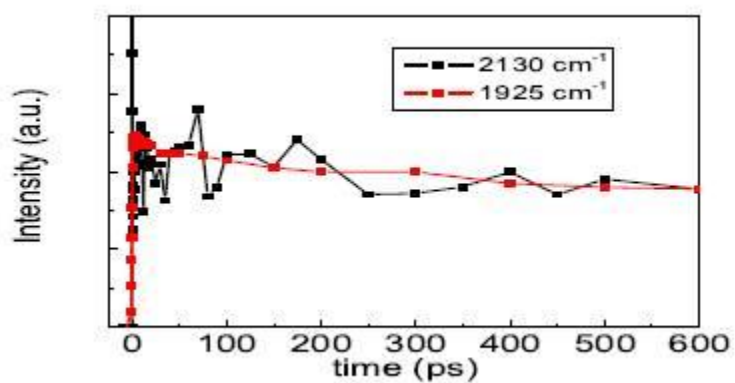


Figure 4. 14: comparison of kinetic traces at 2130 cm^{-1} (black line), corresponding to the maximum absorption in the free CO region in Bs-trHb with the trace at 1925 cm^{-1} (red line), corresponding to the maximum absorption of the coordinated CO.

4.5 Study of CO rebinding in 3F-Tf-trHb

To complete the study about recombination dynamics in order to understand how distal heme pocket structural changes can affect CO recombination dynamics in *Tf-trHb*, time-resolved infrared experiments on the triple mutant protein *3F-Tf-trHb* (YB10F-YCD1F-WG8F) has been performed. As shown in fig. 4.15 the UV-Vis spectrum is quite similar to the *Tf-trHb* while the TF-IR spectrum display an only band centered at 1955 cm^{-1} . As for *Tf-trHb* and *Bs-trHb*, CO dissociation has been triggered by a 550 nm pump pulse and CO rebinding monitored in two mid-IR regions: the region of the $\nu(\text{CO})$ stretching vibration of the iron-bound CO ($1880\text{-}1980\text{ cm}^{-1}$) and the dissociated free CO absorption region ($2030\text{-}2230\text{ cm}^{-1}$). Time resolved spectra of *3F-Tf-trHb* obtained is shown in fig. 4.16. It should be noticed that a single bleaching band centered at 1955 cm^{-1} is observed, in perfect agreement with the maximum absorption band in the TF-IR spectrum. The FWHM average value for the free CO absorption bands in this case is about 15 cm^{-1} , a value about the half of the observed value for the WT protein, attributed to the significant changes in the polarity of molecular environment by the triple Phe mutation.

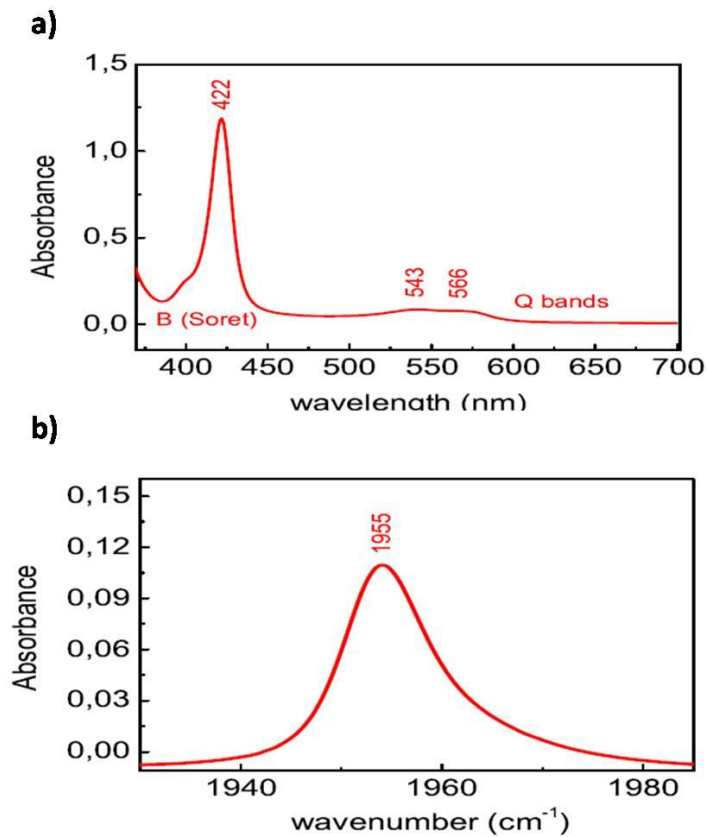


Figure 4. 15. a) UV-Visible spectrum of 3F- Tf -trHb-CO complex. b) FT-IR spectrum of Tf -trHb-CO complex. In both cases, protein solution was prepared by dissolving the lyophilized protein in a TRIS-HCl buffer 0.2 M in D₂O(pD=8). The concentration of 3F-Tf -trHb was 13 mM, the cell pathlength 50 μ m. CO was added after protein reduction with sodium dithionite.

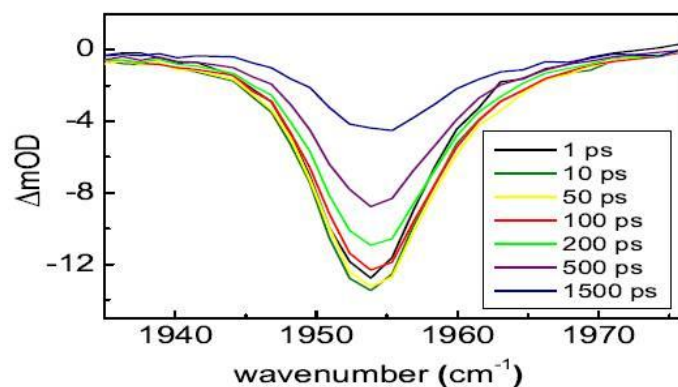


Figure 4. 16. Time resolved spectra recorded at different time delays, recorded at 550 nm, showing the bleaching induced in 3F-Tf-trHb-CO complex in the $\nu(\text{CO})$ stretching region for the coordinated CO.

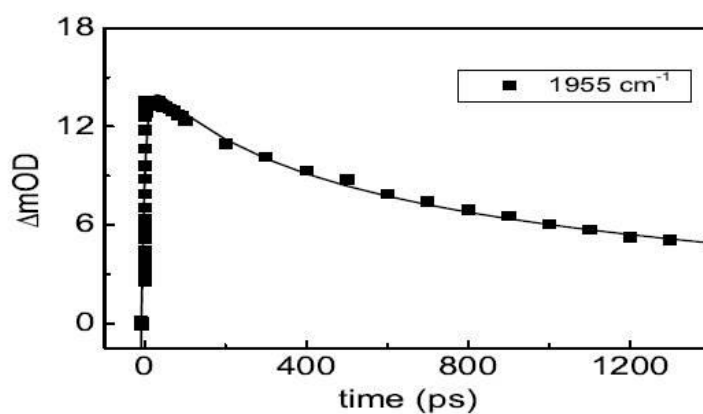


Figure 4. 17. Kinetic trace (scattered points) at 1955 cm^{-1} with the fit (solid line) obtained by global analysis.

The kinetic traces registered at 1955 cm^{-1} are reported in fig.4.17. An accurate observation led to a biphasic recovery occurring within a sub-nanosecond

timescale. The kinetic trace can be satisfactorily fitted with two components, whose time constants are 250 ps and 1.4 ns, respectively. This kinetic behavior is similar to that observed for the WT protein but the fast picosecond component seems to account for a minor fraction of the total recombination process respect to *Tf-trHb*. Fig.4.18 displays time resolved spectra in the free CO region recorded at different time delays after excitation of the sample with a 550 nm laser pulse. The comparison between the kinetic traces recorded for bound CO and dissociated CO, reported in fig. 4.19, are in good agreement confirming that the 250 ps time constant is relative to the fast geminate recombination.

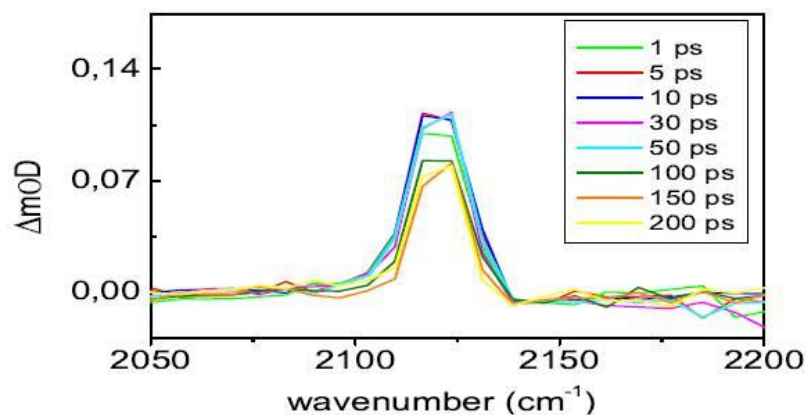


Figure 4. 18. Time resolved spectra in the free CO region recorded at different time delays after excitation of the sample with a 550 nm laser pulse. The spectra have been corrected, as in previous cases, for the presence of a baseline which contributes to the signal.

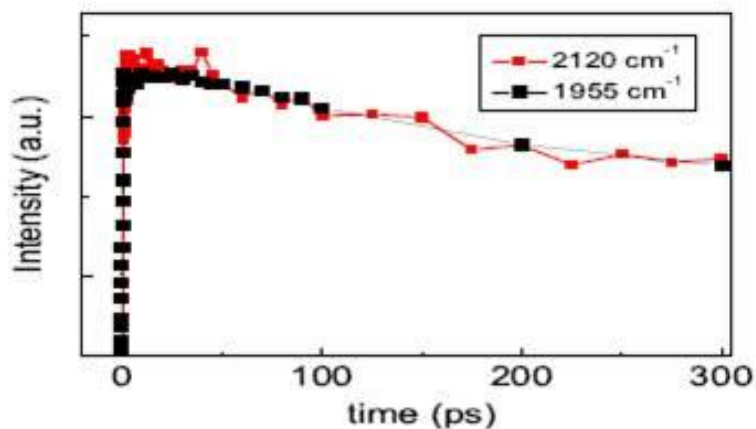


Figure 4. 19. Comparison of kinetic traces at 2120 cm⁻¹ (red line), corresponding to the maximum absorption in the free CO region in 3F-*Tf*-trHb and the kinetic trace at 1955 cm⁻¹ (black line), corresponding to the maximum absorption of the coordinated CO.

4.6 Recombination dynamics comparisons between *Tf-trHb* and *Bs-trHb*

Truncated hemoglobins from *T. fusca* and *B. subtilis* show high structural similarities even though the environments in which they have adapted their self are very different. Actually *Tf-trHb* is capable of efficient O₂ binding and releasing between 55°C and 60°C that is the optimal growth temperature for *Thermobifida fusca*. A comparison between this two proteins is necessary in

order to explain their different ability to adapt to their respectively environments and to identify their not yet defined functions. The results presented in this work show that *Tf-trHb* and *Bs-trHb* are characterized by significant differences in the dynamics of ligand exchange and rebinding. In fig. 4.20 and 4.21 the comparison between the kinetic traces measured for the two bleaching bands of *Tf-trHb* (1940 and 1920 cm^{-1}) with the corresponding bands observed for *Bs-trHb* (1925 and 1988 cm^{-1}) are reported. As highlighted in the figures, although both proteins show fast geminate recombination, they have different relative amount of the picosecond dynamic phase.

Moreover, from the comparison between kinetic traces recorded at the maximum absorption in the free CO region for both proteins, a more intense slow phase and a faster decay in case of *Tf-trHb* with respect to *Bs-trHb* is pointed out (Fig. 4.22).

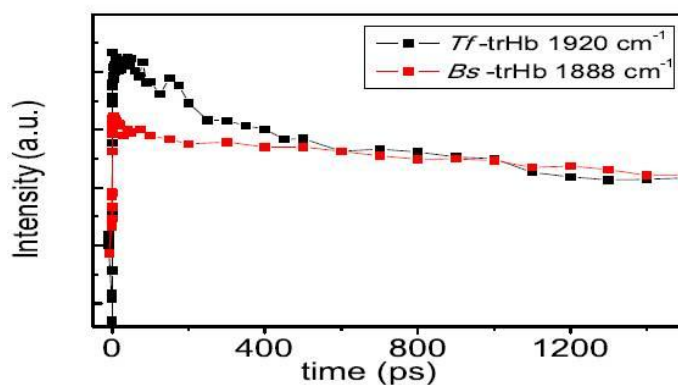


Figure 4. 20. Comparison between the kinetic traces in the bleaching region for *Tf-trHb* and *Bs-trHb* upon excitation at 550 nm. Trace at 1920 cm^{-1} of *Tf-trHb* (black line) is compared to the trace at 1888 cm^{-1} of *Bs-trHb* (red line).

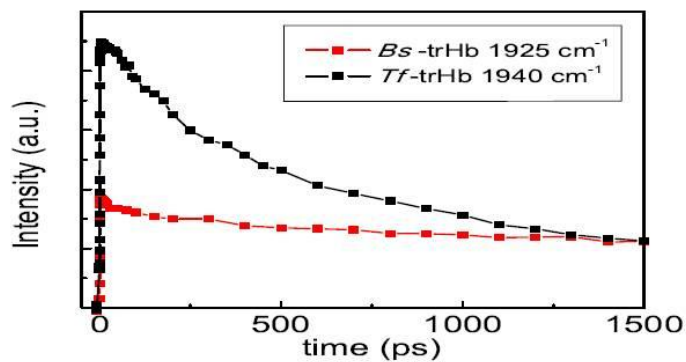


Figure 4. 21. Comparison between the kinetic traces in the bleaching region for Tf trHb and Bs-trHb upon excitation at 550 nm. Trace at 1940 cm⁻¹ of Tf-trHb (black line) is compared to the trace at 1925 cm⁻¹ of Bs-trHb (red line).

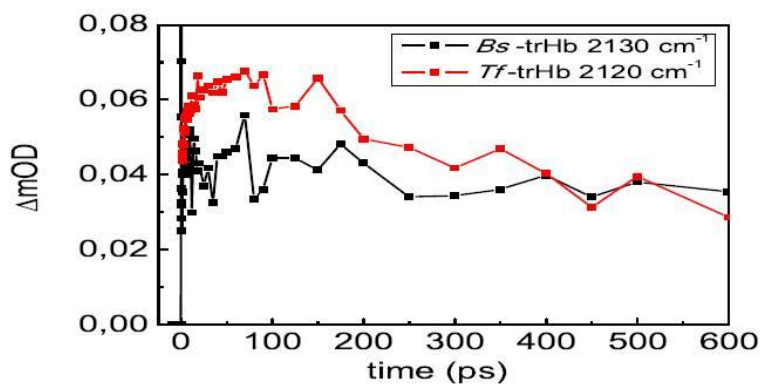


Figure 4. 22. Kinetic trace at 2120 cm⁻¹ recorded at the maximum absorption in the free CO region in Tf-trHb (red line) compared with the corresponding kinetic trace measured in Bs-trHb at 2130 cm⁻¹ (black line).

Thus, both *Tf-trHb* and *Bs-trHb* bind CO in two different conformations: the “open” one characterized by a single hydrogen bond in order to stabilize the ligand and the “closed” one with two hydrogen bond directed towards the CO ligand. The presence of direct hydrogen bonding to the iron ligand is generally considered a key structural requirement for faster recombination after photolysis(68)(73).

CO rebinding investigated in this work, however, showed several unexpected features. In *Bs-trHb* only 10% of photolyzed CO recombines with a 120 ps fast kinetic and the fraction of dynamic phase is the same in both conformations (open and closed), pointing out that it is independent of the number of hydrogen bonds between distal residues and CO. In *Tf-trHb* the recovery is quite different: the fraction of fast recombination is characteristic of open conformation and not in the closed one. These results are in agreement with those obtained for myoglobin in which time resolved infrared spectra measured at low temperature showed the appearance of two bleaching bands (at 1944 and 1926 cm^{-1}), recovering on a different time scale. Even in this case the higher frequency band, corresponding to an ‘open’ configuration, recovers faster than the low frequency one, as observed in *Tf-trHb*(33). Evidently, the reason of these unusual behaviors must be found in the structural flexibility of distal cavity; actually the steric hindrance due to residues around the ligand may prevent CO escape to the solvent and lead to a faster recombination. Accordingly, when the docking site is large enough to accommodate the dissociated ligand, the recombination is slower. The differences in the CO rebinding kinetics registered for two apparently similar proteins such as *Bs-trHb* and *Tf-trHb* highlight the strong

influence played by the structural organization of the distal heme pocket and the interactions among the protein and the heme-ligand complex.

Actually, in *Bs-trHb* GlnE11 is near the ligand and might be able to form an additional, unsuspected, hydrogen bond with CO as TyrB10. Molecular dynamic simulations pointed out that changing between the two conformations GlnE11 opens a cavity in the distal site for CO to escape to the solvent. Moreover the position CD1 in *Bs-trHb* is replaced by Phe residue whose steric hindrance is lesser than in *Tf-trHb* where the position CD1 is occupied by a Tyr residue.

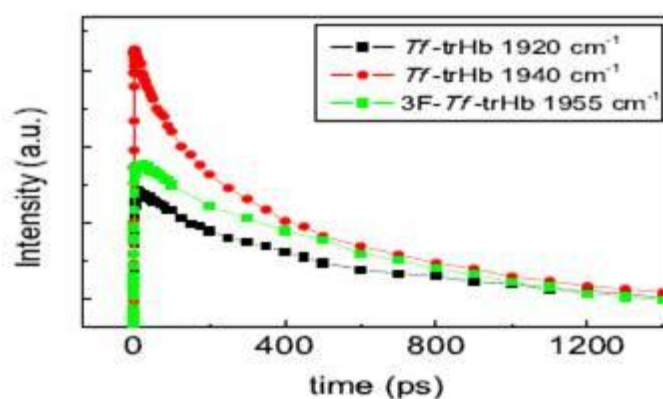


Figure 4. 23. Comparison between the kinetic traces in the bleaching region for *Tf-trHb* and *3F-Tf-trHb* upon excitation at 550 nm. Traces at 1940 cm^{-1} (redline) and 1920 cm^{-1} (black line) of *Tf-trHb* are compared to the trace at 1955 cm^{-1} of *3F-Tf-trHb* (green line). The three kinetic traces have been normalized on the long time scale.

The comparison of *Tf-trHb* and its mutant *3F-Tf-trHb* offers most interesting considerations. On the basis of the H-bonding ligand stabilization network demonstrated for the WT protein, the hydrophobic distal cavity of the triple

mutant protein was expected to affect drastically the dynamics of CO recombination. Accordingly, results indicate that although both proteins (*Tf-trHb* and *3F-Tf-trHb*) show a very fast geminate recombination with similar time courses, the relative amount of the picoseconds recombination phase was very different. A comparison of the kinetic traces measured for the two bleaching bands of *Tf-trHb* (1940 and 1920 cm^{-1}) with the kinetic trace corresponding to bleaching band observed for *3F-Tf-trHb* (1955 cm^{-1}), highlighted many unexpected behaviors for the two proteins [fig.4.23]. First of all, the trace recorded at 1940 cm^{-1} , corresponding to the conformation stabilized by H-bond between CO and the only TrpG8 (thereafter “open conformation”), has shown a faster decay with respect to the band at 1920 cm^{-1} , corresponding to the conformation stabilized by two H-bond between CO and both TrpG8 and TyrCD1 (thereafter “closed conformation”). Probably, in the open conformation the TyrCD1, although not involved in the ligand stabilization, can establish H-bond with the water molecule present in the distal cavity increasing the steric hindrance and constricting the distal cavity volume with a consequent faster recombination. In the closed conformation the geminate recombination is due to the presence of a hydrogen bonding network represented by TyrB10, TyrCD1 and TrpG8 that constitutes a barrier for ligand escaping. The surprising result has been obtained for the triple mutant *3F-Tf-trHb*: the substitution of the three H-bond donors with Phe residues have produced a completely hydrophobic distal cavity without the presence of water, although no ligand stabilization via H-bond could take place in this mutant, a strong recombination dynamic has been registered and the kinetic trace taken at 1955 cm^{-1} display a similar kinetic

behavior with respect to the closed conformation. Similar findings have been reported for *Mycobacterium tuberculosis* trHbO by Vos and coworkers that using femtosecond spectroscopy, analyzed the WT trHbO and two single and one double mutants in which the conserved aminoacids of distal heme pocket TrpG8 (Trp88), TyrCD1 (Tyr36) have been replaced with Phe residues. They found that CO rebinding occurs for 95% predominantly in 1.2 ns in all the analyzed proteins(74).

CONCLUSIONS

The key conclusions of the current research are related to the process of ligand recognition and dynamics not only in the truncated hemoglobins from *Thermobifida fusca* and *Bacillus subtilis* but virtually in all heme proteins. By exploiting the versatility of the model system used in this study, namely the set of distal pocket combinatorial mutants of *Tf-trHb*, it has been possible to evaluate and single out the contributions of short range interactions such as hydrogen bonds, hydrophobicity of the distal pocket and of the overall architecture of the active site to the dynamics of ligands.

H-bonding has always been inferred to play a significant role in determining the heme iron ligand stabilization in the form of single residue-to-ligand H-bonds, water-mediated H-bonds, or even ligand inclusive H-bond networks. In this context, the present work addressed the hydrogen bonding properties of *Tf-trHb* and its combinatorial set of mutants at equilibrium, by probing the ferric fluoride adduct, and under ultrafast photolysis time regime, by probing the dynamics of ferrous CO adduct. Fluoride, as a new probe of hemoglobin active sites, has been studied on a set of mutants where the three amino acids in key topological position of *Tf-trHb* (TrpG8, TyrCD1, TyrB10) are substituted with the non-hydrogen bonding phenylalanine. The RR frequency of the $\nu(\text{Fe-F})$ stretching mode in the low-frequency region provided direct evidence for H-bonding of the fluoride ligand to distal residues via modulation of the Fe-ligand strength. The spectroscopic characterization indicated a clear correlation between $\nu(\text{Fe-F})$

vibrational frequencies and CT1 electronic transition energies. The data obtained have highlighted the presence of two conformers in the fluoride complex of *Tf-trHb*: the first is stabilized by a hydrogen bond between fluoride and TrpG8, and the second in which fluoride is hydrogen bound to both TrpG8 and TyrCD1. These conclusions highlight the usefulness of the Fe-F bond as a sensitive monitor of the distal hydrogen bonding in heme proteins and provide a clear insight into the fine adjustment of the iron ligand bond strength as a function of distal perturbations.

The second conclusion of the present investigation concerns the spectroscopic behavior of a ferrous iron ligand in comparison with the ferric fluoride adduct mentioned before. CO has been shown to be a useful probe of heme-binding sites in Fe(II) proteins, because FeCO back-bonding is modulated by polar interactions with protein residues. The electrostatic field generated by the polar distal pocket amino acids alters the electron distribution in the FeCO unit, changing the order of the C-O bond. Two conformers were observed in the spectra of the CO complexes of both WT and ASV *Tf-trHb*: form 1 with $\nu(\text{FeC})$ and $\nu(\text{CO})$ at 509 and 1938 cm^{-1} and form 2 with $\nu(\text{FeC})$ and $\nu(\text{CO})$ at 518 and 1920 cm^{-1} , respectively. In agreement with the findings obtained for the fluoride adducts, the spectroscopic data and MD simulations demonstrated that CO interacts with TrpG8 in form 1 but with both TrpG8 and TyrCD1 in form 2, while TyrB10 does not directly interact with the bound CO. An empirical linear correlation with negative slope between the frequencies of the $\nu(\text{FeC})$ and $\nu(\text{CO})$ stretching modes has been found for a large class of CO complexes of heme proteins, including bacterial trHb's, and heme model compounds containing

imidazole as the fifth iron ligand. The $\nu(\text{FeC})/\nu(\text{CO})$ position along the correlation line reflects the type and strength of distal polar interactions. Similar conclusions have been reached for fluoride complexes for which a correlation between $\nu(\text{Fe-F})$ wavenumbers and the CT1 transition energy has been demonstrated. The $(\text{CT1})/\nu(\text{Fe-F})$ position along the correlation line appears to reflect the extent of distal H-bonding interactions. Taken together, results on both the ferric fluoride and ferrous CO adducts indicate that the distal pocket residues consistently bridges the iron bound ligand with two hydrogen bonding interactions, the former, and stronger, with TrpG8 indole nitrogen and the latter with TyrCD1. The latter hydrogen bonding interaction is clearly weaker and gives rise to an equilibrium between bonded and non-bonded population under physiological conditions of pH and temperature. MD simulations confirm the overall picture and attribute the weakness of the TyrCD1 hydrogen bonding to the high rotameric freedom of the TyrCD1 residue. The data also highlight the potential of combined resonance Raman (RR) and electronic absorption spectroscopy as a powerful method to investigate relevant properties of the active site of heme proteins.

The third relevant conclusion of the present work concerns the local dynamics of the heme pocket in heme proteins as observed under picoseconds time regime, a time windows in which atoms motion takes place. In particular picoseconds CO recombination dynamics, provides a valuable insight into elementary processes occurring after ultrafast photolysis. For the first time, CO recombination dynamics has been monitored in the mid infrared spectral region, by using *Tf-trHb*, its hydrophobic triple mutant and *Bs-trHb* as model systems.

Measurements in the mid infrared spectral windows are much more specific, with respect to the classical visible pump probe measurements, since they can interrogate the fate of the vibrational bands of the ligand before and after photolysis, thus providing a direct snapshot of the transient state of the photolyzed CO. The comparison of CO recombination dynamics among *Tf-trHb*, its hydrophobic triple mutant (*3F-Tf-trHb*) and *Bs-trHb* brings out a simple, though intriguing, ligand rebinding pathway that is unprecedented among all others hemoproteins investigated to date. First of all, the idea that the polar aminoacid residue, capable to interact with the iron-coordinated CO, are responsible for the high geminate yield in truncated hemoglobins does not hold. In fact, data obtained on the triple mutant, in which the hydrogen bonding network is abolished, indicate that the overall picosecond geminate yield is comparable, if not higher, in the triple mutant than in the WT protein. Moreover the different geminate recombination rates observed for 'open' and 'closed' conformations in *Tf-trHb* but not in *Bs-trHb*, indicate that the percentage of the fast rebinding process is not directly related to the number of H-bonds provided from the relevant aminoacid residues to the ligand. In addition, in all proteins, no metastable CO binding sites have been identified (the transient spectrum of the CO after photolysis is identical to that of free CO in solution).

All together, these observations indicate that the pathway of ligand escape in these proteins is certainly hindered but distal hydrogen bonding interactions do not contribute to the barrier of ligand escape. The behavior of the triple mutant *3F-Tf-trHb* upon ultrafast photolysis is self-explanatory: although it lacks in polar residues capable of forming hydrogen bond to stabilize the ligand and it

does show a consistent picosecond geminate recombination after photolysis. On the basis of these data, and of previous observations on hydrophobic mutants of myoglobins (42), picosecond dynamics in heme proteins must be considered as depending mainly on the polarity of the protein matrix rather than on local hydrogen bonding contributions. Picosecond time scale rearrangements that involve not only selected aminoacid residues next to the ligand may contribute to the creation of metastable docking sites of the ligand or determine preferential pathways on ligand migration but appears to exert limited effects upon ligand recombination.

BIBLIOGRAPHY

1. H.M. Dintzis R.G. Parrish H. Wyckoff D.C. Phillips J.C. Kendrew, G. Bodo. *Nature*, 181, 662, 1958.
2. M. F. Perutz *Annual Review of Biochemistry* 1979, 48, 327-386.
3. H. Wajcman, L. Kiger, M. C. Marden. *Comptes Rendus Biologies* 2009, 332, 273–282.
4. G. Fermi, M.F. Perutz, B. Shaanan. *Journal of Molecular Biologies* 1984, 175, 159-174.
5. E. Antonini, E. Chiancone. *Annual Review of Biophysics and Bioengineering*, 1977, 6, 239-271.
6. T. Brittain. *Comparative biochemistry and physiology*, 1991, 99, 731-740.
7. S. J. Aggarwal, A. Riggs. *The Journal of biological chemistry*, 1969, 244, 2372-2383.
8. R. T. Tam, A. Riggs. *The Journal of biological chemistry*, 1984, 259, 2610-2616.
9. D. Kugelstadt, M. Haberkamp, T. Hankeln, T. Burmester. *Biochemical and biophysical research communications*, 2004, 325, 719-725.

10. R. Changxun Li, S. Z. Guo, S. K. Lee, D. Gozal. *Journal of Cerebral Blood Flow and Metabolism*. 2010, 30, 1874–1882.
11. H. Nishi, R. Inagi, N. Kawada, K. Yoshizato, I. Mimura, T. Fujita, M. Nangaku. *The American journal of pathology*, 2011, 178, 128-139.
12. C.Vazquez-Limona, D. Hoogewijsb, S. N. Vinogradovc, R. Arredondo-Petera. *Plant Science* 2012, 191– 192, 71– 81.
13. T. Ott, J.T. van Dongen, C. Gunther, L. Krusell, G. Desbrosses, H. Vigeolas, V. Bock, T. Czechowski, P. Geigenberger, M.K. Udvarvi, *Current Biology*, 2005, 15, 531–535.
14. P. Bustos-Sanmamed, A. Tovar-Méndez, M. Crespi, S. Sato, S. Tabata, M. Becana. *New Phytologist* 2011, 189, 765–776.
15. D. Bogusz, C. A. Appleby, J. Landsmann, E. S. Dennis, M. J. Trinick, W. J. Peacock. *Nature*, 1988, 331(6152), 178-80.
16. E. R. Taylor, X. Z. Nie, A. W. MacGregor, R. D. Hill. *Plant molecular biology*, 1994, 24, 853-862.
17. R. C. Hardison. *PNAS* 1996, 93, 5675-5679.
18. A. Bonamore, A. Boffi. *IUBMB Life*, 2008, 60, 19–28.
19. S. G. Vasudevan, W. L. Armarego, D. C. Shaw, P. E. Lilley, N. E. Dixon and R. K. Poole. *Molecular and General Genetics*, 1991, 226, 49–58.

- 20.** P. R. Gardner, G. Costantino, A. L. Salzman. *Journal of biological chemistry* 1998, 273,26528-26533.
- 21.** A. Hausladen, A. J. Gow, J. S. Stamler. *PNAS*, 1998, 95, 14100-14105.
- 22.** A. Pesce, M. Couture, S. Dewilde, M. Guertin, K. Yamauchi, P. Ascenzi, L. Moens, M. Bolognesi. *EMBO Journal* 2000, 19, 2424–2434.
- 23.** J. B. Wittenberg, M. Bolognesi, B. A. Wittenberg, M. Guertin. *Journal of Biological Chemistry* 2002, 277, 871–874.
- 24.** M. Couture, H. Chamberland, B. St.-Pierre, J. Lafontaine, M. Guertin. *Molecular and General Genetics*, 1994, 243, 185–197.
- 25.** D. R. Hill, T. J. Belbin, M. V. Thorsteinsson, D. Bassam, S. Brass, A. Ernst, P. Boger, H. Paerl, M. E. Mulligan, M. Potts. *Journal of Bacteriology*, 1996, 178, 6587–6598.
- 26.** S.V. Joseph, G. K. Madhavalatha, R. A. Kumar, S. Mundayoor. *Applied and environmental microbiology*, 2012, 78, 6499-6506.
- 27.** F. P. Nicoletti, A. Comandini, A. Bonamore, L. Boechi, F. M. Boubeta, A. Feis, G. Smulevich, A. Boffi. *Biochemistry*, 2010, 49, 2269-2278.
- 28.** T.G. Spiro, I.H. Wasbotten. *Journal of Inorganic Biochemistry*, 2005, 99, 34–44.
- 29.** S. Abbruzzetti, S. Bruno, S. Faggiano, E. Grandi, A. Mozzarelli, C. Viappiani. *Photochemical and Photobiological Sciences*, 2006, 5, 1109–1120.

- 30.** A. Demidov, X. Ye, P. M. Champion. *Journal of American Chemical Society*, 2002,124, 5914-5924.
- 31.** R.B. Hu, S.G. Boxer, E.S. Park, S.S. Andrews. *Journal of Physical Chemistry B*, 1999,103, 9813.
- 32.** M. K. Hong, D. Braunstein, B. R. Cowen, H. Frauenfelder, P. Ormos. *Biophysical Journal*,1990, 58, 429-426.
- 33.** P. A., Hochstrasser R. M. Moore, J. N., Hansen. *PNAS*, 1988, 85, 5062, 1988.
- 34.** M. H. Vos. *Biochimica et biophysica acta*, 2008, 1777, 15-31.
- 35.** E.R. Henry, W.A. Eaton J. Hofrichter, J.H. Sommer. *PNAS*, 1983, 80, 2235-2239.
- 36.** P.A. Anfinrud, M. Lim, T.A. Jackson. *Nature structural biology*, 1997, 4, 209-214.
- 37.** Nienhaus K, Olson JS, Franzen S, Nienhaus GU. *Journal of American Chemical Society*,2005, 127, 40-41.
- 38.** T. Polack J. P. Ogilvie, S. Franzen, M. H. Vos, M. Joffre, J. L. Martin, A. Alexandrou. *Physical review letters*, 2004, 93, 018102.
- 39.** F. Schotte, M. Lim , T. A. Jackson , A. V. Smirnov , J. Soman , J. S. Olson, G. N. Jr. Phillips , M. Wulff , P. A. Anfinrud . *Science*, 2003, 300, 1944-1947.

- 40.** . Anselmi, D. Roccatano, A. Amadei, B. Vallone, M. Brunori, C.Bossa, A. Di Nola. *Biophysical Journal*, 2004, 86, 3855-3862.
- 41.** A. Di Nola, M. Anselmi, A. Amadei. *Biophysical Journal*, 2008, 94, 4277-4281.
- 42.** R. Regan, R. Elber, J. S. Olson, Q. H.Gibson, T.E. Carver. *Journal of biological chemistry*, 1992, 267,22022-22034.
- 43.** R. Elber, H. Li, J. E. Straub. *Journal of biological chemistry*, 1993, 268, 17908-179016.
- 44.** M. H. Lim, T. A. Jackson, Anfinrud P. A. *Journal of Biological Inorganic Chemistry*, 1997, 2, 531-536.
- 45.** A. Jasaitis, M. H. Vos, G. Silkstone, M. T. Wilson. *Dalton Transactions*, 2005, 21, 3489-3494.
- 46.** . Juszczak, D. Dantsker, U. Samuni, Y. H. B.Ouellet, B. A. Wittenberg, J. M. Friedman, H. Ouellet, M. Guertin. *Biochemistry*, 2003, 42, 5764-5774.
- 47.** A. Feis, B. Catacchio, S. Brogioni, P. Foggi, E. Chiancone, A. Boffi, A. Lapini, G. Smulevich. *Biochemistry*, 47, 902-910, 2008.
- 48.** A. Jasaitis, H. Ouellet, J. C. Lambry, J. L. Martin, J. M. Friedman, M. Guertin, M. H. Vos. *Chemical Physics*, 2012, 396, 10-16.
- 49.** S.A. Asher, M.L. Adams, T.M. Schuste. *Biochemistry*, 1981, 20, 3339–3346.
- 50.** A. Asher, T.M. Schuster. *Biochemistry*, 1979, 18, 5377–5387.

- 51.** S.A. Asher, L.E. Vickery, T.M. Schuster, K. Sauer. *Biochemistry*, 1977, 16, 5849–5856.
- 52.** A. Desbois, M. Lutz, R. Banerjee. *Biochemistry*, 1979, 18, 1510–1518.
- 53.** F. Neri, C. Indiani, K.G. Welinder, G. Smulevich. *European journal of biochemistry*, 1998, 251, 830–838.
- 54.** F. Neri, D. Kok, M. A. Miller, G. Smulevich. *Biochemistry*, 1997, 36, 8947–8953.
- 55.** A. Ilari, L. Giangiacomo, A. Bellelli, V. Morea, A. Bonamore, A. Boffi. *FEBS Journal*, 2005, 272, 4189–4201.
- 56.** M. Milani, A. Pesce, Y. Ouellet, S. Dewilde, J. Friedman, P. Ascenzi, M. Guertin, M. Bolognesi. *Journal of Biological Chemistry*, 2004, 279, 21520–21525.
- 57.** E. Droghetti, F. P. Nicoletti, A. Bonamore, L. Boechi, P. Arroyo Mañez, D. A. Estrin, A. Boffi, G. Smulevich, A. Feis. *Biochemistry*, 2010, 49, 10394–10402, 2010.
- 58.** T. A. Freitas, S. Hou, E. M. Dioum., J. A. Saito, J. Newhouse, G. Gonzalez, M. A. Gilles-Gonzalez, M. Alam. *PNAS*, 2004, 101, 6675–6680.
- 59.** L. Giangiacomo, A. Boffi, V. Morea, E. Chiancone, A. Ilari, *Journal of Biological Chemistry*, 2005, 280, 9192–9202.

- 60.** Y. Ouellet, M. Guertin, J. M. Friedman, S. R. Yeh, U. Samuni. *Journal of American Chemical Society*, 2004, 126, 2682-2683.
- 61.** A. Marcelli, A. Abbruzzetti, J. P. Bustamante, A. Feis, A. Bonamore, A. Boffi, C. Gellini, P. R. Salvi, D. A. Estrin, S. Bruno, C. Viappiani, P. Foggi. *PLoS ONE*, 2012, 7, e39884.
- 62.** T.G. Spiro, in A.B.P. Lever, H.B. Gray (Eds.), *Iron Porphirins, Part II*, Addison-Wesley Reading, MA, 1983, pp. 89–152.
- 63.** N.T. Yu, E.A. Kerr, T.G. Spiro, *Biological Application of Raman Spectroscopy*, Vol. 3, Wiley-Interscience, New York, 1988, pp. 39–95.
- 64.** M. Lim, P. A. Anfinrud, T. A. Jackson. *Journal of American Chemical Society*, 2004, 126 (25), 7946-7957.
- 65.** A. Feis, J. N. Rodriguez-Lopez, R. N. Thorneley, G. Smulevich. *Biochemistry* 1998, 37, 13575–13581.
- 66.** G. Smulevich, A. R. Mantini, M. Paoli, M. Coletta, G. Geraci. *Biochemistry*, 1995, 34, 7507–7516.
- 67.** P. A. Anfinrud, C. Han, R. M. Hochstrasser. *PNAS*, 1989, 86 (21), 8387-8391.
- 68.** P. Nuernberger, K. F. Lee, A. Bonvalet, L. Bouzhir-Sima, J. C. Lambry, U. Liebl, M. Joffre, M. H. Vos. *Journal of American Chemical Society*, 2011, 133 (43), 17110-17113.

- 69.** M. Lim, T. A. Jackson, P. A. Anfinrud. *Journal of Chemical Physics*, 1995,102,4355-4367.
- 70.** D. E. Sagnella, J. E. Straub, T. A. Jackson , M. Lim , P. A. Anfinrud. *PNAS*, 1999, 96, 25, 14324-14329.
- 71.** P. Nuernberger, K.F. Lee, A. Bonvalet, M.H. Vos, M. Joffre. *Journal of Physocal Chemistry B*, 2011, 115, 18, 5554–5563.
- 72.** M. H. Lim, T. A. Jackson, P. A. Anfinrud. *Journal of Physical Chemistry*, 1996, 100, 29, 12043-12051.
- 73.** A. Jasaitis, K. Hola, L. Bouzhir-Sima , J. C. Lambry , V. Balland , M. H. Vos, U. Liebl. *Biochemistry*, 2006, 45 (19), 6018-6026.
- 74.** A. Jasaitis, H. Ouellet, J. C. Lambry, J. L. Martin, J. M. Friedman, M. Guertin, M. H. Vos. *Chemical Physics*, 2012, 396, 10-13.
- 75.** A.V. Soldatova, A.M. Ibrahim, J.S. Olson, R.S. Czernuszewicz, T.G. Spiro. *Journal of American Chemical Society*, 2010, 132, 4614–4625.
- 76.** M. Milani, A. Pesce, M. Nardini, H. Ouellet, Y. Ouellet, S. Dewilde, A. Bocedi, P. Ascenzi, M. Guertin, L. Moens, J.M. Friedman, J.B. Wittenberg, M. Bolognesi. *Journal of Inorganic Biochemistry*, 2005, 99, 97–109.
- 77.** J. Al-Mustafa, J.R. Kincaid. *Biochemistry* 1994, 33, 2191–2197.
- 78.** T. Egawa, S.R. Yeh. *Journal of Inorganic Biochemistry*, 2005, 99, 72–96.

79. S. Faggiano, S. Abbruzzetti, F. Spyarakis, E. Grandi, C. Viappiani, S. Bruno, A. Mozzarelli, P. Cozzini, A. Astegno, P. Dominici, S. Brogioni, A. Feis, G. Smulevich, O. Carrillo, P. Schmidtke, A. Bidon-Chanal, F.J. Luque. *Journal of Physical Chemistry B*, 2009.

80. J. Belyea, C.M. Belyea, S. Lappi, S. Franzen. *Biochemistry*, 2006, 14275–14284.

81. M. Tsubaki, R.B. Srivastava, N.T. Yu. *Biochemistry* 1981, 20, 946–952.

82. F.P. Nicoletti, M.K. Thompson, S. Franzen, G. Smulevich. *Journal of Biological Inorganic Chemistry*, 2011, 16, 611–619.

ACKNOWLEDGEMENTS

The experimental work presented in this thesis was carried on at the Department of Biochemical Sciences A. Rossi-Fanelli of University of Rome “Sapienza” and supported by Istituto Pasteur – Fondazione “Cenci-Bolognetti” and by the following projects: “Progetto Italia-Argentina Ministero degli Affari Esteri” (MAE), “Progetti di ricerca di interesse nazionale 2008” (PRIN 2008) and “Fondo per gli investimenti della ricerca di base 2008” (FIRB 2008).

I am particularly grateful to Professor Alberto Boffi, who gave me the possibility to work in his group, for the continuous supervision of my work and the fundamental support he gave me in many ways.

I wish to express my gratitude and my affection to Dr. Alessandra Bonamore and Dr. Paola Baiocco who introduced me in this group, supporting me during experiments, giving me important suggestions and tricks, actively participating to my professional growth and showing to me great friendship.

Many thanks go also to Dr. Alberto Macone, Dr Maurizio Gargano and Dr. Manuela Fornara who shared with me many funny moments during these years.

Finally, Resonance Raman experiments was carried out at the University of Florence in collaboration with Prof. Giulietta Smulevich while Ultrafast Infrared spectroscopy experiments was realized at European Laboratory for Non-Linear

Spectroscopy (LENS)-University of Florence in collaboration with Prof. Paolo Foggi. I really thank them for these interesting experiments.

More in general, I would like to express all my affection and my gratitude to each of my colleagues in the Department of Biochemical Sciences, who always kindly collaborated and showed to me great friendship.

APPENDIX



Contents lists available at ScienceDirect

Journal of Inorganic Biochemistry

journal homepage: www.elsevier.com/locate/jinorgbio



The optical spectra of fluoride complexes can effectively probe H-bonding interactions in the distal cavity of heme proteins

Enrica Droghetti^{a,1}, Francesco P. Nicoletti^{a,1}, Alessandra Bonamore^b, Natascia Sciamanna^b, Alberto Boffi^b, Alessandro Feis^a, Giulietta Smulevich^{a,*}

^a Dipartimento di Chimica "Ugo Schiff", Università di Firenze, Via della Lastruccia 3–13, I-50019 Sesto Fiorentino (FI), Italy

^b Istituto Pasteur, Fondazione Cenci Bolognietti, Department of Biochemical Sciences and CNR Institute of Molecular Biology and Pathology, University of Rome "La Sapienza", Piazzale Aldo Moro 5, I-00185 Rome, Italy

ARTICLE INFO

Article history:

Received 24 February 2011
Received in revised form 17 June 2011
Accepted 20 July 2011
Available online 28 July 2011

Keywords:

Resonance Raman
Charge transfer bands
Bacterial hemoglobin
Fluoride complexes
H-bonds

ABSTRACT

Fluoride complexes of heme proteins are characterized by unique spectroscopic properties, that provide a simple and direct means to monitor the interactions of the distal heme pocket environment with the iron-bound ligand. In particular, a strong correlation has been demonstrated between the wavelength of the iron-porphyrin charge transfer band at 600–620 nm (CT1) and the strength of H-bonding donation from the distal amino acid side chains to the fluoride ion. In parallel, resonance Raman spectra with excitation within either the CT1 band or the charge transfer band at 450–460 nm (CT2) have revealed that the iron-fluoride stretching frequency is directly affected by H-bonding to the fluoride ion. On this basis, globins and peroxidases display distinct spectroscopic features, which are strongly dependent on the capability of their distal residues (i.e. histidine, arginine and tryptophan) to be involved in H-bonding with the ligand. In particular, in peroxidases strong H-bonding corresponds to a low iron-fluoride stretching frequency and to a red-shifted CT1 band. The reverse is observed in myoglobin. Interestingly, a truncated hemoglobin of microbial origin (*Thermobifida fusca*) investigated in the present work, displays the specific spectroscopic signature of a peroxidase, in agreement with the presence of strong H-bonding residues, i.e., tyrosine and tryptophan, within the distal pocket.

© 2011 Elsevier Inc. All rights reserved.

1. Introduction

The process of ligand recognition in heme proteins is a complex phenomenon, its description requiring a full understanding of the environment experienced by ligands in heme binding pockets. Over the last three decades, notable research efforts have been devoted to the development of experimental spectroscopic methods able to probe the ligand binding site of diverse heme proteins [1]. Descriptive analyses of the physicochemical properties of the active site in heme proteins have been obtained by using iron ligands with different chemical properties. Carbon monoxide is possibly the most widely used Fe(II) ligand. The most remarkable properties of the CO complexes are concerned with the high thermodynamic stability coupled to photolability of the iron carbon bond, a feature that opened the way to both steady-state [2] and time-resolved spectroscopic [3] studies. Carbon monoxide is a useful vibrational probe of heme-binding sites in proteins, because FeCO backbonding is modulated by

polar interactions with protein residues, and by variations in the donor strength of the trans ligand. This modulation is sensitively monitored by the CO and FeC stretching frequencies, which are readily detectable in infrared and resonance Raman spectra [2]. Nitric oxide Fe(II) complexes are emerging as a useful extension of the studies with CO, particularly in view of its important physiological roles in certain heme proteins [4]. Cyanide complexes have also been often employed in the characterization by NMR spectroscopy and X-ray crystallography [5]. Nevertheless, the electronic absorption spectra of low-spin (LS) Fe(III) CN⁻ complexes of heme proteins are not sensitive to the heme pocket environment. Instead, resonance Raman spectra of cyanide complexes have yielded insights into the distal cavity structure [6–8]. Although isoelectronic with Fe(II)CO adducts, Fe(III)(CN⁻) adducts experience much less backbonding, and the FeC stretching frequency are not markedly affected. However, the Fe(III) (CN⁻) unit is easier to bend, and bent conformations are characterized by vibrational behavior quite distinct from that of the essentially linear conformer, giving indications of steric and/or electrostatic distal interactions [9].

Less studied anionic ligands are azide, which gives a mixture of high spin/low spin (HS/LS) complexes [10,11], and sulfide which gives

* Corresponding author. Tel.: +39 055 457 3083; fax: +39 055 457 3077.
E-mail address: giulietta.smulevich@unifi.it (G. Smulevich).

¹ These authors contributed equally to this work.

rise to a 1S complex. This latter anion has been recently suggested as a potential physiological ligand for heme proteins in bacteria [12] and for dehaloperoxidase isolated from the marine worm *Amphitrite ornata* [13].

In this work, we propose to reconsider the opportunities yielded by spectroscopic studies on the fluoride complexes of heme proteins. Fluoride coordinates to Fe(III) hemes with the formation of 6-coordinate (6c) HS complexes. Their electronic absorption spectra display an interesting feature in the 600–620 nm range, where a weak band due to a charge transfer transition (CT1) appears. A clear correlation between the absorption maxima of the CT1 and the H-bonding to the bound anion has been found in a series of mutated heme containing peroxidases, thus indicating that fluoride is a sensitive probe of the distal environment in peroxidases [14]. Besides UV–Vis spectroscopy, resonance Raman (RR) spectroscopy is a very powerful tool for investigating the interaction between exogenous ligands and heme iron. In general, the metal ligand stretching modes can be selectively enhanced by tuning the laser frequency within the Soret or charge transfer transition bands [15,16].

The nature and sensitivity of the metal–ligand bond to heme structure and heme environment make the frequency of the stretching mode an ideal probe able to provide detailed information on the heme–ligand–protein interactions. However, unlike CO, CN⁻, NO and O₂ ligands, whose metal ligand stretch can be easily identified on the basis of its frequency shift observed using isotopic substitution of the exogenous ligands, fluoride isotopes are not practicable due to the high radioactivity and instability of ¹⁸F. As a consequence, the Fe–ligand stretching modes could only be assigned on the basis of ⁵⁶Fe/⁵⁴Fe isotopic shift [17]. However, the very small isotopic shift (about 2 cm⁻¹) and the laborious experimental procedure, which requires preparation of the ⁵⁴Fe heme, make the isotope based assignment impractical.

In order to gain more insight into the ligand recognition processes operating in heme proteins, we investigated the fluoride binding mode to the truncated hemoglobin (trHb) from the actinobacterium *Thermotoga fusca* (TF-trHb), by combining UV–Vis electronic absorption with RR spectroscopy. Tr-Hbs are characterized by a typical structural fold with a two-over-two helical structure, and by a remarkable variability in the nature of the amino acid residues within the heme active site. On the basis of the amino acid sequence, they have been classified into three groups, namely I (HbN), II (HbO) and III (HbP) [18]. In spite of many biochemical and physiological observations, pointing to possible NO [19], sulfide [12] or oxygen reactive species [19] scavenging activities, the functional role of these proteins remains unclear. TF-trHb, the first identified thermostable truncated hemoglobin [20], exemplifies the structural properties of group II trHbs. Its crystal structure revealed that the active site is characterized by the invariant Fe–histidine covalent link on the proximal side, and by a highly polar distal environment in which TrpG8, TyrCD1, and TyrB10 provide three potential H-bond donors in the distal cavity to stabilize the incoming ligands [20]. Very recent work has clearly indicated that TrpG8 and TyrCD1 are the residues mainly involved in the stabilization of exogenous ligands, namely sulfide in the Fe(III) state [12] and CO in the Fe(II) state [21].

The data obtained for the fluoride complex of TF-trHb are compared with those obtained for myoglobin (Mb) and peroxidases. In fact, in vertebrate globins, the key role of the highly conserved distal HisE7 residue in controlling ligand binding has been established through a number of structural, thermodynamic, and kinetic studies on naturally occurring and properly engineered heme proteins [22]. In heme containing peroxidases along with the distal His, an Arg residue is determinant to the anion binding via a strong H-bond between the positively charged guanidinium group and the anion [23].

The very good correlation between the vibrational and electronic features found for various fluoride complexes of heme proteins provides a simple method for testing the polarity of the distal cavity.

The combined analysis of the electronic absorption and RR spectra allows us to rationalize the CT1 wavelengths and the wavenumbers of the $\nu(\text{Fe}-\text{F})$ stretching mode, enhanced by excitation in the charge-transfer band at 450–460 nm (CT2), in terms of the strength and the number of the H-bonds between the anionic ligand and the distal residues of heme proteins. The fluoride anion is strongly stabilized by H-bonds with the distal residues in TF-trHb. The spectra resemble those of heme containing peroxidases suggesting that the polarity of its distal cavity is similar to that of the peroxidases.

2. Materials and methods

Fluoride and phosphate salts, and isotopically enriched water D₂O (99.8%) were obtained from Merck AG (Darmstadt, Germany), and Sephadex G-25 from Pharmacia Biotech (Uppsala, Sweden). Horse heart Mb (hhMb), sperm whale Mb (swMb), and 2-[N-Morpholino]ethanesulfonic acid (MES) were bought from Sigma-Aldrich (Steinheim, Germany) and Horseradish peroxidase isoenzyme C (HRPC) from Biozyme Laboratories (South Wales, UK). All chemicals were of analytical or reagent grade and were used without further purification. TF-trHb was obtained and purified as previously described [21].

Sample preparation hhMb and HRPC samples were prepared by simply solubilising the commercial products (powder) in appropriate buffer. swMb samples were obtained by diluting the commercial buffered protein solution (0.02 M Tris HCl pH 8.0) in the appropriate buffer until the desired pH was obtained. Fe(III) TF-trHb was obtained after the oxidation of the Fe(II) form using excess potassium ferricyanide followed by gel filtration on a Sephadex G-25 column to remove the oxidant. The fluoride complexes were prepared by adding a 0.5 M buffered solution of NaF to the samples, giving a final concentration of 0.46 M. 0.1 M phosphate and MES buffers were used for experiments at pH 7.0 and 5.2, respectively. The sample concentration was in the range of 25–200 μM . Deuterated hhMb and HRPC-fluoride complexes were prepared by simply solubilising the commercial products (powder) in buffered [0.1 M phosphate buffer (pD 7.0) and 0.1 M MES buffer (pD 5.1)]. The deuterated fluoride complex of TF-trHb was prepared by adding 5 μL of proteins, in 0.1 M natural abundance buffers, to 60 μL of 0.5 M fluoride in 0.1 M D₂O phosphate buffer.

2.1. Spectroscopic characterization

Electronic absorption spectra, measured with a double-beam spectrophotometer (Varian Cary 5), were recorded using a 1 cm cuvette, and a 600 nm/min scan rate. Absorption spectra (using a 5-mm NMR tube) were measured both prior to and after RR measurements, ensuring that no degradation had taken place under the experimental conditions. For the differentiation process, the Savitzky–Golay method was applied using 15 data points. No changes in the wavelength or in the bandwidth were observed when the number of points was increased or decreased.

RR spectra were measured with 406.7 nm (Kr⁺ laser, Coherent, Innova 300 C) and 441.6 nm (He–Cd laser, Kimmon IK4121R-G) excitations using a triple spectrometer (consisting of two Acton Research SpectraPro 2300i working in the subtractive mode, and a SpectraPro 2500i in the final stage with a 3600 grooves per millimeter grating), equipped with a liquid-nitrogen cooled CCD detector (Roper Scientific Princeton Instruments). RR spectra were calibrated with indene, n-pentane and carbon tetrachloride as standards to an accuracy of 1 cm⁻¹ for intense isolated bands. All RR measurements were repeated several times under the same conditions to ensure reproducibility. To improve the signal-to-noise ratio, a number of spectra were accumulated and summed only if no spectral differences were noted.

3. Results and discussion

3.1. Electronic absorption spectroscopy

The complexes of heme proteins with fluoride yield spectra typical of a 6cHS complex [24–27] whose $\pi \rightarrow \pi^*$ transitions give rise to the strong Soret band with maxima between 404–406 nm, and the weaker Q band at 490 nm. Charge transfer transitions occur between 607 and 617 nm [CT1 due to $a_{2u}(\pi) \rightarrow e_g(d_{\pi})$ transition] and between 450 and 460 nm [CT2 due to $a'_{2u}(\pi) \rightarrow a_{1g}(d_{\pi}^2)$] [28]. This latter transition gives rise to a very weak band in the electronic absorption spectra, but it is clearly detected in the magnetic circular dichroism (MCD) spectra [29,30].

Fig. 1 compares the electronic absorption and its second derivative spectra of the fluoride complexes of horse myoglobin (hhMb) at pH 7.0 and 5.2, horseradish peroxidase (HRPC), and Tf-trHb at pH 7.0. The spectrum of Fe(III) Tf-trHb is also reported being consistent with a mixture of an aquo 6cHS heme and a hydroxo 6cLS. These data are summarized in Table 1 together with those of swMb, cytochrome c peroxidase (CCP) and its distal variants His52Leu, Trp51Phe and Arg48Leu.

It can be seen that the Soret and Q band maxima are very similar within the various heme proteins and the CT2 band is found between 451 and 454 nm. In contrast, small yet significant differences in the wavelength of the CT1 band are observed. The wavelength of the CT1 band is a sensitive probe of axial ligand polarity and of its interaction with the distal protein residues. It blue-shifts when the p and/or π donor capability of the axial ligands increases or when the ligand acts as a H-bond donor (e.g., H_2O or H_3O^+) since the interaction between the p/ π orbitals of the ligand and the iron d_{π} orbitals raises the energy of the latter. The opposite effect is observed when the ligand acts as an H-bond acceptor [31,32 and references therein]. An extensive study on heme peroxidases from various organisms [33] suggested that the position of the CT1 maximum could be related to structural properties of the protein cavity surrounding the bound fluoride anion. Such correlation is further strengthened by the observed effect of distal mutations on the CT1 position of the fluoride complex of CCP, while

proximal mutations affecting the Fe–N imidazole bond strength do not affect the CT1 maxima [33]. The CT1 maximum is observed at 617 nm as a result of three H-bonds donated to the fluoride by Arg48, Trp51, and a water molecule, consistent with the crystal structure of the CCP–F complex [34]. A blue-shift of the CT1 is observed in the mutant W51F where replacement of the distal Trp by a non-H-bonding Phe residue reduces the number of H-bonds involving the ligand with the protein matrix from three to two. A similar blue-shift is observed in HRPC, consistent with the fact that HRPC lacks the distal Trp residue (not conserved in heme containing peroxidases) and two H-bonds are present: one is with the distal Arg, and the other is likely with a water molecule which is in turn H-bonded with the distal His [33].

In the case of Mb–F complex, the X-ray structure shows that the anion is doubly H-bonded, with a water molecule and the distal His [35]. The observed CT1 band occurs at 607 nm, blue-shifted with respect to HRPC. It was suggested that this difference might be ascribed to the different type of H-bond involving the fluoride anion, i.e., with neutral His in Mb and with the positively charged guanidinium group of Arg in HRPC [33]. This conclusion is reinforced by the observation that for Mb–F at acidic pH, where a protonated histidine interacts with the ligand, the CT1 maximum (609 nm) becomes comparable with that of HRPC (611 nm) and of the Arg48Leu mutant of CCP (610 nm). On the basis of these findings the CT1 maximum at 613 nm observed for Tf-trHb–F is consistent with the presence of multiple H-bonds donated to the fluoride by the distal residues.

3.2. Resonance Raman spectroscopy

In addition to the UV–Vis spectra, the RR frequency of the $\nu(\text{Fe–F})$ stretching mode in the low-frequency region would provide direct evidence for H-bonding of the fluoride ligand to distal residues via information on the Fe–ligand strength. Asher and coworkers demonstrated that the specific enhancement of the $\nu(\text{Fe–F})$ stretching vibrational modes occurs when excitation is within the CT1 band [24,36,37]. Utilizing a tunable dye laser which can excite within the CT1 bands (600–640 nm) they investigated the ligation properties of the complexes of fluoride with swMb and human adult hemoglobin. The $\nu(\text{Fe–F})$ stretching modes appeared in the region between 380 and 470 cm^{-1} . In particular, in the case of the fluoride complex of swMb, at neutral pH, both bands at 422 and 462 cm^{-1} have been assigned as Fe–F stretching bands. The latter band had also been observed upon excitation at 441.6 nm for the fluoride complex of hhMb [17], and assigned to the Fe–F stretching mode on the basis of the 2 cm^{-1} up-shift observed upon $^{56}\text{Fe}/^{54}\text{Fe}$ isotopic substitution. In addition, the band at 462 cm^{-1} has been reported to be pH sensitive, as its intensity decreased upon acidification with the concomitant appearance of a band at 399 cm^{-1} . This result was interpreted as an acid–base equilibrium with $\text{pK}=5.5$, being due to protonation of the distal His and formation of a strong H-bond to the fluoride ligand in swMb [24]. Based on the results obtained by Desbois, we attempted to identify the $\nu(\text{Fe–F})$ stretching mode of the fluoride complexes using excitation in the CT2 band, which is clearly evident in the electronic absorption and in the second derivative spectra of fluoride complexes at about 450 nm (Fig. 1). As previously reported [17] the best intensity enhancement of the $\nu(\text{Fe–F})$ stretching mode has been obtained by excitation with the 441.6 nm line of a HeCd laser.

Fig. 2 compares the RR spectra in the low frequency region of hhMb, HRPC and Tf-trHb at pH 7.0 taken with excitation in resonance with the Soret band (406.7 nm) and the CT2 band (441.6 nm). The RR frequencies of the $\nu(\text{Fe–F})$ stretching modes obtained with two different excitations for the fluoride complexes of Tf-trHb, selected heme containing peroxidases and hh- and sw-Mb are reported in Table 1, where the last column indicates the suggested distal residues H-bonded to the fluoride ligand. Visual inspection of the spectra

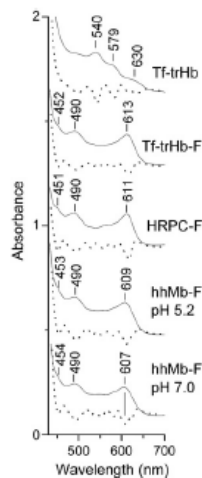


Fig. 1. Electronic absorption (continuous line) and second derivative (dotted line) spectra of Fe(III) Tf-trHb, together with the fluoride complexes of Tf-trHb, HRPC and hhMb at pH 7.0 (0.1 M phosphate), and hhMb at pH 5.2 (0.1 M MES).

Table 1
Soret and CT1 band maxima (nm), and $\nu(\text{Fe-F})$ stretching band wavenumbers (cm^{-1}) of the fluoride complexes of various heme proteins.

Proteins	Soret nm	Q nm	CT1 nm	CT2 nm	$\nu(\text{Fe-F})$ (cm^{-1}) Exc. CT1 Exc. CT2	H-bonds with fluoride
Tf-trHb	405	490	613	452	383	Trp28 TyrCD1, H ₂ O
CCP(MI) ^a	406		617			Trp51 Arg48 H ₂ O
His52Leu CCP(MI) ^a	406		617			Trp51 Arg48 H ₂ O
Trp51Phe CCP(MI) ^a	406		613			Arg48 H ₂ O
Arg48Leu CCP(MI) ^a	406		610			Trp51 (H2O)
HRPC ^b	404	490	611	451	385 ^b	Arg38 H ₂ O
Arg38Leu HRPC ^c		Does not bind fluoride				
swMb, pH 7.0 ^d		490	607		461, 422	His64, H ₂ O ^e
swMb, pH 5.4 ^d		491	609		399, 422	His64 ⁺ , H ₂ O
hhMb, pH 7.0 ^f				453		His64, H ₂ O
hhMb, pH 7.0	406	490	607	454		His64, H ₂ O
hhMb, pH 5.2	406	490	609	453		His64 ⁺ , H ₂ O
swMb, pH 7.0	406	490	607	454		His64, H ₂ O
swMb, pH 5.2	406	490	609			His64 ⁺ , H ₂ O

^a [33].^b [38].^c [39].^d [24].^e [35].^f [17].

clearly indicates that changing the excitation frequency causes changes in the intensity of some bands in the 380–460 cm^{-1} region, where the $\nu(\text{Fe-F})$ stretch is expected. In particular, as previously observed [17], the RR spectrum of hhMb shows the enhancement of the 460 cm^{-1} band in resonance with the CT2 transition (441.6 nm). At pH 5.2, this band decreases in intensity, in agreement with the

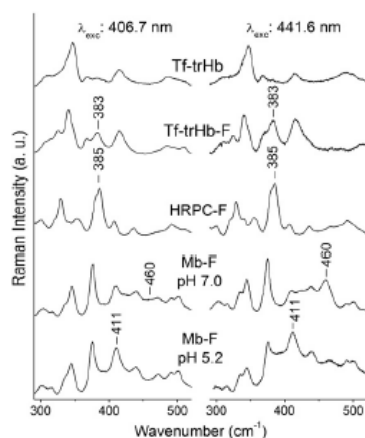


Fig. 2. Resonance Raman spectra in the low-frequency region of Fe(III) Tf-trHb, together with the fluoride complexes of Tf-trHb, HRPC and hhMb at pH 7.0 (0.1 M phosphate), and hhMb at pH 5.2 (0.1 M MES), taken with excitation in resonance with the Soret (406.7 nm) and with the CT2 band (441.6 nm). Experimental conditions, 406.7 nm excitation wavelength; 1 cm^{-1} spectral resolution, 6 mW laser power at the sample, average of ten spectra with 1800 s integration time (Fe(III) Tf-trHb), average of three spectra with 1800 s integration time (Tf-trHb-F), average of six spectra with 600 s integration time (HRPC-F and hhMb-F at pH 7.0), average of six spectra with 650 s integration time (hhMb-F at pH 5.2); 441.6 nm excitation wavelength; 1 cm^{-1} spectral resolution, 10 mW laser power at the sample, average of two spectra with 1800 s integration time (Fe(III) Tf-trHb), average of four spectra with 900 s integration time (Tf-trHb-F), 24 mW laser power at the sample, average of three spectra with 2700 s integration time (HRPC-F), average of six spectra with 600 s integration time (hhMb-F at pH 5.2), average of nine spectra with 600 s integration time (hhMb-F at pH 7.0). A baseline has been subtracted from the spectra of Tf-trHb, Tf-trHb-F, and Mb-F at pH 7.0.

previously reported RR spectra with CT1 excitation [24], whereas a band at 411 cm^{-1} strongly increases.

In order to verify whether the enhancement of the $\nu(\text{Fe-F})$ stretching mode in the RR spectra obtained in resonance within the CT2 band is a general behavior for heme proteins, we recorded the spectra of the fluoride complex of HRPC. A very strong band, assigned to the $\nu(\text{Fe-F})$ stretching mode, was previously found at 385 cm^{-1} upon excitation in the CT1 band at 603 nm [38]. This very low frequency has been interpreted as due to two strong H-bonds between the fluoride anion and both the distal arginine (Arg38) and a water molecule [33,38]. This is consistent with the observation that fluoride does not appreciably bind to Fe in the Arg38Leu variant of HRPC (Table 1 and [39]). The RR spectrum of HRPC-F with both 406.7 nm and 441.6 nm excitation is shown in Fig. 2. The most intense band in the low-wavenumber range is in the region 380–385 cm^{-1} , in agreement with previous results.

The RR spectrum of the Tf-trHb fluoride complex is quite similar to that of HRPC-F, with the enhancement of a band at 383 cm^{-1} , as compared to the protein without ligand. In analogy with HRPC-F, the low frequency of the $\nu(\text{Fe-F})$ stretch indicates the presence of strong H-bonding interactions between fluoride and the distal cavity residues.

Experiments carried out in deuterated buffers clearly showed frequency/intensity changes in the region of the $\nu(\text{Fe-F})$ stretching bands (Fig. 3). Both hhMb-F bands at 460 cm^{-1} and 411 cm^{-1} , which are intense at pH 7 and 5.2 respectively, shifts up by 2 cm^{-1} in D₂O, yielding additional evidence of their $\nu(\text{Fe-F})$ stretching nature. The upshift is caused by a slightly stronger Fe–F bond following the weakening of the H-bond. No other changes are observed in the spectra. In the case of HRPC and Tf-trHb, deuteration affects the intensity and the frequency of the doublets observed at 380–385 cm^{-1} (HRPC) and 369–383 cm^{-1} (Tf-trHb) (see Fig. 3). In spite of the overlap between $\nu(\text{Fe-F})$ stretch and the propionyl bending modes, the observed sensitivity to the H/D exchange within this spectral window supports the presence of a $\nu(\text{Fe-F})$ stretch with a strongly H-bonded F-ligand. In fact, the isotopic sensitivity in the low frequency region is observed only in the ligated proteins, since the RR spectra obtained in H₂O and D₂O buffers of ferric HRPC and Tf-trHb are identical (data not shown).

The effects of deuteration on the frequency of the $\nu(\text{Fe-F})$ stretch are an upshift in the case of hhMb-F and a downshift for HRPC-F. For Tf-trHb a clear shift could not be estimated. This finding can be possibly rationalized, since it has been theoretically predicted that H/D substitutions may give rise to different effects on the H/D-bond

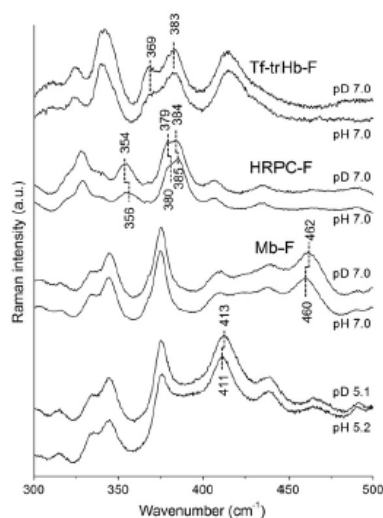


Fig. 3. Resonance Raman spectra in the low-frequency region of fluoride adducts of Tf-trHb, HRPC and hhMb at pH 7.0 and pD 7.0 (0.1 M phosphate), and hhMb at pH 5.2 and pD 5.1 (0.1 M MES) taken with excitation in resonance with the CT2 band (441.6 nm). Experimental conditions, 1 cm^{-1} spectral resolution, 27 mW laser power at the sample, average of five spectra with 1800 s integration time (Tf-trHb-F), average of six spectra with 600 s integration time (HRPC-F), average of seventeen spectra with 300 s integration time (hhMb-F at pH and pD 7.0), average of fifteen spectra with 300 s integration time (hhMb-F at pH 5.2 and pD 5.1). A baseline has been subtracted from the spectra of Tf-trHb-F and Mb-F at pH 7.0.

strength in differently charged model systems [40]. Interestingly, in HRPC-F also the band at 356 cm^{-1} downshifts by 2 cm^{-1} in D_2O . A fairly strong band observed in the RR Soret excitation spectrum of the ferric HRPC (without F) at 350 cm^{-1} has been assigned to the ν_8 (A_{1g}) mode [41]. However, we cannot rule out that this band corresponds to an out of plane mode which is enhanced upon excitation in the CT2 band. Changes in this region have been also observed in the Soret excitation RR spectra of ferric HRP-OH formed at alkaline pH. In this case the doublet at 343 (γ_6) – 350 cm^{-1} (ν_8) changes the relative intensity and shifts to 343 – 352 cm^{-1} , respectively in the deuterated buffer [42].

The presence of strong H-bonding interactions between fluoride and the distal cavity residues in both HRPC and Tf-trHb agrees well with the recent studies on the complexes of sulfide and CO with Fe(II) and Fe(III) Tf-trHb, respectively [12,21]. In particular, for the CO complex, the spectroscopic and computational results carried out on the wild-type protein and selected distal variants demonstrate the existence of two CO conformers. CO interacts with TrpG8 in one form and with both TrpG8 and TyrD1 in the other, while TyrB10 does not directly interact with the bound CO. On the basis of these findings, we propose that the fluoride anion is equally stabilized by two H-bonds donated by TrpG8 and TyrD1. In addition, in analogy with the other heme proteins, a third H-bond with a distal water molecule cannot be ruled out, since in the absence of the ligand the protein is an aquo 6cHS species.

In agreement with previous conclusions for the CO complex, the present results clearly indicate that the polarity of the Tf-trHb distal cavity is very close to that of the heme-containing peroxidases, consistent with recent findings of the genuine peroxidase activity possessed by Tf-trHb [43] and other bacterial truncated hemoglobins,

such as the truncated hemoglobin O from *M. tuberculosis* [44]. Moreover, the possibility that the Trp-Tyr pair may mimic the His-Arg couple is consistent with the previously observed decrease in the peroxidase activity in the Trp-Phe mutants [43].

4. Conclusions

The high sensitivity of the fluoride anion as a probe of the polarity of the distal cavity has been used to demonstrate the “peroxidase character” of a prototypic representative of the “truncated globin” subfamily. In fact, in Tf-trHb, a low $\nu(\text{Fe-F})$ stretching frequency has been shown to correlate with a red-shifted CT1 band in the visible region as a consequence of strong H-bonding to distal pocket residues. The present experimental results, taken together with relevant literature data, provide a clear picture of the correlation between the iron-fluoride bond strength and the polarity of the distal pocket. Re-analysis of hhMb, swMb and HRPC fluoride complexes with excitation in the more readily achievable CT2 band complete the overall picture, thus offering an experimentally easy method to access the physicochemical properties of the simplest model compounds in heme protein chemistry, composed of a monoatomic ligand able to sensitively monitor the important interactions with distal pocket residues.

5. Abbreviations

Tf-trHb	truncated hemoglobin from <i>Thermobifida fusca</i>
CCP	cytochrome c peroxidase
HRPC	horseradish peroxidase isoenzyme C
hhMb	horse heart myoglobin
swMb	sperm whale myoglobin
MCD	magnetic circular dichroism
RR	resonance Raman
6c	6-coordinate
HS	high spin
LS	low spin
CT	charge transfer

Acknowledgment

This work was supported by Institute Pasteur Fondazione Cenci Bolognetti (A. Boffi), MIUR FIRB RBF08F41U_002 (A. Bonamore), and MIUR PRIN 2008BFJ34R (A. Feis and A. Boffi).

References

- [1] R.G. Shulman, *J. Biol. Chem.* 276 (2001) 351–357.
- [2] T.G. Spiro, I.H. Wasbotten, *J. Inorg. Biochem.* 99 (2005) 34–44.
- [3] S. Abbruzzetti, S. Bruno, S. Faggiano, E. Grandi, A. Mozzarelli, C. Viappiani, *Photochem. Photobiol. Sci.* 5 (2006) 1109–1120.
- [4] A.V. Soldatova, A.M. Ibrahim, J.S. Olson, R.S. Czernuszewicz, T.G. Spiro, *J. Am. Chem. Soc.* 132 (2010) 4614–4625.
- [5] M. Milani, A. Pesce, M. Nardini, H. Ouellet, Y. Ouellet, S. Dewilde, A. Bocedi, P. Ascenzi, M. Guertin, L. Moens, J.M. Friedman, J.B. Wittenberg, M. Bolognesi, *J. Inorg. Biochem.* 99 (2005) 97–109.
- [6] J. Al-Mustafa, J.R. Kincaid, *Biochemistry* 33 (1994) 2191–2197.
- [7] T. Egawa, S.R. Yeh, *J. Inorg. Biochem.* 99 (2005) 72–96.
- [8] S. Faggiano, S. Abbruzzetti, F. Spyralis, E. Grandi, C. Viappiani, S. Bruno, A. Mozzarelli, P. Cazzini, A. Astegno, P. Dominici, S. Brogioni, A. Feis, G. Smulevich, O. Carrillo, P. Schmidtke, A. Bidon-Chanal, F.J. Luque, *J. Phys. Chem. B* 113 (2009) 16028–16038.
- [9] T. Deng, I.D. Macdonald, M.C. Simiani, M. Sykora, J.R. Kincaid, S.G. Sligar, *J. Am. Chem. Soc.* 123 (2001) 269–278.
- [10] J. Belyea, C.M. Belyea, S. Lappi, S. Franzen, *Biochemistry* 45 (2006) 14275–14284.
- [11] M. Tsubaki, R.B. Srivastava, N.T. Yu, *Biochemistry* 20 (1981) 946–952.
- [12] F.P. Nicoletti, A. Comandini, A. Bonamore, I. Boechi, F.M. Boubeta, A. Feis, G. Smulevich, A. Boffi, *Biochemistry* 49 (2010) 2269–2278.
- [13] F.P. Nicoletti, M.K. Thompson, S. Franzen, G. Smulevich, *J. Biol. Inorg. Chem.* 16 (2011) 61–619.
- [14] F. Neri, C. Indiani, K.G. Welinder, G. Smulevich, *Eur. J. Biochem.* 251 (1998) 830–838.

- [15] T.G. Spiro, in: A.B.P. Lever, H.B. Gray (Eds.), *Iron Porphyrins, Part II*, Addison-Wesley Reading, MA, 1983, pp. 89–152.
- [16] N.T. Yu, E.A. Kerr, in: T.G. Spiro (Ed.), *Biological Application of Raman Spectroscopy*, Vol. 3, Wiley-Interscience, New York, 1988, pp. 39–95.
- [17] A. Desbois, M. Lutz, R. Banerjee, *Biochemistry* 18 (1979) 1510–1518.
- [18] J.B. Wittenberg, M. Bolognesi, B.A. Wittenberg, M. Guertin, *J. Biol. Chem.* 277 (2002) 871–874.
- [19] G. Wu, L.M. Wainwright, R.K. Poole, *Adv. Microb. Physiol.* 47 (2003) 255–310.
- [20] A. Bonamore, A. Ilari, L. Giangiacomo, A. Bellelli, V. Morea, A. Boffi, *FEBS J.* 272 (2005) 4189–4201.
- [21] E. Droghetti, F.P. Nicoletti, A. Bonamore, L. Boechi, P. Arroyo Manes, D.A. Estrin, A. Boffi, G. Smulevich, A. Feis, *Biochemistry* 49 (2010) 10394–10402.
- [22] B.A. Springer, S.G. Sligar, J.D. Olson, J.C.N. Phillips, *Chem. Rev.* 94 (1994) 699–714.
- [23] G. Smulevich, A. Feis, B.D. Howes, *Acc. Chem. Res.* 38 (2005) 433–440.
- [24] S.A. Asher, M.L. Adams, T.M. Schuster, *Biochemistry* 20 (1981) 3339–3346.
- [25] J. Beetlestone, P. George, *Biochemistry* 3 (1964) 707–714.
- [26] M. Tamura, *Biochim. Biophys. Acta* 243 (1971) 249–258.
- [27] T. Yonetani, D.F. Wilson, B. Seamounts, *J. Biol. Chem.* 241 (1966) 5347–5352.
- [28] M.W. Makinen, A.K. Churg, in: A.B.P. Lever, H.B. Gray (Eds.), *Iron Porphyrins, Part I*, 1983, pp. 143–225.
- [29] L. Vickery, T. Nozawa, K. Sauer, *J. Am. Chem. Soc.* 98 (1976) 343–350.
- [30] A.E. Pond, M. Sono, E.A. Elenkova, D.B. Goodin, A.M. English, J.H. Dawson, *Biospectroscopy* 5 (1999) 542–552.
- [31] G. Smulevich, F. Neri, M.P. Marzocchi, K.G. Welinder, *Biochemistry* 35 (1996) 10576–10585.
- [32] G. Smulevich, M. Paoli, G. De Sanctis, A.R. Mantini, F. Ascoli, M. Coletta, *Biochemistry* 36 (1997) 640–649.
- [33] F. Neri, D. Kok, M.A. Miller, G. Smulevich, *Biochemistry* 36 (1997) 8947–8953.
- [34] S.L. Edwards, T.L. Poulos, *J. Biol. Chem.* 265 (1990) 2588–2595.
- [35] S. Aime, M. Fasano, S. Paoletti, F. Cutruzzola, A. Desideri, M. Bolognesi, M. Rizzi, P. Ascenzi, *Biophys. J.* 70 (1996) 482–488.
- [36] S.A. Asher, T.M. Schuster, *Biochemistry* 18 (1979) 5377–5387.
- [37] S.A. Asher, L.E. Vickery, T.M. Schuster, K. Sauer, *Biochemistry* 16 (1977) 5849–5856.
- [38] N.T. Yu, in: J.F. Riordan, B.L. Vallee (Eds.), *Methods in Enzymology*, Vol. 130, Academic Press, New York, 1986, pp. 350–409.
- [39] B.D. Howes, J.N. Rodriguez-Lopez, A.T. Smith, G. Smulevich, *Biochemistry* 36 (1997) 1532–1543.
- [40] M. Tachikawa, M. Shiga, *J. Am. Chem. Soc.* 127 (2005) 11908–11909.
- [41] Q. Huang, R. Schweitzer-Stenner, *J. Raman Spectr.* 36 (2005) 363–375.
- [42] A. Feis, M.P. Marzocchi, M. Paoli, G. Smulevich, *Biochemistry* 33 (1994) 4577–4583.
- [43] R. Torge, A. Comandini, B. Catacchio, A. Bonamore, B. Botta, A. Boffi, *J. Mol. Catal. B Enzymatic* 61 (2009) 303–308.
- [44] H. Ouellet, K. Rangelova, M. Labarre, J.B. Wittenberg, B.A. Wittenberg, R.S. Magliozzo, M. Guertin, *J. Biol. Chem.* 282 (2007) 7491–7503.

Fluoride as a Probe for H-Bonding Interactions in the Active Site of Heme Proteins: The Case of *Thermobifida fusca* Hemoglobin

Francesco P. Nicoletti,^{†,‡} Enrica Droghetti,^{†,‡} Leonardo Boechi,[‡] Alessandra Bonamore,[§] Natascia Sciamanna,[§] Dario A. Estrin,[†] Alessandro Feis,[†] Alberto Boffi,[§] and Giulietta Smulevich^{*,†}

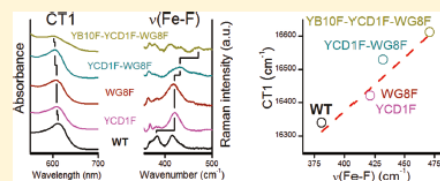
[†]Dipartimento di Chimica "Ugo Schiff", Università di Firenze, Via della Lastruccia 3-13, I-50019 Sesto Fiorentino (FI), Italy

[‡]Departamento de Química Inorgánica, Analítica y Química Física/INQUIMAE-CONICET, Facultad de Ciencias Exactas y Naturales, Universidad de Buenos Aires, Ciudad Universitaria, Pabellón II, Buenos Aires (C1428EHA), Argentina

[§]Institute Pasteur, Fondazione Cenci Bolognietti, Department of Biochemical Sciences and CNR, Institute of Molecular Biology and Pathology, University of Rome "La Sapienza", Piazzale Aldo Moro 5, I-00185 Rome, Italy

Supporting Information

ABSTRACT: The structural and functional properties of the active site of the bacterial hemoglobin from *Thermobifida fusca* are largely determined by three polar amino acids: TrpG8, TyrCD1, and TyrB10. We have exploited the availability of a combinatorial set of mutants, in each of which these three amino acids have been singly, doubly, or triply replaced by a Phe residue, to perform a detailed study on H-bonding interactions between the protein and heme-bound fluoride. By appropriate choice of the excitation conditions, $\nu(\text{Fe}-\text{F})$ stretching bands have been detected in the resonance Raman spectra. In the wild-type protein and one of the mutants, two $\nu(\text{Fe}-\text{F})$ bands have been observed and assigned to the presence of two protein conformers where fluoride is singly or doubly H-bonded. Furthermore, by plotting the CT1 charge-transfer transition energy vs the $\nu(\text{Fe}-\text{F})$ wavenumbers, an empirical correlation has been found. The data are well fitted by a straight line with a positive slope. The position along the correlation line can be considered as a novel, general spectroscopic indicator of the extent of H-bonding in the active site of heme proteins. In agreement with the spectroscopic results, we have observed that the rate of ligand dissociation in stopped-flow kinetic measurements progressively increases upon substitution of the H-bonding amino acids. Molecular dynamics simulations have been performed on the fluoride complexes of native and mutated forms, indicating the prevalent interactions at the active site. All the techniques yield evidence that TrpG8 and TyrCD1 can form strong H bonds with fluoride, whereas TyrB10 plays only a minor role in the stabilization of the ligand.



INTRODUCTION

One of the key objectives of current research in heme proteins is to find well-defined correlations between functional aspects and chemical properties of the active site. There are three main determinants for the reactivity of the active site of heme proteins, namely, oxidation and spin state of the iron ion, "proximal" iron coordination to the protein matrix, and "distal" cavity environment. The latter is essentially defined by the protein amino acids which can stabilize (or destabilize) the iron-bound ligands through a manifold of interactions. H-bonding often appears to play a significant role in determining the degree of ligand stabilization, in the form of single residue-to-ligand H-bonds,^{1,2} water-mediated H-bonds,³ or even ligand inclusive H-bond networks.⁴⁻⁷ Therefore, experimental methods which can selectively and sensitively probe H-bonding interactions are highly valuable.

Optical spectroscopic methods have been employed in research on heme protein chemistry both with physiological and nonphysiological ligands. Advanced technique⁸ and site-directed

mutagenesis⁹ were extensively applied to globins in general, and myoglobin in particular, thus contributing to create the concept of "myoglobin as a molecular laboratory".¹⁰ More recently, however, the discovery of novel natural variations on the globin theme has provided new impetus on heme protein research. In particular, a large family of globins of bacterial origin characterized by a two-over-two helical structure (instead of the typical three-over-three), and by a remarkable variability in the nature of the amino acid residues within the heme active site, have been identified as truncated hemoglobins (trHbs).¹¹ The trHb from the actinomyces *Thermobifida fusca* (Tf-trHb)¹² exemplifies the structural properties of this subfamily of proteins. Its polar distal residues, TrpG8, TyrCD1, and TyrB10, provide three potential H-bond donors to stabilize the incoming ligands. The role of these residues has been recently addressed in a combinatorial set of mutants in which each amino acid has been replaced singly by a

Received: October 3, 2011

Published: November 17, 2011

The residue, and also by preparation of double and triple mutants. This unique collection of mutants, in which the highly polar distal environment is progressively transformed in a fully hydrophobic cavity, has been investigated by functional and spectroscopic studies that clearly indicated that TrpG8 and TyrCD1 are the residues mainly involved in the stabilization of exogenous ligands, namely sulfide in the Fe(III) state¹³ and CO in the Fe(II) state.¹⁴

In the present work, we exploit the high sensitivity of fluoride complexes to probe H-bonding in the distal cavity of Tf-trHb. Our results rest on a very recent rediscovery of the potential of combined resonance Raman (RR) and electronic absorption spectroscopy of fluoride-bound heme proteins.¹⁵ We have now tested this method on the benchmark of the combinatorial set of Tf-trHb mutants. The spectroscopic results for the eight proteins are compared with kinetic and computational results, showing a good agreement. The analysis of the results leads to a novel correlation between the $\nu(\text{Fe}-\text{F})$ vibrational frequency and the CT1 transition energy.

EXPERIMENTAL SECTION

Abbreviations. trHb, truncated hemoglobin; Tf, *Thermotifida fusca*; ASV, acidic surface variant of Tf containing two single site mutations Phe107Glu and Arg91Glu; DHP, dehaloperoxidase; HRP, horseradish peroxidase isoenzyme C; hhMb, horse heart myoglobin; swMb, sperm whale myoglobin; MES, 2-[N-morpholino]ethanesulfonic acid; TRIS, tris(hydroxymethyl)aminomethane; MD, molecular dynamics; RR, resonance Raman; 6c, six-coordinate; HS, high spin; CT, charge transfer; WT, wild type.

Genetic Engineering Procedures. Wild type (WT) Tf-trHb was expressed as a recombinant protein in *Escherichia coli* cells and purified as described previously.¹² As previously reported,¹⁴ the acidic surface variant (ASV) of Tf-trHb differs from the WT protein by mutation of both Phe107 and Arg91 to glutamic acid to increase protein solubility during recombinant expression, without affecting thermostability or ligand binding properties. Therefore, ASV was taken as an engineered scaffold of the WT protein for subsequent site-directed mutagenesis studies on the relevant residues of the distal heme pocket. In particular, our study included the single, double, and triple mutants in which the polar distal amino acids [TyrB10(54), TyrCD1(67), and TrpG8(119)] were replaced with Phe residues. Seven distal mutants of ASV were studied, namely, TrpG8→Phe (hereafter WG8F), TyrCD1→Phe (YCD1F), TyrB10→Phe (YB10F), TyrB10→Phe-TrpG8→Phe (YB10F-WG8F), TyrCD1→Phe-TrpG8→Phe (YCD1F-WG8F), TyrB10→Phe-TyrCD1→Phe (YB10F-YCD1F), and TyrB10→Phe-TyrCD1→Phe-TrpG8→Phe (YB10F-YCD1F-WG8F).

Sample Preparation. All measurements were performed at room temperature. Fluoride and phosphate salts were obtained from Merck AG (Darmstadt, Germany), and Sephadex G-25 from Pharmacia Biotech (Uppsala, Sweden). 2-[N-morpholino]ethanesulfonic acid (MES) and tris(hydroxymethyl)aminomethane (TRIS) were bought from Sigma-Aldrich (Steinheim, Germany). All chemicals were of analytical or reagent grade and were used without further purification. The fluoride complexes were prepared by adding a 0.5 M buffered solution of NaF to the Fe(III) proteins, giving a final concentration of 0.2 M. Buffers (0.1 M) were used for experiments at pH 8.5 (TRIS), 7.0 (phosphate), 5.5 (MES). The sample concentration was in the range of 50–100 μM . The fluoride complexes of the YB10F-WG8F, YCD1F-WG8F, YB10F-YCD1F, YB10F-YCD1F-WG8F Tf-trHb mutants were obtained after the oxidation of the Fe(II) form (present in a mixture with the Fe(III) form) using excess potassium ferricyanide followed by gel filtration on a Sephadex G-25 column to remove the oxidant.

Spectroscopic Characterization. Electronic absorption spectra, measured with a double-beam spectrophotometer (Varian Cary 5), were recorded using a 1 cm cuvette and a 600 nm/min scan rate. Absorption spectra (using a 5-mm NMR tube) were measured both prior to and after RR measurements, ensuring that no degradation had taken place under the experimental conditions used. RR spectra were measured with excitation at 406.7 nm (Kr⁺ laser, Coherent, Innova 300C) and 441.6 nm (He–Cd laser, Kimmon IK4121R-G) using a triple spectrometer (consisting of two Acton Research SpectraPro 2300i working in the subtractive mode, and a SpectraPro 2500i in the final stage with a 3600 grooves per millimeter grating), equipped with a liquid-nitrogen cooled CCD detector (Roper Scientific Princeton Instruments). RR spectra were calibrated with indene, *n*-pentane, and carbon tetrachloride as standards to an accuracy of 1 cm^{-1} for intense isolated bands.

All RR measurements were repeated several times under the same conditions to ensure reproducibility. To improve the signal-to-noise ratio, a number of spectra were accumulated and summed only if no spectral differences were noted. To determine peak bandwidth and positions, a curve-fitting program (Lab Calc; Galactic) was used to simulate the spectra using a mix of (50%) Gaussian and (50%) Lorentzian line shapes. Bandwidths (full width at half-maximum) varied as follows: 9–12 cm^{-1} for the $\delta(\text{C}_\beta\text{C}_\alpha)$ propionyl modes, 11–12 cm^{-1} for the $\delta(\text{C}_\beta\text{C}_\alpha)$ vinyl modes, 13–20 cm^{-1} for the $\nu(\text{Fe}-\text{F})$ stretching mode.

Kinetic Measurements. Ligand binding and release were carried out by stopped flow measurements using an Applied Photophysics apparatus (Leatherhead, UK). Fluoride and azide binding kinetics were measured by mixing Fe(III) WT or mutated proteins with increasing concentrations of NaF or NaN₃ solutions in 50 mM phosphate buffer at pH 7.0. Protein concentrations were in the range 4–8 μM , and observation wavelengths were 404 nm for fluoride and 414 nm for azide. Fluoride release kinetics were measured according to the ligand displacement methods by mixing fluoride-bound proteins with 0.1 M NaN₃ solutions in 50 mM phosphate buffer at pH 7.0 and monitoring the absorbance decrease at 404 nm. Under these experimental conditions, given the higher affinity and faster binding kinetics of N₃⁻ with respect to fluoride, the observed signal decay reflected uniquely the contribution from the fluoride release process. Ligand binding data were fitted to standard second-order equations, and ligand release to mono-exponential decays by using the Matlab program (South Natick, MA).

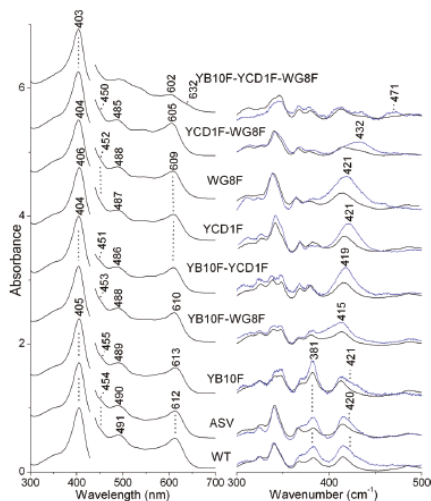
Molecular Dynamics Simulations. The simulations were performed starting from the crystal structure of WT Tf-trHb, solved at 2.48 Å resolution (PDB entry: 2BMM.pdb). The fluoride was added in the distal site, bound to Fe with a bond distance of 1.8 Å. Each simulation was performed using WT and ASV proteins, single mutant (YB10F, WG8F), double mutant (YCD1F-WG8F), and triple mutant proteins (YB10F-YCD1F-WG8F). The system was then immersed in a box of TIP3P water molecules.¹⁶ The minimum distance between protein and wall was 10 Å, and all systems were simulated employing periodic boundary conditions and Ewald sums for treating long-range electrostatic interactions.¹⁷ The shake algorithm was used to keep bonds involving H atoms at their equilibrium length. This allowed us to employ a 2 fs time step for the integration of Newton's equations. The parm99 set of parameters implemented in AMBER was used to describe the protein.¹⁸ The charges and parameters for Fe(III) heme–fluoride were determined by the standard procedure: partial charges were computed using the restricted electrostatic potential (RESP) recipe and DFT electronic structure calculations with the PBE functional and 6-31G** basis sets (Table S1, Supporting Information). The calculation has been performed in the high spin state, which is known to be the ground state. Equilibrium distance and angles, as well as force constants, were computed using the same methods and basis set used for computed charges. The Lennard–Jones parameters of the coordinated fluoride were taken from parm99 parameters. The temperature and pressure were regulated with the Berendsen thermostat and barostat, respectively, as

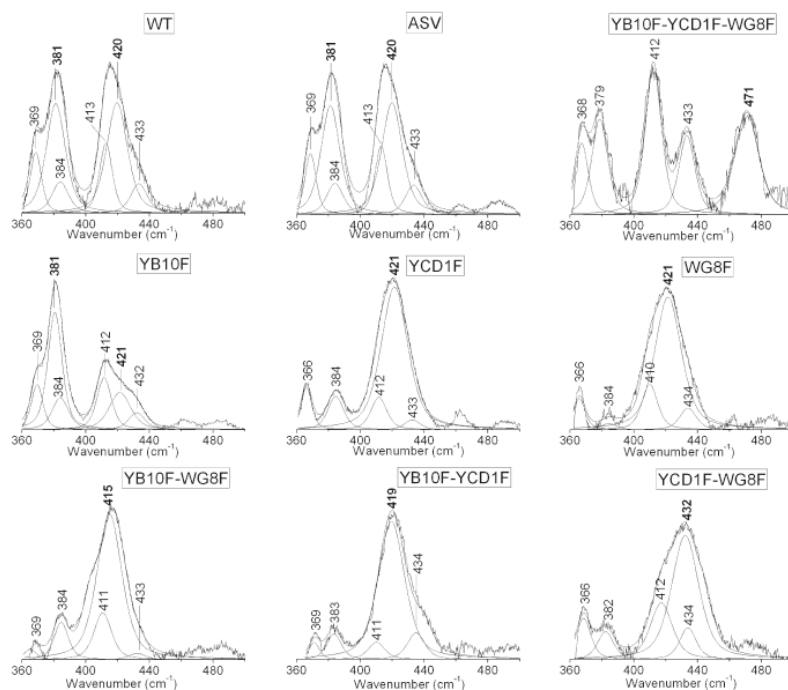
implemented in AMBER. All systems were minimized to optimize any possible structural clashes. Subsequently, the systems were heated slowly from 0 K to 300 K using a time step of 0.1 fs, under constant volume conditions. Finally, a short simulation at constant temperature of 300 K, under constant pressure of 1 bar, was performed using a time step of 0.1 fs, to allow the systems to reach proper density. These equilibrated structures were the starting point for 30 ns of MD simulations. All systems were stable during the time scale of the simulations as shown by the inspection of the root-mean-square displacements (rmsd) depicted in Figure S1, Supporting Information.

RESULTS

Spectroscopy. We first investigated the electronic absorption and RR spectra (recorded with both 406.7 and 441.6 nm excitation wavelengths) of the fluoride complexes of WT and ASV Tf-trHb, and of the combinatorial set of the distal mutants. The UV-visible absorption spectra (Figure 1) displayed Soret bands at 406–403 nm and Q bands at 485–491 nm. These features, and the high-frequency RR spectra obtained with 441.6 nm excitation (data not shown), are characteristic of six-coordinate (6c) HS forms, with fluoride coordinated as the sixth ligand of the iron ion. In the low frequency RR spectra, the $\nu(\text{Fe}-\text{F})$ stretching mode was assigned on the basis of its intensity enhancement upon excitation near the CT2 band, as shown by the comparison of the RR spectra obtained with excitation 406.7 and 441.6 nm (Figure 1, right).¹⁵ The spectra of the various proteins differed in the wavelength of the CT1 band and the wavenumber of the $\nu(\text{Fe}-\text{F})$ stretching mode, indicating a different interaction between the bound fluoride and the distal polar residues. WT and ASV were characterized by almost identical spectra with a CT1 maximum at 612 nm and the $\nu(\text{Fe}-\text{F})$ stretch at 381 cm^{-1} , overlapping a propionyl bending mode. The low energy of the CT1 band, together with the low frequency of the $\nu(\text{Fe}-\text{F})$ stretch, indicates the presence of strong H-bonding interactions between fluoride and the distal cavity residues, consistent with the presence of multiple H-bonds donated to the fluoride by the distal residues.¹⁵ In addition, we assigned a band at 420 cm^{-1} to a second $\nu(\text{Fe}-\text{F})$ stretching mode on the basis of both CT2 excitation enhancement (Figure 1, right) and correlation with the $\nu(\text{Fe}-\text{F})$ frequencies of the set of mutants (see below). This band indicates the presence of a second complex with a weakly H-bonded fluoride. The frequencies of the two $\nu(\text{Fe}-\text{F})$ bands are identical for both WT and ASV, and their relative intensities are very similar, as shown by a band-fitting analysis (Figure 2).

Distal mutations affected the spectral position of both the CT1 and $\nu(\text{Fe}-\text{F})$ stretch to different extents. Among the singly mutated variants, minor changes were observed upon mutation of TyrB10 to Phe: an upshift by 1 nm of the CT1 band and an increase of the $\nu(\text{Fe}-\text{F})$ band at 381 cm^{-1} at the expense of the one at 421 cm^{-1} (Figures 1 and 2). On the other hand, the spectra of the YCD1F and WG8F mutants gave rise to spectra which were similar to each other but different from those of WT and ASV. The CT1 band shifted to 609 nm, and a single $\nu(\text{Fe}-\text{F})$ band at 421 cm^{-1} was observed. In regard to the doubly mutated variants, YB10F-YCD1F, in which both distal Tyr residues are missing, and YB10F-WG8F, in which TyrB10 and TrpG8 are mutated, gave rise to similar results. The YB10F-WG8F variant had a CT1 at 610 nm and the $\nu(\text{Fe}-\text{F})$ band at 415 cm^{-1} , while the YB10F-YCD1F variant had a CT1 at 609 nm and the $\nu(\text{Fe}-\text{F})$ band at 419 cm^{-1} . However, in the





Protein	$\delta(C_{\beta}C_{\alpha}C_{\delta})$		$\delta(C_{\beta}C_{\alpha}C_{\beta})$		$\nu(\text{Fe-F})$	
YB10F-YCD1F-WG8F	368 (9)	379 (12)	412 (11)	433 (12)	471 (18)	
YCD1F-WG8F	366 (9)	382 (12)	412 (11)	434 (12)	432 (20)	
WG8F	366 (9)	384 (12)	410 (11)	434 (12)	421 (20)	
YCD1F	366 (9)	384 (12)	412 (11)	433 (12)	421 (20)	
YB10F-YCD1F	371 (9)	383 (12)	411 (11)	434 (12)	419 (20)	
YB10F-WG8F	369 (9)	384 (12)	411 (11)	433 (12)	415 (18)	
YB10F	369 (9)	384 (12)	412 (11)	432 (12)	421 (16)	381 (13)
ASV	369 (9)	384 (12)	413 (11)	433 (12)	420 (16)	381 (15)
WT	369 (9)	384 (12)	413 (11)	433 (12)	420 (16)	381 (15)

Figure 2. RR spectra in the 360–490 cm^{-1} region with the corresponding band-fitting analysis. Experimental conditions: see Figure 1. The $\nu(\text{Fe-F})$ bands are indicated in bold. The table reports the assignment of the bands with their frequency and bandwidth (in brackets) as obtained by the band-fitting analysis.

Table 1 reports the CT1 band maxima together with the frequencies of the $\nu(\text{Fe-F})$ and the $\nu(\text{C=C})$ stretching modes (see below) for the proteins under investigation. The data for sperm whale myoglobin (swMb), horse heart myoglobin (hhMb), dehaloperoxidase (DHP), and horseradish peroxidase isoenzyme C (HRPC) are also included for comparison.

Fluoride Binding and Release Kinetics. Ligand binding kinetics, measured in stopped flow experiments, revealed slight differences in the second-order binding rates among the different

mutated proteins. As reported in Table 2, fluoride binding proceeded at rates between 4 and 8 $\text{mM}^{-1} \text{s}^{-1}$, whereas azide binding rates were about 80-fold higher. In turn, 200-fold differences were observed in the rates of fluoride release among the different mutants, the WT protein being the slowest (1.2 s^{-1}) and YB10F-YCD1F-WG8F being the fastest (242 s^{-1}). Azide dissociation constants could not be measured directly and were calculated from the ratio between the second-order ligand binding rates and the measured thermodynamic constants

Table 1. CT1 Band Maxima (expressed in nm and cm^{-1}) Together with the Wavenumbers of the $\nu(\text{Fe}-\text{F})$ and the Vinyl Group $\nu(\text{C}=\text{C})$ Stretching Modes for the Proteins under Investigation^a

protein	CT1 (nm)	CT1 (cm^{-1})	$\nu(\text{Fe}-\text{F})^b$ (cm^{-1})	$\nu(\text{C}=\text{C})$ (cm^{-1})
YB10F-YCD1F-WG8F	602	16611	471	1626
DHP ^d	605	16529	462	1620s, 1632w
YCD1F-WG8F	605	16529	432	1626
hhMb (pH 7.0) ^c	607	16475	460	1620
swMb (pH 7.0) ^c	607	16475	462	1620
WG8F	609	16420	421	1627
YCD1F	609	16420	421	1627
YB10F-YCD1F	609	16420	419	1628
hhMb (pH 5.2) ^c	609	16420	411	1620
swMb (pH 5.2) ^c	609	16420	410	1620
YB10F-WG8F	610	16393	415	1626
HRPC ^c	611	16367	385	1621w, 1631s
WT	612	16340	420 (54%); 381 (46%)	1628
ASV	612	16340	420 (53%); 381 (47%)	1628
YB10F	613	16313	421 (32%); 381 (68%)	1627

^aThe data for sperm whale myoglobin (swMb), horse heart myoglobin (hhMb), dehaloperoxidase (DHP), and horseradish peroxidase isoenzyme C (HRPC) are also included for comparison. ^bThe relative percentage of the two $\nu(\text{Fe}-\text{F})$ conformers, as found by the curve-fitting analysis, is reported in brackets. ^cReferences 15 and 32. ^dReference 39.

Table 2. Fluoride Binding and Dissociation Kinetics for Tf-trHb and Its Distal Side Mutants^a

protein	$k_{\text{on}}(\text{F}^-)$, $\text{mM}^{-1} \text{s}^{-1}$	$k_{\text{off}}(\text{F}^-)$, s^{-1}
ASV	6.4 ± 0.6	1.2 ± 0.08
WT	6.5 ± 0.4	1.7 ± 0.07
YB10F	5.5 ± 0.3	29 ± 0.11
YCD1F	4.2 ± 0.6	9 ± 0.12
WG8F	4.5 ± 0.5	30.2 ± 0.26
YB10F-YCD1F	6.0 ± 0.5	49 ± 0.09
YB10F-WG8F	5.4 ± 0.3	106 ± 0.35
YCD1F-WG8F	6.6 ± 0.4	117 ± 1.25
YB10F-YCD1F-WG8F	7.6 ± 0.4	242 ± 12.75

^aAll experiments were carried out in 50 mM phosphate buffer at pH 7.0 at 25 °C. Ligand dissociation rates were obtained by fluoride displacement with 0.1 M sodium azide.

(see Table S2, Supporting Information). Azide release rates were found to follow the same trend as the fluoride release rates, although the overall effect of the mutations was slightly damped with respect to fluoride.

Computer Simulations. To obtain the charge distribution of the active site, we performed DFT electronic structure calculations using the PBE functional and the 6-31G** basis set of a model system composed of fluoride coordinated to an isolated Fe(III) heme with imidazole as the sixth ligand. The calculations were performed on the HS state as identified by the spectroscopic measurements. In agreement with the experimental results, the optimized Fe-F bond distance was found to be ~ 1.8 Å and the coordinated fluoride exhibited a negative charge (partial charge of $-0.36 e^-$), highlighting that positive residues should stabilize the coordinated fluoride, similar to the results found for the heme-bound O_2 .^{19–22}

Classical molecular dynamics (MD) simulations of Fe(III) Tf-trHb with coordinated fluoride were then performed to shed light on the nature of the H-bond network stabilizing the

coordinated fluoride, as suggested by the spectroscopy data. No significant structural differences were found in the active site environment during the time scale of the simulation between WT and ASV (Figure 3A and S2), confirming that Phe107 and Arg91 mutations do not affect the ligand binding properties. Moreover, in both the WT and ASV proteins, the coordinated fluoride is stabilized by a H-bond with the indole N proton of the WG8 and the hydroxylic hydrogen of the YCD1, while the TyrB10 residue is not involved (Figure 3A). The same result was found for the YB10F mutant (Figure 3B), indicating that the YB10 residue has a minor role in the stabilization of the coordinated fluoride. Accordingly, when TrpG8 is replaced by Phe, the YCD1 residue mainly stabilizes the coordinated fluoride, while the YB10 is not able to form a strong H-bond with the ligand (Figure 3C). However, the hydroxylic hydrogen of the YB10 residue is able to interact with the coordinated fluoride when both WG8 and YCD1 are absent, as revealed for the YCD1F-WG8F double mutant (Figure 3D).

The triple mutant YB10F-YCD1F-WG8F was able to accommodate two water molecules in the active site (Figure 4, upper panel). To characterize the internal water interactions, we evaluated the radial distribution function $g(r)$ for the O atom of water molecules, centered in the coordinated fluoride for the last 25 ns of the simulation. The integration of the $g(r)$ function confirmed the presence of two water molecules around the F^- anion (Figure 4, lower panel). The profiles show a clear peak at 2.75 Å, indicating the presence of water molecules interacting strongly with the coordinated fluoride.

DISCUSSION

Distal Cavity Interactions. Fluoride is a common ligand for heme proteins in the Fe(III) state. It is not known as a physiological ligand, and only recently has it been reported that it can modulate the reactivity of a heme protein.²³ Nevertheless, fluoride complexes of heme proteins as model systems have been actively researched with optical and magnetic methods during

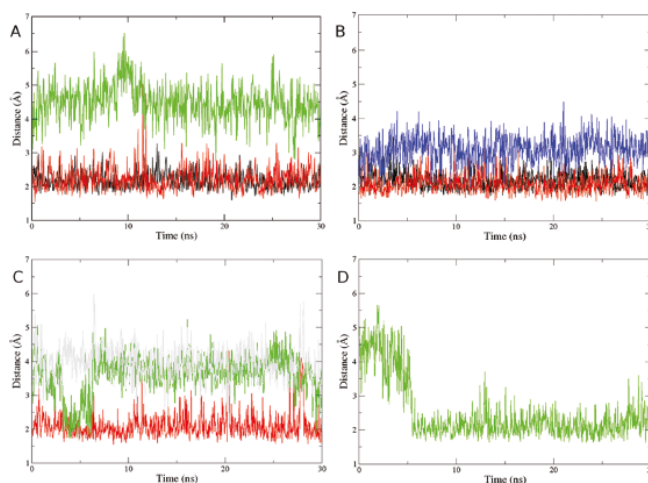


Figure 3. Time evolution of selected distances of Tf-trHb. (A) WT protein; (B) YB10F mutant; (C) WG8F mutant; (D) YCD1F-WG8F mutant. (Black) Distances between fluoride and indole N proton of the WG8; (red) distances between fluoride and hydroxylic hydrogen of the YCD1; (green) distances between fluoride and hydroxylic hydrogen of the YB10; (blue) distances between indole N proton of the WG8 and the hydroxylic oxygen of the YCD1; (gray) distances between hydroxylic hydrogen of the YCD1 and the hydroxylic oxygen of the YB10.

recent decades. Fluoride is a weak-field ligand; therefore, it binds heme proteins, giving rise to 6cHS complexes, characterized by a strong Soret band with maxima between 404 and 406 nm and a weaker Q-band at 490 nm.^{24–27} In addition, ligand-to-metal charge transfer transitions between 607 and 617 nm [CT1 due to $a_{2u}(\pi) \rightarrow e_g(d_x)$ transition, with x,y polarization] and between 450 and 460 nm [CT2 due to $a'_{2u}(\pi) \rightarrow a_{1g}(d_z)$ with z -polarization] are observed.²⁸ The $\nu(\text{Fe}-\text{F})$ stretching mode is intensified in the Raman spectra obtained in resonance with either the CT1 or the CT2 band.^{15,24,29–31} Fluoride builds four sp^3 hybrid orbitals and coordinates to the heme iron via σ - and π -bonding. An (lone pair) sp^3 hybrid orbital forms a σ bond with the d_z^2 Fe orbital. In this case the d_x^2 metal orbitals (d_{xz} , d_{yz} , d_{xy}) do not interact with the ligand orbitals and remain as nonbonding orbitals centered on the metal. Fluoride is also capable of π -bonding, acting as a π -donor. In this case the occupied ligand orbitals are lower in energy than the d_x^2 metal orbitals which become π^* and are shifted to higher energy.

We have recently shown¹⁵ that the spectroscopic properties of the fluoride complexes provide a simple and direct method to monitor the interactions of the distal heme pocket environment with the iron-bound ligand. In particular, we have demonstrated a strong correlation between the wavelength of the CT1 band and the strength of H-bonding donation from the distal amino acid side chains to the fluoride ion. In fact, the CT1 maximum wavelength is a sensitive probe of axial ligand polarity and of its interaction with the distal protein residues. It red-shifts when the π -donor capability of the axial ligands decreases, or when the ligand acts as a H-bond acceptor, because the destabilizing interaction between the π orbitals of the ligand and the iron d_x^2 orbitals is reduced in these cases.³² In parallel, RR spectra with excitation within the CT2 band (450–460 nm) have revealed

that the $\nu(\text{Fe}-\text{F})$ stretching frequency is directly affected by H-bonding to the fluoride ion. This is mainly due to the reduction of the Fe–F bond strength in H-bonded complexes, as a consequence of a decreased electron density on fluoride. A low $\nu(\text{Fe}-\text{F})$ stretching frequency has been shown to correlate with a red-shifted CT1 band in the complexes where fluoride is strongly H-bonded to distal pocket residues. We found that WT and ASV Tf-trHb are characterized by a $\nu(\text{Fe}-\text{F})$ band at 381 cm^{-1} together with a CT1 at 612 nm, similar to the spectroscopic signature of a peroxidase, in agreement with the presence of strong H-bonding residues. The present results show that the distal mutations markedly affect the spectroscopic markers of the fluoride adducts. In particular, because in the absence of either TrpG8 or TyrCD1, the $\nu(\text{Fe}-\text{F})$ band shifts from 381 cm^{-1} to higher frequency, with a concomitant blue-shift of the CT1 band, we clearly demonstrate that the $\nu(\text{Fe}-\text{F})$ band at 381 cm^{-1} together with the CT1 at 612 nm correspond to a conformer where the bound fluoride is stabilized by H-bond interactions donated by both TrpG8 and TyrCD1. Interestingly, in the presence of TrpG8 and TyrCD1, TyrB10 does not interact with the ligand. In contrast, its absence favors a strengthening of the H-bond, as observed in the single YB10F and in the double YB10F-WG8F and YB10-YCD1 mutants. TyrB10 is able to weakly interact with fluoride only when H-bond interactions with both TrpG8 and TyrCD1 are missing, i.e., in the YCD1F-WG8F double mutant. Accordingly, MD simulations revealed that in the WG8F mutant only the TyrCD1 residue stabilizes the coordinated fluoride, and the TyrB10 residue is not able to form a H-bond with the ligand. However, in the double mutant YCD1F-WG8F, the TyrB10 residue is now able to interact with the coordinated fluoride.

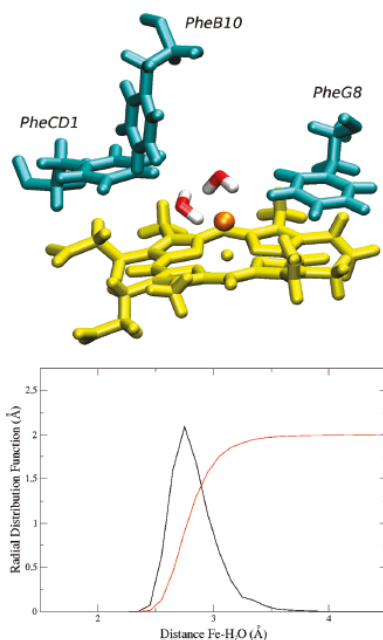


Figure 4. MD simulation obtained for the YB10F-YCD1F-WG8F Tf-trHb triple mutant. Upper panel: Representative snapshot of the active site. Heme group (yellow) with coordinated F^- (orange), relevant residues (cyan), and water molecules inside the active site are depicted. Lower panel: Radial distribution function $g(r)$ plot for the O atom of water molecules, centered in the coordinated fluoride (black). The integrated function, which indicates the total number of water molecules around fluoride, is depicted in red.

A second form of the fluoride complex, which is characterized by a $\nu(\text{Fe}-\text{F})$ band at 420 cm^{-1} , has been found in both the WT and ASV RR spectra. This heterogeneity can be compared with previous results obtained for the fluoride complexes of globins. X-ray diffraction of fluoride-bound hemoglobin indicated an equilibrium between two species, with and without H-bonding between the anion and a water molecule.³³ Accordingly, RR spectra displayed two $\nu(\text{Fe}-\text{F})$ stretches at 443 and 471 cm^{-1} .²⁹ Two pH-dependent forms were found for fluoride-bound myoglobin. The strong band observed at about 460 cm^{-1} at pH 7.0^{15,24,30} decreased in intensity at pH 5.2, with the concomitant growth of a new band at about 410 cm^{-1} .¹⁵ Furthermore, the downshift of the $\nu(\text{Fe}-\text{F})$ stretching mode was accompanied by a 2 nm red shift of the CT2 band (from 607 to 609 nm).^{15,24} These pH-dependent spectral variations were interpreted as due to changes in the iron-fluoride bond distance and/or change in the H-bonds involving the ligand, a water molecule, and the distal His.²⁴ The X-ray structure of the fluoride complex of swMb at pH 7.0 indicated that fluoride is H-bonded to the distal His64 and to a water molecule which, interacting also with the distal His,

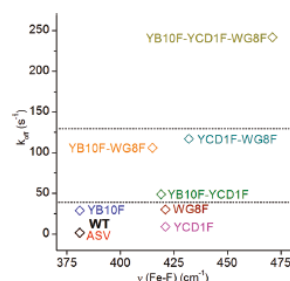


Figure 5. Correlation between the $\nu(\text{Fe}-\text{F})$ wavenumbers (Table 1) and the dissociation kinetics constant (Table 2). The dashed lines separate groupings of triple, double, and single mutants.

stabilizes the coordinated fluoride ion.³⁴ Therefore, protonation of the distal His can occur at acid pH. In the case of WT and ASV Tf-trHb, no spectroscopic changes are observed in the spectra between pH 5.5 and 8.5 (data not shown). We assign the $\nu(\text{Fe}-\text{F})$ band at 420 cm^{-1} to a second conformer, whose bound fluoride is stabilized by a single strong H-bond. Only this form, in fact, is observed in the mutants where either the WG8 or YCD1 residues have been replaced by Phe (Table 1). However, within the time scale of the simulation, only one conformation has been sampled by MD simulations in WT, ASV, and YB10F Tf-trHb, exhibiting stable H-bonds with both WG8 and YCD1. The absence of the second conformation detected in the RR experiments is probably due to limitations of the classical MD approach employed.

An interesting result is provided by the triple mutant that shows a reduced affinity for fluoride. The spectra of the fluoride-bound YB10F-YCD1F-WG8F mutant display the highest energy CT1 band in the Tf-trHb mutant series (i.e., at 603 nm) together with the highest $\nu(\text{Fe}-\text{F})$ stretch at 471 cm^{-1} . Nevertheless, the heme environment, where fluoride is surrounded by three Phe residues, does not appear to be apolar as would be expected. MD simulations clearly indicate that two water molecules interacting with the coordinated fluoride ion are accommodated into the active site. These data resemble closely those of the swMb-F adduct (607 nm and 462 cm^{-1}), whose anionic ligand is H-bonded to the distal His64 (2.74 \AA) and a water molecule (2.71 \AA), deeply buried in the distal side of the heme cavity.³⁴

In general, the Fe-F stretching frequencies and the MD simulations are consistent with the dissociation kinetic rate constants, because the fluoride complexes of the mutants with multiple H-bonding interactions exhibit lower dissociation rate constants. In agreement with the spectroscopic results, the progressive removal of distal H-bonding contributions to the bound fluoride brings about an increase in the observed rate of ligand release. An exponential correlation between the rate of ligand release and the overall fluoride binding energy would be expected if the Fe-F bond is the only determinant of the ligand dissociation process.⁹ Analysis of the data reported in Table 2 and plotted in Figure 5 indicate that there is a clear correspondence between the Fe-F stretching frequencies and the rates of ligand release. The singly, doubly or triply mutated species appear to gather into separate groups within the "stretching frequency/kinetic rate" correlation plot (see Figure 5). It is noteworthy that

Table 3. Comparison between the Spectroscopic Data Obtained for the CO^a and Fluoride^b Complexes of Tf-trHb, hhMb, swMb, DHP, and HRPC Together with the Proposed Distal H-Bond Interactions with the Exogenous Ligand

protein	$\nu(\text{Fe}-\text{CO})$ (cm ⁻¹)	$\nu(\text{CO})$ (cm ⁻¹)	H-bond interaction	$\nu(\text{Fe}-\text{F})$ (cm ⁻¹)	H-bond interaction
YB10F-YCD1F-WG8F	494	1955	—	471	H ₂ O
YCD1F-WG8F	488	1967	—		
	498	1952		432	YB10
WG8F	491	1962	—		
	497	1942		421	YCD1
YCD1F	505	1943	WG8	421	WG8
YB10F-YCD1F	511	1931	WG8	419	WG8
YB10F-WG8F	493	1966	—		
	511	1936		415	YCD1
YB10F	507	1942	WG8	421	WG8
	522	1926	WG8	381	WG8
ASV Tf-trHb	509	1938	WG8	420	WG8
	518	1920	WG8	381	WG8
			YCD1	420	YCD1
WT Tf-trHb	509	1938	WG8	420	WG8
	518	1920	WG8	381	WG8
			YCD1	420	YCD1
HRPC	516	1933		H42	
	539	1904	R38	H42	R38
swMb pH 7.0	507	1947		H64	H64
hhMb pH 7.0	509	1944		H64	H64
swMb pH 5.1	508 ^d			H64	
swMb pH 5.4 ^c				399 ^f 410	H64 ^d
swMb pH 3.9	491			H64 ^e	H ₂ O
DHP pH 7.0	500	1950		H55	H55
				462	H ₂ O

^a The data of the CO adducts have been taken from the following: Tf-trHb and its mutants;¹⁴ HRPC;³⁸ swMb pH 7.0;⁴¹ hhMb pH 7.0;⁴⁰ swMb pH 5.1 and pH 3.9;⁴⁷ DHP.³⁷ ^b References 15 and 39. ^c Reference 24. ^d It appears that the pK for H64 protonation is higher in the fluoride complex than in the CO complex.

the YB10F mutants (YB10F, YB10F-WG8F, YB10F-YCD1F, and YB10F-YCD1F-WG8F) display a consistent increase in the kinetics of ligand release with respect to the YB10-containing mutants (YCD1F, WG8F, YCD1F-WG8F), indicating that this residue, though not prominently involved in fluoride ligand hydrogen bonding, is still capable of influencing the ligand release process.

The effects on the dissociation kinetics upon distal mutation maybe more complex than the effects on the Fe–F stretching vibrational frequency. In fact, the latter is related to the H-bonding(s) involving fluoride, whereas the barriers fluoride has to overcome in the whole dissociation pathway will be related to H-bond breaking and, additionally, to the presence of diverse migration paths within the protein matrix. For instance, the fact that dissociation from the single TrpG8→Phe mutant is faster than that from the single TyrCD1→Phe mutant could be interpreted on the basis of the hindrance of the Trp side chain. A detailed interpretation, though, would be speculative at the present stage. Moreover, the presence of two conformers could complicate the picture. In principle, two different rates should be observed, although a single rate is observed if the conformers interconvert rapidly (see, e.g., refs 35 and 36).

Comparison with CO Complexes. Table 3 compares the spectroscopic data for the complexes of Tf-TrHb, hhMb, DHP, and HRPC with CO and fluoride, together with the proposed distal H-bonds involving the ligands.^{14,15,37–41} CO has been shown to be a useful probe of heme-binding sites in Fe(II) proteins, because FeCO back-bonding is modulated by polar interactions with protein residues, and by variations in the donor

strength of the trans ligand.⁴¹ The electrostatic field generated by the polar distal pocket amino acids alters the electron distribution in the FeCO unit, changing the order of the C–O bond. A positively charged electrostatic field favors back-donation, which strengthens the Fe–C bond and correspondingly weakens the C–O bond, thereby increasing the $\nu(\text{FeC})$ vibrational frequency and decreasing the $\nu(\text{CO})$ frequency, readily detectable in infrared and RR spectra. A linear correlation with negative slope between the frequencies of the $\nu(\text{FeC})$ and $\nu(\text{CO})$ stretching modes has been found for a large class of CO complexes of heme proteins, including bacterial trHb's, and heme model compounds containing imidazole as the fifth iron ligand.^{4,14} The $\nu(\text{FeC})/\nu(\text{CO})$ position along the correlation line reflects the type and strength of distal polar interactions.⁴¹

Two conformers were observed in the spectra of the CO complexes of both WT and ASV Tf-trHb: form 1 with $\nu(\text{FeC})$ and $\nu(\text{CO})$ at 509 and 1938 cm⁻¹ and form 2 with $\nu(\text{FeC})$ and $\nu(\text{CO})$ at 518 and 1920 cm⁻¹, respectively. The spectroscopic data and MD simulations demonstrated that CO interacts with TrpG8 in form 1 but with both TrpG8 and TyrCD1 in form 2, while TyrB10 does not directly interact with the bound CO.¹⁴ The present results suggest that the two fluoride conformers in the WT and ASV proteins are stabilized in a similar manner.

When the effects of the mutations are considered, it can be seen that the data obtained from CO complexes and those obtained from fluoride complexes (Table 3) follow a common trend, although the corresponding complexes cannot be placed in the same order. In fact, it is expected that Trp and Tyr mutation to Phe

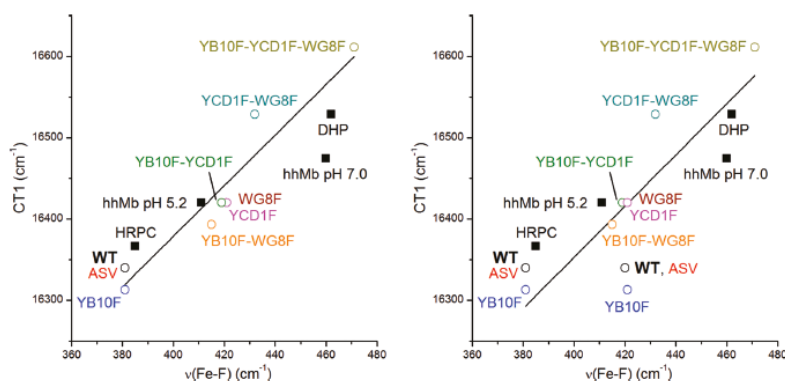


Figure 6. Empirical correlation plot between the $\nu(\text{Fe-F})$ wavenumbers and the CT1 energy. The frequencies of the CT1 are plotted as a function of the frequencies of the Fe-F stretching modes for the following proteins: WT, ASV, YB10F, YCD1F, WG8F, YB10F-WG8F, YB10F-YCD1F-WG8F, HRPC, DHP, hhMb pH 7.0, hhMb pH 5.2. Experimental data are reported in Tables 1 and 3. The lines represent two different least-squares fits for the experimental data of WT Tf-trHb and the combinatorial set of mutants, namely, considering only the strongly H-bonded forms of WT, ASV, and YB10F with $\nu(\text{Fe-F})$ stretch at 381 cm^{-1} (left) and both conformers (right).

decreases both the back-bonding in the CO complexes and the H-bonding interactions in the fluoride complexes. However, the single mutants YCD1F and WG8F, which share very similar CT1 maximum wavelengths and $\nu(\text{Fe-F})$ stretching frequencies in their fluoride complexes, display very different vibrational frequencies of the FeCO unit. Another divergent mutant is the triple YB10-YCD1F-WG8F, which displays the highest $\nu(\text{Fe-F})$ stretching frequency but an intermediate back-bonding in the CO complex. There are several possible explanations for these differences. Clearly, back-bonding in the CO complexes depends on all kinds of polar interactions with the neighboring amino acids,⁴² whereas H-bonding is the only effective stabilization for the heme-bound fluoride. Moreover, it should be considered that the two types of complexes have different chemical properties, namely (i) carbon monoxide is neutral (and almost apolar), whereas fluoride retains a negative charge, and (ii) H-bonding to CO is directional, whereas there is no directionality in F-HX bonding because of the spherical symmetry of fluoride.

CT1 Energy/ $\nu(\text{Fe-F})$ Wavenumber Correlation. In an attempt to find an empirical correlation between the $\nu(\text{Fe-F})$ wavenumbers and the CT1 transition energy, we have plotted our experimental data for all the Tf-trHb fluoride complexes together with the available literature data (Figure 6, left). The data are fitted well by a straight line with positive slope. The (CT1)/ $\nu(\text{Fe-F})$ position along the correlation line appears to reflect the extent of distal H-bonding interactions. Fluoride complexes which are stabilized by multiple, strong H-bond interactions, like those of the WT, ASV Tf-trHb, and YB10F conformer ($\nu(\text{Fe-F})$ at 381 cm^{-1}), are located at the extreme left side. In fact, H-bonding decreases both the $\nu(\text{Fe-F})$ stretching frequency and the energy of the $e_g(d_{xy})$ orbitals, thereby lowering the energy of the $a_{2u}(\pi) \rightarrow e_g(d_{xy})$ CT1 transition. At the other extreme of the line, fluoride complexes with very weak H-bond interactions are found, like that of the YB10F-YCD1F-WG8F mutant. Unlike the points for the 381 cm^{-1} conformer, those for the second conformer of WT, ASV Tf-trHb,

and YB10F ($\nu(\text{Fe-F})$ at $420\text{--}421\text{ cm}^{-1}$) fall off the line (Figure 6, right). In fact, the presence of two conformers should give rise to two CT1 absorption bands. Based on the CT1 energy measured for WG8F, YCD1F, and YCD1F-YB10F mutants which show only the second conformer, the expected energy difference between the two conformers is about 200 cm^{-1} . Because the CT1 band is relatively weak and broad, in practice we observe a single maximum. Therefore, given the impossibility to single out two different CT1 bands for WT, ASV, and YB10F, we correlate the two different Raman Fe-F stretches with the same energy value. As a consequence for the proteins with multiple conformers, some points are off the line.

Some deviations from this linear correlation can be expected as a consequence of different vinyl/heme conjugation. In general, the absorption maxima of the heme prosthetic group, including the Soret, Q, and CT1 bands, are related not only to the coordination/spin state of the heme but also to the degree of conjugation between the heme group and its two vinyl substituents, which can cause up to 10 nm red-shift of the electronic transitions.⁴³ In heme proteins, the vinyl groups are found to give rise to $\nu(\text{C=C})$ polarized Raman bands between 1620 and 1635 cm^{-1} .⁴⁴ A direct relationship between the $\nu(\text{C=C})$ stretching wavenumbers and the orientations of the vinyl groups, as induced by specific protein interactions, clearly showed that a lower frequency corresponds to a higher degree of conjugation between the C=C vinyl group and the porphyrin π system.⁴⁵ Increased conjugation from the vinyl groups shifts the energy not only of the $\pi \rightarrow \pi^*$ transition but also of the $a_{2u}(\pi) \rightarrow e_g(d_{xy})$ (CT1) to lower energy, thus shifting the maxima to the red.^{32,45,46}

The RR spectra of Tf-trHb fluoride complexes are characterized by two overlapping $\nu(\text{C=C})$ bands at 1628 cm^{-1} , corresponding to vinyl groups with a low degree of conjugation with the heme. Mutations do not change the orientation of the vinyl group and, therefore, do not affect their conjugation, because the maximum frequency change of the $\nu(\text{C=C})$ stretches in the

Tf-trHb mutant series is 2 cm^{-1} (Table 1). Therefore, the observed changes of the CT1 maxima are solely due to different H-bonding interactions. In contrast, when the fluoride adducts of Mb, HRPC, and DHP are compared, the effect of the $\nu(\text{C}=\text{C})$ conjugation on the energy of the CT1 band must be taken into account. Mb-F is characterized by a higher degree of conjugation between the vinyl group and the porphyrin π system, as suggested by the presence of two overlapping $\nu(\text{C}=\text{C})$ at 1621 cm^{-1} .³² As a consequence, the CT1 band is at a lower energy compared to those of the Tf-trHb-F adducts. Less deviation from the line based on the Tf-trHb-F adducts is found for DHP, because a second weak vinyl mode is found at 1630 cm^{-1} .³⁹ Finally, the CT1 of the HRPC-F adduct is found at an energy higher than that of the Tf-trHb-F adducts. In fact, two vinyl stretches have been observed, as the band with a very low degree of conjugation between the vinyl group and the porphyrin π system (1631 cm^{-1}) is the most intense.³²

CONCLUSION

The present results can be considered as a unique data set, because they have been obtained for a complete group of mutants where the three key amino acids of Tf-trHb (WG8, YCD1, YB10) are progressively substituted with the non-hydrogen bonding phenylalanine. The spectroscopic characterization of the fluoride complexes has unveiled a well-defined correlation between $\nu(\text{Fe}-\text{F})$ vibrational frequencies and CT1 electronic transition energies. The validity of this correlation is confirmed by its being applicable to literature data, including important model proteins such as myoglobin and horseradish peroxidase. This indicates its general usefulness as an additional method to investigate relevant properties of the active site of heme proteins. For the case of Tf-trHb, we have obtained a detailed picture of H-bonding in the distal cavity environment. The interpretation of the spectroscopic data is strengthened by the close relation with the observed fluoride dissociation kinetics and molecular dynamics simulations. All the techniques yield evidence that TrpG8 and TyrCD1 can form strong H bonds with fluoride, whereas TyrB10 can only interact weakly.

ASSOCIATED CONTENT

S Supporting Information. Plot of rmsd vs time of MD simulation for the complexes between fluoride and WT Tf-trHb, YB10F, WG8F, YCD1F-WG8F, YB10F-YCD1F-WG8F mutants; time evolution of selected distances between distal residues of ASV Tf-trHb. The distances are defined as those between the coordinated fluoride and the following distal site atoms: indole N proton of the WG8, hydroxylic hydrogen of the YCD1, and the hydroxylic hydrogen of the YB10. Charges of selected atoms used in the simulation are given in Table S1. Kinetics of azide binding and release are given in Table S2. Azide release kinetics was calculated from the product of the measured thermodynamic and kinetic ligand binding data. This material is available free of charge via the Internet at <http://pubs.acs.org>.

AUTHOR INFORMATION

Corresponding Author
giulietta.smulevich@unifi.it

Author Contributions

^aThese authors contributed equally to this work.

ACKNOWLEDGMENT

This work was supported by Institute Pasteur Fondazione Cenci Bolognietti (A. Boffi), MIUR FIRB RBF08F41U_002 (A. Bonamore), MIUR PRIN 2008BFJ34 (A. Feis and A. Boffi), University of Buenos Aires (grant X074), CONICET, and European Union FP7 project NOSTress (D. Estrin), and the Italian Ministero dell'Istruzione, dell'Università e della Ricerca (MIUR), Direzione Generale per l'Internazionalizzazione della Ricerca, Progetti di Grande Rilevanza Italia-Argentina.

REFERENCES

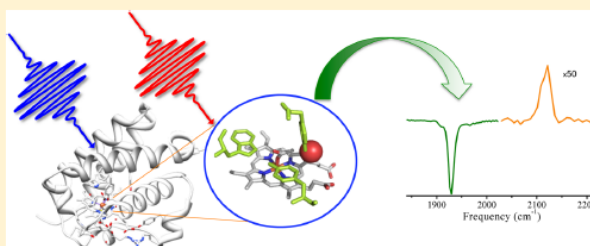
- (1) Ma, L. H.; Liu, Y.; Zhang, X.; Yoshida, T.; La Mar, G. N. *J. Am. Chem. Soc.* **2006**, *128*, 6657–6668.
- (2) Streit, B. R.; Blanc, B.; Lukat-Rodgers, G. S.; Rodgers, K. R.; DuBois, J. L. *J. Am. Chem. Soc.* **2010**, *132*, 5711–5724.
- (3) Edwards, S. L.; Poulos, T. L. *J. Biol. Chem.* **1990**, *265*, 2588–2595.
- (4) Egawa, T.; Yeh, S. R. *J. Inorg. Biochem.* **2005**, *99* (1), 72–96.
- (5) Feis, A.; Lapini, A.; Catacchio, B.; Brogioni, S.; Foggi, P.; Chiancone, E.; Boffi, A.; Smulevich, G. *Biochemistry* **2008**, *47*, 902–910.
- (6) Ouellet, H.; Juszcak, L.; Dantsker, D.; Samuni, U.; Ouellet, Y. H.; Savard, P. Y.; Wittenberg, J. B.; Wittenberg, B. A.; Friedman, J. M.; Guertin, M. *Biochemistry* **2003**, *42*, 5764–5774.
- (7) Rodriguez, J. C.; Zeng, Y.; Wilks, A.; Rivera, M. *J. Am. Chem. Soc.* **2007**, *129*, 11730–11742.
- (8) Ye, X.; Demidov, A.; Rosca, F.; Wang, W.; Kumar, A.; Ionascu, D.; Zhu, L.; Barrick, D.; Wharton, D.; Champion, P. M. *J. Phys. Chem. A* **2003**, *107*, 8156–8165.
- (9) Springer, B. A.; Sligar, S. G.; Olson, J. S.; Phillips, G. N. *J. Chem. Rev.* **1994**, *94*, 699–714.
- (10) Quillin, M. L.; Li, T.; Olson, J. S.; Phillips, G. N., Jr.; Dou, Y.; Ikeda-Saito, M.; Regan, R.; Carlson, M.; Gibson, Q. H.; Li, H.; et al. *J. Mol. Biol.* **1995**, *245*, 416–436.
- (11) Wittenberg, J. B.; Bolognesi, M.; Wittenberg, B. A.; Guertin, M. *J. Biol. Chem.* **2002**, *277*, 871–874.
- (12) Bonamore, A.; Ilari, A.; Giangiacomo, L.; Bellelli, A.; Morea, V.; Boffi, A. *FEBS J.* **2005**, *272*, 4189–4201.
- (13) Nicoletti, F. P.; Comandini, A.; Bonamore, A.; Boechi, L.; Boubeta, F. M.; Feis, A.; Smulevich, G.; Boffi, A. *Biochemistry* **2010**, *49*, 2269–2278.
- (14) Droghetti, E.; Nicoletti, F. P.; Bonamore, A.; Boechi, L.; Arroyo Manez, P.; Estrin, D. A.; Boffi, A.; Smulevich, G.; Feis, A. *Biochemistry* **2010**, *49*, 10394–10402.
- (15) Droghetti, E.; Nicoletti, F. P.; Bonamore, A.; Sciamanna, N.; Boffi, A.; Feis, A.; Smulevich, G. *J. Inorg. Biochem.* **2011**, *105*, 1338–1343.
- (16) Jorgensen, W. L.; Chandrasekar, J.; Madura, J.; Impey, R. W.; Klein, M. L. *J. Chem. Phys.* **1983**, *79*, 926–935.
- (17) Luty, B. A.; Tironi, I. G.; Van Gunsteren, W. F. *J. Chem. Phys.* **1995**, *103*, 3014–3021.
- (18) Pearlman, D. A.; Case, D. A.; Caldwell, J. W.; Ross, W. S.; Cheatham, T. E.; Debolt, S.; Ferguson, D.; Seibel, G.; Kollman, P. *Comput. Phys. Commun.* **1995**, *91*, 1–41.
- (19) Boechi, L.; Manez, P. A.; Luque, F. J.; Marti, M. A.; Estrin, D. A. *Proteins* **2010**, *78*, 962–970.
- (20) Boechi, L.; Marti, M. A.; Milani, M.; Bolognesi, M.; Luque, F. J.; Estrin, D. A. *Proteins* **2008**, *73*, 372–379.
- (21) Crespo, A.; Marti, M. A.; Kalko, S. G.; Morreale, A.; Orozco, M.; Gelpi, J. L.; Luque, F. J.; Estrin, D. A. *J. Am. Chem. Soc.* **2005**, *127*, 4433–4444.
- (22) Marti, M. A.; Capece, L.; Bikiel, D. E.; Falcone, B.; Estrin, D. A. *Proteins* **2007**, *68*, 480–487.
- (23) Ye, L.; Spittler, D.; Ullrich, R.; Boland, W.; Nuske, J.; Diekert, G. *Biochemistry* **2010**, *49*, 7264–7271.
- (24) Asher, S. A.; Adams, M. L.; Schuster, T. M. *Biochemistry* **1981**, *20*, 3339–46.

- (25) Beetlestone, J.; George, P. *Biochemistry* 1964, 3, 707–714.
- (26) Tamura, M. *Biochim. Biophys. Acta* 1971, 243, 249–258.
- (27) Yonetani, T.; Wilson, D. F.; Seamonds, B. *J. Biol. Chem.* 1966, 241, 5347–5352.
- (28) Makinen, M. W.; Churg, A. K., in *Iron Porphyrins*, Lever, A.P.B. P; Gray, H.B. Eds, Addison-Wesley Publishing Company, Reading, USA, Part 1. 1983, 143–225.
- (29) Asher, S. A.; Vickery, L. E.; Schuster, T. M.; Sauer, K. *Biochemistry* 1977, 16, 5849–5856.
- (30) Desbois, A.; Lutz, M.; Banerjee, R. *Biochemistry* 1979, 18, 1510–1518.
- (31) Yu, N. T. *Methods Enzymol.* 1986, 150, 350–409.
- (32) Neri, F.; Kok, D.; Miller, M. A.; Smulevich, G. *Biochemistry* 1997, 36, 8947–8953.
- (33) Deatherage, J. F.; Loe, R. S.; Anderson, C. M.; Moffat, K. *J. Mol. Biol.* 1976, 104, 687–706.
- (34) Aime, S.; Fasano, M.; Paoletti, S.; Cutruzzola, F.; Desideri, A.; Bolognesi, M.; Rizzi, M.; Ascenzi, P. *Biophys. J.* 1996, 70, 482–488.
- (35) Coletta, M.; Ascoli, F.; Brunori, M.; Traylor, T. G. *J. Biol. Chem.* 1986, 261, 9811–9814.
- (36) Feis, A.; Santoni, E.; Neri, F.; Ciaccio, C.; De Sanctis, G.; Coletta, M.; Welinder, K. G.; Smulevich, G. *Biochemistry* 2002, 41, 13264–13273.
- (37) Belyea, J.; Belyea, C. M.; Lappi, S.; Franzen, S. *Biochemistry* 2006, 45, 14275–14284.
- (38) Feis, A.; Rodriguez-Lopez, J. N.; Thorneley, R. N.; Smulevich, G. *Biochemistry* 1998, 37, 13575–13581.
- (39) Nicoletti, F. P.; Thompson, M. K.; Howes, B. D.; Franzen, S.; Smulevich, G. *Biochemistry* 2010, 49, 1903–1912.
- (40) Smulevich, G.; Mantini, A. R.; Paoli, M.; Coletta, M.; Geraci, G. *Biochemistry* 1995, 34, 7507–7516.
- (41) Spiro, T. G.; Wasbotten, I. H. *J. Inorg. Biochem.* 2005, 99, 34–44.
- (42) Phillips, G. N., Jr.; Teodoro, M. L.; Li, T.; Smith, B.; Olson, J. S. *J. Phys. Chem. B* 1999, 103, 8817–8829.
- (43) Spiro, T. G.; Li, X.-Y. In *Biological application of Raman Spectroscopy*; Spiro, T. G., Ed.; Wiley Interscience: New York, 1988; Vol. 3, pp 1–37.
- (44) Kalsbeck, W. A.; A., G.; Pandey, R. K.; Smith, K. M.; Bocian, D. M. *J. Am. Chem. Soc.* 1995, 117, 10959–10968.
- (45) Marzocchi, M. P.; Smulevich, G. *J. Raman Spectrosc.* 2003, 34, 725–736.
- (46) Neri, F.; Indiani, C.; Baldi, B.; Vind, J.; Welinder, K. G.; Smulevich, G. *Biochemistry* 1999, 38, 7819–7827.
- (47) Sage, J. T.; Morikis, D.; Champion, P. M. *Biochemistry* 1991, 30, 1227–1237.

Carbon Monoxide Recombination Dynamics in Truncated Hemoglobins Studied with Visible-Pump MidIR-Probe Spectroscopy

Andrea Lapini,^{¶,†} Mariangela Di Donato,^{¶,†,‡} Barbara Patrizi,[†] Agnese Marcelli,[†] Manuela Lima,[†] Roberto Righini,[†] Paolo Foggi,^{†,‡,§} Natascia Sciamanna,[‡] and Alberto Boffi[‡][¶]LENS (European Laboratory for Nonlinear Spectroscopy) via N. Carrara 1, 50019 Sesto Fiorentino (FI), Italy[†]INO (Istituto Nazionale di Ottica), Largo Fermi 6, 50125 Firenze, Italy[‡]Dipartimento di Chimica, Università di Perugia, via Elce di Sotto 8, 06123 Perugia, Italy[§]Istituto Pasteur, Fondazione Cenci Bolognetti c/o Dipartimento di Scienze Biochimiche, Università "La Sapienza", piazzale Aldo Moro 5, 00185 Roma, Italy

Supporting Information



ABSTRACT: Carbon monoxide recombination dynamics upon photodissociation with visible light has been characterized by means of ultrafast visible-pump/MidIR probe spectroscopy for the truncated hemoglobins from *Thermobifida fusca* and *Bacillus subtilis*. Photodissociation has been induced by exciting the sample at two different wavelengths: 400 nm, corresponding to the heme absorption in the B-band, and 550 nm, in the Q-bands. The bleached iron–CO coordination band located at 1850–1950 cm^{-1} and the free CO absorption band in the region 2050–2200 cm^{-1} have been observed by probe pulses tuned in the appropriate infrared region. The kinetic traces measured at 1850–1950 cm^{-1} reveal multiexponential subnanosecond dynamics that have been interpreted as arising from fast geminate recombination of the photolyzed CO. A compared analysis of the crystal structure of the two proteins reveals a similar structure of their distal heme pocket, which contains conserved polar and aromatic amino acid residues closely interacting with the iron ligand. Although fast geminate recombination is observed in both proteins, several kinetic differences can be evidenced, which can be interpreted in terms of a different structural flexibility of the corresponding heme distal pockets. The analysis of the free CO band-shape and of its dynamic evolution brings out novel features about the nature of the docking site inside the protein cavity.

INTRODUCTION

Truncated hemoglobins (trHbs) are a family of small oxygen binding proteins widely distributed among bacteria, plants, and protozoa.^{1,2} They are characterized by a high structural variability of the heme pocket residues, suggesting diverse functions, possibly related to the physiological response in the defense from oxygen reactive species and in the presence of other bimolecular ligands such as NO or CO. On the basis of the nature of the amino acid residues in key topological positions within the distal heme pocket, trHbs are usually divided into three groups, each presenting a certain number of conserved residues. Truncated hemoglobins from *Thermobifida fusca* (Tf-trHb) and *Bacillus subtilis* (Bs-trHb) both belong to group II, which is characterized by the presence of a Trp

residue on the bottom of the heme distal pocket (G8 position).¹ The resolution of the crystal structure of a number of group II truncated hemoglobins has revealed a common general pattern of the heme pocket, characterized by an ensemble of polar residues capable of forming hydrogen bonds with the iron-bound ligand, usually defined as “ligand inductive hydrogen bonding network” (see Figure 1). It has been suggested that TrpG8 plays an important role in ligand binding and stabilization, though other amino acids in topological positions E7, E11, CD1, and B10 can modify drastically the

Received: February 27, 2012

Revised: June 22, 2012

Published: July 3, 2012

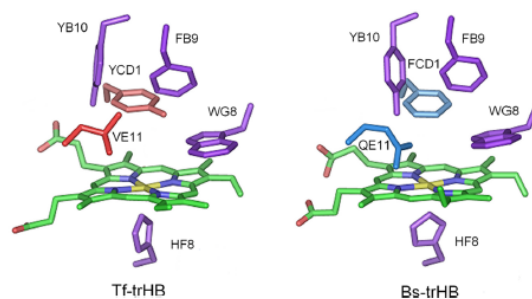


Figure 1. Close-up view of the active sites in *Thermobifida fusca* and *Bacillus subtilis* truncated hemoglobins. The key topological positions in contact with the iron bound ligand (E11, B9, B10, CD1, and G8) are shown for both proteins. Conserved residues in both proteins are colored magenta. Nonconserved amino acids are in red (Tf-trHb) or in cyan (Bs-trHb). Pictures generated with PyMol (DeLano Scientific LLC).

interaction network.^{3–5} The structure and sequence analysis of group II trHbs shows that the nature of the residue at position CD1 is correlated with the nature of the site E11. When the protein has a Tyr at CD1, a nonpolar residue is found at E11; in contrast, when a non-hydrogen bond donor replaces the TyrCD1, a hydrogen bond donor is present at the E11 site. TyrB10 and TrpG8 are instead invariant residues.^{6,7} The crystal structure of both Tf-trHb⁸ and Bs-trHb⁹ has been resolved, confirming a high degree of similarity among these two proteins. In the case of Tf-trHb, the heme distal pocket involves, beside TrpG8, two Tyr residues, TyrB10 and TyrCD1, which are in close proximity with the iron-bound ligand. In Bs-trHb, the more closely ligand interacting residues besides TrpG8 are TyrB10 and GlnE11.

Given the high sensitivity of the $\nu(\text{CO})$ stretching vibration of the hemoglobin-CO adduct to the electric field generated by the protein environment, Resonance Raman and FTIR spectra have been used to probe the local structural characteristics of the heme binding pocket for the heme-bound CO state of both Tf-trHb and Bs-trHb. It has been found that each of these two proteins can adopt two different conformations, differing by the number of hydrogen bonds formed with the iron-coordinated CO.^{3,10,11}

In the case of Tf-trHb, the comparison of the FTIR spectra of the wild type protein and of a series of combinatorial mutants in which TrpG8, TyrCD1, and TyrB10 have been changed into Phe, revealed that in one conformation both TrpG8 and TyrCD1 are hydrogen bonded to the iron-coordinated CO, while in the other conformer only the H-bond with TrpG8 is maintained. The FTIR spectrum of the CO adduct of the wild type protein showed two bands attributable to the $\nu(\text{CO})$ stretching vibration, located at 1920 and 1940 cm^{-1} , respectively. These features have been ascribed to the presence of two conformers in which the iron coordinated CO is either doubly H-bonded to both TrpG8 and TyrCD1 or singly bonded only to TrpG8, respectively.¹⁰

Very similar structural characteristics are observed also for Bs-trHb. In the latter protein, the FTIR spectrum of the CO adduct also shows two bands assigned to the $\nu(\text{CO})$ stretching vibration: one extremely downshifted, at 1888 cm^{-1} , and the other at 1925 cm^{-1} . The spectra have been interpreted along the same line as in Tf-trHb, that is, by assuming the presence of a doubly H-bonded species in which TrpG8 and TyrB10 are

hydrogen bonded to the iron coordinated CO, and a singly H-bonded adduct in which TrpG8 is the sole H-bonding residue. The extreme downshift of the $\nu(\text{CO})$ stretching vibration at 1888 cm^{-1} indicated a highly polar environment around the bound CO, in which the double H-bond dominates the ligand dissociation and rebinding dynamics properties of Bs-trHb.³ The sizably lower frequency of the $\nu(\text{CO})$ stretching band in Bs-trHb, as compared to Tf-trHb, can be a consequence of a more favorable orientation of the coordinating residues toward the ligand. Such sterically favorable conformation is suggested to generate a stronger H-bonding interaction and consequently a higher degree of electron back-donation toward the iron. This finding may account for the 1 order of magnitude higher oxygen affinity in Bs-trHb with respect to Tf-trHb despite the similar structural characteristics of the distal heme pockets in the two proteins.³

The structural features of the heme distal pocket are known to govern the dynamics of ligand escape and recombination in globins. Recombination dynamics can vary substantially, spanning from the millisecond time scale of myoglobin and hemoglobin^{12,13} to the subnanosecond time scale observed for instance in the oxygen sensory protein FixL.^{14,15} In Bs-trHb CO recombination dynamics has been studied by transient visible absorption spectroscopy, revealing the existence of a very fast geminate recombination dynamics with a time constant of about 770 ps.³ The occurrence of fast geminate recombination suggests that the ligand is confined within the distal pocket with little possibility for the CO molecule to escape from the protein matrix to the solvent.

To capture further details on the way such proteins operate we analyzed the CO escape and rebinding processes after dissociation induced by a short laser pulse by applying visible-pump MidIR-probe spectroscopy in both Bs-trHb and Tf-trHb. The combination of the high temporal resolution given by short laser pulses with the structural information achieved by the infrared probe, provides unique pieces of information on the microscopic environments experienced by the ligand molecule after photodetachment, unattainable by UV-vis probe pulses. This technique has been widely applied in the past to study carbon monoxide recombination dynamics in a number of similar systems, such as myoglobin, hemoglobin, and the oxygen sensory protein FixL.^{13–19} In the present study, the comparison between two proteins investigated in further details

provides insight on the factors influencing the amount and the dynamics of geminate recombination and on the microscopic environment determining the impaired escape of the ligand after photolysis.

■ MATERIAL AND METHODS

Protein Expression and Purification-Sample Preparation. *Bacillus subtilis* and *Thermobifida fusca* hemoglobins were obtained and purified as described previously.^{8,9} In addition, Tf-trHb was successfully obtained as a lyophilized sample.

Protein solution for vis-pump MidIR-probe measurements were prepared by dissolving the samples in a Tris-HCl buffer, 0.2 M, in D₂O (pD = 8). In the case of Tf-trHb, a 10 mM solution was prepared by dissolving a lyophilized protein preparation in the buffer, while for Bs-trHb, solutions at 4 mM concentration were obtained by microcentrifugation with Millipore ultracon filters. The reduction of proteins was accomplished by adding a freshly prepared anaerobic solution of sodium dithionite in stoichiometric excess to the protein solution, previously degassed with nitrogen. Carbon monoxide (Rivoira), was gurgled at low flux intensity, and the sealed protein solution was saturated with 1 atm CO for 15 min. In this way CO is homogeneously distributed despite the high viscosity of the sample. Samples for transient infrared measurements were prepared by squeezing about 40 μ L of solution between two calcium fluoride windows (3 mm thickness) separated by a 50 μ m Teflon spacer (in the case of Bs-trHb, a 100 μ m spacer was used). The OD at the excitation wavelength was about 0.8 for all samples.

Visible-Pump/MidIR-Probe Spectroscopy. Measurements were performed probing both the absorption region of the $\nu(\text{CO})$ stretching vibration of the iron-bound CO (1880–1990 cm^{-1} for Tf-trHb and 1825–1975 for Bs-trHb) and the dissociated free CO absorption (2030–2230 cm^{-1}). CO dissociation was induced by pumping the systems either with a 400 or a 550 nm laser pulse. The experimental setup for the infrared differential absorption measurements has been described in detail in ref 20. Briefly, a Ti:sapphire oscillator/regenerative amplifier, operating at 1 kHz, (Legend, Coherent) was used to pump a home-built optical parametric generator and amplifier with difference frequency generation, which produced a tunable output (2.5–10 μ m) with a spectral width of \sim 200 cm^{-1} . The output of a HgCdTe camera system, placed behind a spectrograph, was read out every shot at a repetition rate of 1 kHz and a sampling resolution either of 3 or 6 cm^{-1} . In case of the blue excitation, another part of the Legend output was frequency doubled in a BBO crystal to generate the pump-pulses at 400 nm (\sim 6 nm fwhm) which were attenuated to provide 200–500 nJ and focused to a spot of \sim 150 μ m in diameter. Excitation pulses at 550 nm (energy = 200 nJ) were obtained by sum frequency generation of the idler output of a commercial optical parametric generator (TOPAS, Light Conversion) with a portion of the fundamental output at 800 nm. A moveable delay line made it possible to increase the time-of-arrival-difference of the pump and probe beams up to 1.8 ns. The pump beam polarization was set to magic angle with respect to the probe beam by rotating a $\lambda/2$ plate. Furthermore anisotropy measurements were executed by setting the pump beam polarization either at 0 or 90 degrees with respect to the probe beam. The sample was moved with a home-built scanner to refresh the solution and avoid photo-degradation. Home-written software was used to collect the data over the two different spectral windows, respectively,

between 1880 and 1975 cm^{-1} and 2030–2230 cm^{-1} . Every window was recorded with a freshly prepared sample and measured at least three times. To obtain a good signal-to-noise ratio in the case of the free CO signal, which has a small absorption cross section, a number of data sets, corresponding to about 12000 laser shots were collected and averaged. The integrity of the sample has been checked by FTIR (Bruker Alpha-T) and visible absorption (Perkin-Elmer LAMBDA 950) before and after the time-resolved measurements.

Data Analysis. For the quantitative analysis of the time-resolved spectral data we used a combined approach, consisting of singular values decomposition (SVD) and the simultaneous fitting of all the collected kinetic traces (global analysis). To avoid the contribution due to perturbed free induction decay and cross-phase modulation,^{21–25} we excluded from our analysis the spectra measured for delays shorter than 500 fs. First, we extrapolated the number of components using SVD;^{26–28} then we analyzed the whole ensemble of kinetic data by means of a global fitting procedure. The combination of global analysis and SVD is a very helpful analysis protocol, as it provides a good control on the number of components used to fit the data.^{29–34} The time constants resulting from the fitting of the right singular vectors were used as the starting point for the subsequent global analysis. The aim of global analysis is to decompose the two-way data matrix into time-independent spectra and wavelength-independent kinetics.^{33–36} Once the number of components has been identified, the second step involves the parametrization of the time evolution of the relative intensities of the spectral components. This was accomplished by assuming a first-order kinetics, describing the overall temporal evolution as the sum or combination of exponential functions. Global analysis was performed using the GLOTARAN package (<http://glotaran.org>).^{34,37–40} We employed a linear unidirectional “sequential” model. The solution for the system of differential equations for the “sequential” model with increasing lifetimes is

$$c_j(t) = \sum_{j=1}^l b_{ji} \exp(-k_j t)$$

$$b_{ji} = \prod_{m=1}^{j-1} k_m / \prod_{\substack{n=1 \\ n \neq j}}^j (k_n - k_j)$$

$c_j(t)$ represent the temporal evolution of the selected component, k_j is the decay rate of component j and the amplitudes b_{ji} of the exponential decays are defined for $j \leq l$ assuming $b_{j1} = 1$. In discussion of our results the spectra associated to the various time constants are termed “evolution associated difference spectra” (EADS).

■ RESULTS

Thermobifida fusca. Initial experiments on Tf-trHb were performed by exciting the sample with a 400 nm pump pulse, whose energy was varied between 200 and 500 nJ. The spectrum recorded immediately after excitation shows the appearance of a bleaching signal in the spectral region where the $\nu(\text{CO})$ stretching vibration is expected, indicating photolysis of the ligand. A main bleaching band and a small shoulder are visible, respectively peaking at 1920 and 1940 cm^{-1} , in good correspondence with the absorption bands measured in the FTIR spectrum of the CO adduct for this protein, see Figure 2a. Experiments were repeated by setting

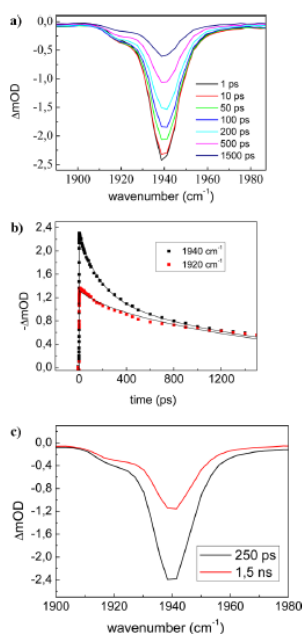


Figure 2. (a) Time resolved spectra recorded at different time delays, showing the bleaching induced by the excitation at 400 nm in the $\nu(\text{CO})$ stretching region for the coordinated CO; (b) Kinetic traces (scattered points) at selected frequencies together with the fit (solid line) obtained by global analysis. The trace at 1920 cm^{-1} has been scaled to overlap the trace at 1940 cm^{-1} on the long time scale; (c) EADS obtained by globally analyzing all the kinetic traces recorded in the 1850–1950 cm^{-1} spectral range.

the pump pulse polarization either to 0 or 90 degrees with respect to the probe pulse, and the time-dependent anisotropy of the transition was calculated, resulting in an average value of -0.18 . Considering that the heme behaves like a circular absorber when excited at 400 nm,^{14,42} it can be calculated that the coordinated CO is oriented in way that its dipole forms an angle smaller than 15 degrees with respect to the heme normal, similarly to what observed for other globin proteins.^{14,17,43}

The analysis of the kinetic traces revealed a biphasic recovery, occurring within the subnanosecond time scale. As clearly visible by inspecting the kinetic traces reported in Figure 2b, the bleaching band at 1940 cm^{-1} recovers faster than the bleaching at 1920 cm^{-1} . We have analyzed the data using a global fit with a sequential decay scheme, obtaining the EADS reported in Figure 2c. The kinetic traces can be satisfactorily fitted with two components, whose time constants are 250 ps and 1.5 ns, respectively. The fast kinetic phase accounts for almost 30% of the recombination dynamics at 1940 cm^{-1} . An inspection of the kinetic traces reported in Figure 2b brings out that the relative weight of the fast component is much higher

for the 1940 cm^{-1} band with respect to the low frequency band (1920 cm^{-1}).

Bleaching recovery on a subnanosecond time scale can be directly associated to fast geminate recombination if it is assumed that the recombined CO and CO in the non-photolyzed portion of the sample have the same spectrum as the ligated CO at equilibrium.⁴³ To further investigate the dynamics following CO photodissociation we also analyzed the free CO absorption band, which is expected to appear at about 2100–2150 cm^{-1} . Because of the low absorption cross section of the free CO vibration and the substantial water absorption in that region, it is difficult to obtain reliable kinetic traces and time-dependent spectra with a good signal to-noise-ratio. Tentative measurements, carried out by exciting the sample with a 400 nm pump pulse, revealed a significant baseline problem, due to water absorption, heating, and excess energy dissipation in the system. To minimize these unwanted contributions, CO photolysis was triggered by exciting the heme in the Q-band absorption region (550–600 nm) instead of the B-band region. Under these experimental conditions the amount of energy dissipated by the system was significantly reduced.

Measurements were thus carried out by setting the excitation pulse at 550 nm and probing both the $\nu(\text{CO})$ stretching region for the coordinated CO and the free CO absorption region. The dynamic evolution in the bleaching region was substantially identical to what was previously observed by exciting the sample at 400 nm. Instead, significant improvement was obtained in the free CO region, where time traces with good signal-to-noise ratio could be recorded.

Spectra collected in the free CO region are reported in Figure 3a while Figure 3b shows the kinetic trace measured at the absorption maximum and compared with that of the 1940 cm^{-1} bleaching band, which has been scaled to match the

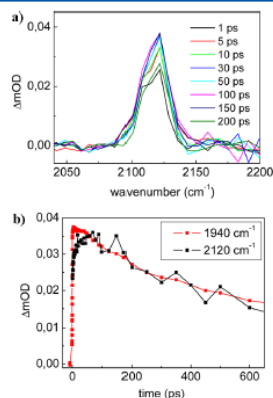


Figure 3. (a) Time resolved spectra in the free CO region recorded at different time delays after excitation of the sample with a 550 nm laser pulse; (b) kinetic traces at 2120 cm^{-1} (red line), corresponding to the maximum absorption in the free CO region. This trace has been superimposed with the kinetic trace at 1940 cm^{-1} (black line), corresponding to the maximum absorption of the coordinated CO, opportunely scaled.

intensity of the free CO signal. As noticed from Figure 3b, the two kinetic traces are well matched, except for the short time scale, where the signal corresponding to the CO absorption (2120 cm^{-1}) shows an initial rise component.

Spectra in Figure 3a have been corrected for the presence of a baseline, which still contributes in this region although at a more minor extent than in the previous measurements with 400 nm excitation. The baseline is removed by subtracting a third order polynomial fit (initial raw data and baseline subtracted are shown in Supporting Information). To avoid the influence of the baseline correction procedure on the dynamic behavior of the system, the region between 2080 and 2150 cm^{-1} , where the signal is observed, was removed for the fit. Our data show a ratio in the absorption cross section between the coordinated and docked CO of about 50, in agreement with previous findings.⁴³ Baseline problems are less significant in the bleaching region, which is free from water absorption. In this region, the amplitude of background fluctuation has a negligible influence on the kinetics (see Supporting Information for details).

As reported in Figure 3b, the dynamic evolution in the free CO absorption region matches that of the 1940 cm^{-1} bleaching, thus confirming that also the fast 250 ps component has to be ascribed to geminate recombination. At the early measured times a rise of the free CO absorption signal is observed, which can be fitted with a time constant of 30 ps. An initial rise component for a docked CO band has been previously observed also for myoglobin¹⁷ and interpreted in terms of protein relaxation around the photolyzed CO molecule. In that case however the rise component had a much faster time constant of about 1.6 ps. Furthermore thermal relaxation has also been observed to occur for myoglobin excited at 597 nm, with a time constant of 6.2 ps.⁴⁴ The longer time scale observed in this case for the rise component may indicate a combination of slower cooling process and/or a more significant protein rearrangement, possibly involving the rotation or reorientation of one or more amino acid side chains in the CO docking site. Such structural adjustment most likely modifies the electrostatic interactions around the CO molecule thus increasing the oscillator strength.⁴⁵ This is probably the consequence of a more flexible heme pocket structure, also brought out by the presence of a water molecule, which could rearrange by breaking/forming H-bonds with the tyrosine amino acids (TyrB10 and TyrCD1) located at a short distance from the heme.

Besides the 30 ps component, a global fit of the kinetic traces collected in the free CO region ($2050\text{--}2200\text{ cm}^{-1}$) results in two additional decay components, with time constants of 300 ps and 1.2 ns, respectively. These time constants qualitatively agree with those measured for the bleaching recovery, thus confirming that the process responsible for the dynamic evolution of the system is a fast geminate recombination of the photolyzed CO. The EADS obtained by globally analyzing the kinetic traces in the $2050\text{--}2150\text{ cm}^{-1}$ region with a sequential decay scheme are reported in the Supporting Information. To take into account of the bandwidth variation with time, we estimated the temporal evolution of the integrated area of the CO band, and we compared it with the kinetic trace at 2120 cm^{-1} , corresponding to band maximum. The two traces are qualitatively in good agreement (see Supporting Information).

The measured CO absorption peak is quite asymmetrical and has a rather large bandwidth (fwhm 30 cm^{-1}), which suggests

the presence of an inhomogeneous distribution of two unresolved bands behind the measured line shape. The signal dynamically evolves by slightly shifting to the blue, but no substantial line shape variations are observed. Although it has been shown that in similar systems a certain percentage (reported values span between 3.6 and 13%) of the photolyzed CO is initially in a vibrationally hot state^{13,14,17,19,46,47} no vibrational hot band could be resolved in the present case. Since the CO anharmonicity has been estimated to be $27\text{--}30\text{ cm}^{-1}$,⁴⁸ hot bands are probably not resolved due to baseline fluctuation problems.

Bacillus subtilis. Also in the case of Bs-trHb, time-resolved spectra in the bleaching region were collected by exciting the sample both with a 400 nm and a 550 nm laser pulse. Again, no significant differences were observed in the dynamic evolution of the system between the two excitation wavelengths. Following CO photodissociation, two bleaching bands are observed at 1925 cm^{-1} and 1888 cm^{-1} , respectively, whose positions well correspond with the measured FTIR spectrum of the CO adduct for this protein, see Figure 4a. The

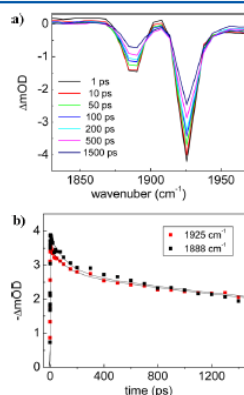


Figure 4. (a) Time resolved spectra recorded at different time delays, showing the bleaching induced in Bs-trHb in the $\nu(\text{CO})$ stretching region for the coordinated CO. Excitation wavelength was 550 nm. (b) Kinetic traces (scattered points) together with the fit (solid line) obtained by global analysis at selected frequencies, corresponding to the two maximum absorptions in the iron coordinated CO region. The trace at 1888 cm^{-1} has been scaled to overlap the trace at 1925 cm^{-1} .

corresponding kinetic traces, reported in Figure 4b can be fitted with two time constants of 120 ps and 2 ns, respectively. In contrast to what was observed in Tf-trHb, the two bleaching bands in Bs-trHb recover with the same kinetics. In this case the faster kinetic component has a very low weight, only accounting for less than 10% of the recombination dynamics for both bleaching bands, implying that the fraction of picosecond geminate recombination is lower than that observed in Tf-trHb. Fast geminate recombination in Bs-trHb has been previously observed through time-resolved measurements in the visible spectral range.⁵ In the present infrared measurements a 30 ps component, previously identified by transient absorption measurements in the visible region, is not observed. Since the currently probed spectral range is only sensitive to

CO vibrations, we conclude that this 30 ps component is not associated to fast ligand recombination, but probably represents a relaxation process of the heme.

The free CO region was probed by exciting the sample at 550 nm. The time-resolved spectra in this region are qualitatively similar for both proteins, but striking differences are observed in their kinetics. Also for Bs-trHb only one band is observed, whose dynamic evolution follows that of the bleaching signals, though with minor intensity. The peak shape of the docked CO is not completely symmetrical and the fwhm is about 30 cm^{-1} . Time resolved spectra of the free CO in Bs-trHb, shown in Figure 5a, show a blue shift on a 10 ps

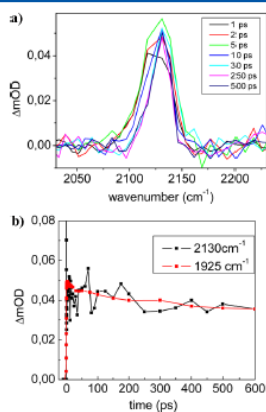


Figure 5. (a) Time resolved spectra in the free CO region recorded at different time delays after excitation of the sample with a 550 nm laser pulse; (b) Kinetic traces at 2130 cm^{-1} (black line), corresponding to the maximum absorption in the free CO region in Bs-TrHb. The trace has been superimposed with the kinetic trace at 1925 cm^{-1} (red line), corresponding to the maximum absorption of the coordinated CO.

time scale, which could be an indication for vibrational cooling. Alternatively there could be two bands hidden under the observed line shape, with a population exchange occurring on this time scale. Given the low signal-to-noise ratio of the measurements, these observations have to be considered with care, and in order to better rationalize this spectral evolution, measurements should be repeated with a higher spectral resolution.

The kinetic trace for the maximum of the absorption band, compared with that of the scaled bleaching trace measured at 1925 cm^{-1} is reported in Figure 5b. In Figure 6, the kinetic traces corresponding to the maximum absorption of the free CO band are compared for the two analyzed proteins. The observed signals bring out clearly a more intense slow phase and a faster decay in the case of Tf-trHb with respect to Bs-trHb.

DISCUSSION

The possibility to follow CO recombination dynamics in the infrared spectral window, after photolysis induced by a short laser pulse, provides unique information about the influence of structural and electrostatic properties of the distal heme pocket

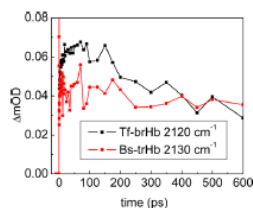


Figure 6. Kinetic trace at 2120 cm^{-1} recorded at the maximum absorption in the free CO region in Tf-trHb (black line) compared with the corresponding kinetic trace measured in Bs-trHb at 2130 cm^{-1} (red line).

on the ligand dissociation and rebinding processes occurring in globin proteins. While pump-probe measurements in the visible spectral range give only indirect information on the recombination dynamics, since they can only probe the evolution in the electronic state of the heme moiety after excitation, measurements in the infrared are much more specific, since they can probe the dynamics of the vibrational bands of the ligand before and after photolysis, thus providing a direct snapshot of the transient state of the photolyzed CO molecule. In this work we have shown that, in the case of Bs-trHb, the infrared probe has allowed the unambiguous assignment of a 30 ps component previously identified by visible transient absorption measurements.³ The absence of this kinetic component in the current measurements within the infrared spectral range, leads to the conclusion that it is not associated to fast ligand recombination, but most likely represents a relaxation process of the heme.

Furthermore, important information on the influence of the distal pocket structure on the recombination dynamics can be retrieved with this technique. In this study we have compared two truncated hemoglobins, *Thermobifida fusca* and *Bacillus subtilis*, whose distal heme pockets, shown in Figure 1, are at a first sight very similar.

Despite the structural similarities in the architecture of the heme pocket, Tf-trHb and Bs-trHb display significant differences in the dynamics of ligand exchange and rebinding. Present results indicate that although both proteins show fast geminate recombination, the relative amount of the picosecond dynamic phase is not the same. To highlight these differences we have compared in Figure 7a and 7b the kinetic traces measured for the two bleaching bands of Tf-trHb (1940 and 1920 cm^{-1}) with the corresponding bands observed for Bs-trHb (1925 and 1988 cm^{-1}).

For both proteins two different conformations have been identified on the basis of FTIR measurements, herein referred as an "open" conformation, characterized by a single amino acid H-bonded to the ligand and a "closed" conformation, characterized as having two H-bonded residues.^{3,10}

In the case of Tf-trHb, the dynamics of bleaching recovery of the open and closed conformations are different. The open conformation, responsible for the infrared band at 1940 cm^{-1} substantially recovers with a fast 250 ps component, while for the closed one, the picosecond component only accounts for a minor fraction of signal recovery.

It is commonly accepted in the literature that the presence of H-bonds between the residues in the distal pocket and the heme bound CO favors the occurrence of fast recombination.

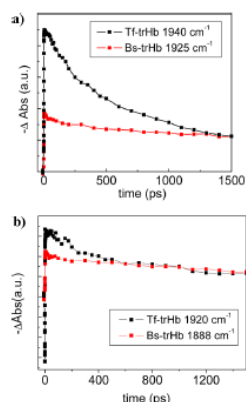


Figure 7. Comparison between the kinetic traces in the bleaching region for Tf-trHb and Bs-trHb upon excitation at 550 nm. (a) Trace at 1940 cm^{-1} of Tf-trHb (black line) compared to the trace at 1925 cm^{-1} of Bs-trHb (red line). The two kinetic traces have been scaled to overlap on the long time scale. (b) The 1920 cm^{-1} of Tf-trHb (black line) compared to the trace at 1925 cm^{-1} of Bs-trHb (red line).

For instance it was recently shown that in the oxygen sensory protein FixL, the introduction of a residue capable of forming H-bonds with the iron bound CO, through the mutation R220H, determines the occurrence of substantial contribution to geminate recombination on a 250 ps time scale.^{14,48}

On that basis one would expect to observe a substantial amount of picosecond geminate recombination also in Bs-trHb, since, for this protein, the highly downshifted $\nu(\text{CO})$ stretching measured by FTIR indicated the presence of strong H-bonds between the iron coordinated CO and the residues in the distal pocket. Nevertheless our results show that only a minor fraction of the photolyzed CO, corresponding to less than 10% of the total, recombines with a 120 ps kinetics. The fraction of the fast dynamic phase is the same for both the open and closed conformations of the protein, being thus independent of the number of H-bonds formed by the coordinated ligand. We also note that, in Tf-trHb, the higher fraction of fast recombination is observed in the open conformation, that is, the one with only one H-bond and not, as it would be expected at a first sight, when both TyrCD1 and TrpG8 are H-bonded to the coordinated CO. A similar behavior has been observed in the case of myoglobin, in which time-resolved infrared spectra measured at low temperature showed the appearance of two bleaching bands (at 1944 and 1926 cm^{-1}), recovering on a different time scale. Even in this case the higher frequency band, corresponding to an open configuration, recovers faster than the low frequency one, like in Tf-trHb.¹²

Therefore it appears that a simple structural analysis only accounting for the number of hydrogen bond interactions of the iron coordinated ligand is not sufficient to interpret the kinetic differences observed among different globin proteins.

By comparing the behavior of the two truncated hemoglobins here studied, it can be suggested that one of the main factors influencing the amount of fast geminate recombination is the structural flexibility of the heme pocket.

The steric hindrance of the residues surrounding the ligand, which can act as a cage confining the CO in the docking site, avoids its escape toward the solvent. If the docking site of the photolyzed CO is sufficiently large, because of the presence of smaller residues in the distal pocket, the recombination is slower. On the contrary if bulky residues impair ligand escape, the CO molecule may possibly recombine with the iron atom on a faster time scale.

These observations are still not sufficient to explain the different dynamics observed for the two conformations of Tf-trHb. In this protein, the residue TyrCD1, which in the closed conformation is at H-bond distance from the iron coordinated CO, is believed to have a high structural flexibility, being alternatively capable of forming a H-bond either with a water molecule localized in its proximity or with the ligated CO. It would be expected that, when this residue is rotated toward the ligand, as in the closed conformation, it would prevent the photolyzed CO from escaping far from the heme. In the open conformation TyrCD1 is rotated away from the ligand instead, so it may allow the CO molecule to move further away from the heme upon photolysis. In contrast, in the experimental conditions used in this work, we observe a faster rebinding for the open conformation. This may indicate that the differences among the two protein conformations can involve more rearrangements than TyrCD1 rotation. One possibility is that when TyrCD1 is rotated away from the ligand, the conserved water molecule located in the distal site assumes a position such to block the CO exit. Alternatively there could be rearrangements in the position of other residues, not identified in the currently available crystal structure, acquired without coordinated CO,⁸ which eventually make the open conformation even more restrained than the closed one. It thus appears that in case of this protein it is not totally correct to refer to the two conformations as open or closed, only considering the number of hydrogen bonds formed with the iron-bound CO, while it would be more appropriate to identify them as a less constraining and more constraining conformation.

For Bs-trHb we have described until now the closed conformation as the one where both TrpG8 and TyrB10 are H-bonded to the ligand, and the open conformation as the one where only the H-bond with TrpG8 is maintained. In this case there is little difference in the dynamics of CO recombination between them. Possibly, the configuration adopted by TrpG8 and the other pocket residues is not very different for the two conformations, so that the volume of the docking cavity remains always similar. Furthermore the other residue which in the distal pocket of Bs-trHb is located at a short distance from the coordinated CO is GlnE11, whose hindrance is certainly lower if compared to that of TyrB10, which in Tf-trHb is also at short distance from the CO, besides TrpG8 and TyrCD1. It is worth noting that the importance of GlnE11 in stabilizing the coordinated ligand in Bs-trHb has been recently highlighted. According to molecular dynamic simulations, GlnE11 can adopt two different conformations, forming a H-bond alternatively either with the iron-bound CO or with TyrB10.⁴⁹ By switching among these two conformations, GlnE11 would open a cavity directly connecting the heme distal pocket with the solvent, thus favoring ligand escape. This finding would explain the high oxygen affinity observed for Bs-trHb and strengthen the suggestion that the volume of the heme cavity and its structural flexibility have a strong influence on the fraction of fast geminate recombination.⁴⁹ Compared to Tf-trHb, in this case there is less protein reorganization after

photolysis, possibly because the docking site is already sufficiently large to accommodate the dissociated ligand, due to the topological substitution between TyrCD1 with PheCD1 and LeuE11 with GlnE11. A lower degree of protein rearrangement induced by the ligand dissociation could also explain the absence of a rise component in the kinetics of the photodissociated CO.

Similar considerations regarding the caging effect^{50,51} played by the amino-acid residues surrounding the photolyzed CO can also be applied to other recently studied systems. Picosecond geminate recombination has also been found in the CO complex of nonglobin proteins, such as microperoxidase and in the chemically modified form of cytochrome *c*, termed carboxymethyl cytochrome *c*.⁵² In the former system a time constant of 110 ps has been estimated for concentrated samples,⁵³ while in the latter system a multiphasic recombination with time constant of 16 ps, 120 ps, and 1 ns has been measured.⁵⁴ The authors attributed the three phases to CO rebinding from different locations within the distal pocket site. The high efficiency of the ligand rebinding has been interpreted even in this case as a consequence of a sterically hindered and "caged" nature of the distal heme pocket, from which it is difficult for the ligand to escape. In these systems, the short time scale of the geminate rebinding has been correlated to a protein configuration that assures the restraint of the reorganization energy of the active site.⁵⁴

As a final comment, it should be pointed out that the kinetic analysis presented until now does not take into account that a fraction of the photolyzed CO escapes to the solvent, and recombines on a much slower time scale with a bimolecular process. A direct estimation of the relative amount of geminate and bimolecular recombination would require following the system dynamics on a time scale spanning from picoseconds to milliseconds, which is not feasible with the currently used experimental set up. However, it is possible to have an estimate of the amount of geminate recombination occurring on the picoseconds time scale by evaluating the ratio between the areas of the EADS obtained by global analysis. In the case of Tf-trHb it can be estimated that about 40% of CO undergoes picosecond geminate recombination. The evaluation of kinetic component in the nanosecond regime is affected by a large (~20%) indeterminateness due to the lack of data regarding the bimolecular recombination.

CONCLUSIONS

Time resolved vibrational spectroscopy, employed to study carbon monoxide photodissociation and rebinding in two truncated hemoglobins, has revealed key structural and dynamic properties of the ligand binding process in these unusual globins. The results of this study highlight striking differences between the dynamics of CO recombination in the truncated hemoglobins with respect to other globins, such as vertebrate myoglobins and hemoglobins. Both the truncated hemoglobins from *Thermobifida fusca* and *Bacillus subtilis* exhibit subnanosecond multiexponential geminate recombination, which account for at least 50% of the total yield of CO recombination. Several conserved residues in the distal heme pocket of both the analyzed proteins, capable of interacting with the iron coordinated ligand through the formation of H-bonds, acts as a cage on the dissociated CO, preventing its escape toward the solvent and confining it in the heme cavity, thus favoring fast rebinding. This effect is even more pronounced in the case of Tf-trHb, where at least 40% of

geminate recombination occurs in less than 300 ps. The occurrence of fast geminate rebinding and the differences in the CO rebinding kinetics registered for two apparently similar proteins highlight the strong influence played by the structural organization of the distal heme pocket and the interactions among the protein and the heme-ligand complex. Globin proteins are not the only example where such an effect is observed. Other systems where protein ligand interactions can have a strong influence on the photodynamics are found for instance in the rhodopsin family, where strong differences in the dynamics of retinal photoisomerization have been measured between visual pigments and microbial rhodopsin.⁵⁵ It is evident that a detailed understanding of such interactions is necessary in order to completely characterize the photodynamics of these systems. Regarding the two proteins analyzed in this study, further analysis on site directed mutants will allow an even more accurate characterization of the specific interactions of each of the residues present in the distal pocket with the ligand, which will eventually help to clarify the behavior of these proteins in their living environment.

ASSOCIATED CONTENT

Supporting Information

Baseline subtraction procedure for data at 2050–2150 cm^{-1} ; EADS of time-resolved data in the free CO absorption region; influence of the baseline in the bleaching region; comparison between the kinetics at 2120 cm^{-1} ; and the time dependence of the integrated area of the CO band. This material is available free of charge via the Internet at <http://pubs.acs.org>.

AUTHOR INFORMATION

Author Contributions

†These two authors have equally contributed to this work

Notes

The authors declare no competing financial interest.

ACKNOWLEDGMENTS

The authors acknowledge the Italian 'Ministero dell'Istruzione dell'Università e della Ricerca' (PRIN 2008, 2008BFJ34R) and Istituto Pasteur Fondazione Cenci Bolognietti. A.L. and A.M. acknowledge the financial support of the Regione Toscana through the found POR FSE 2007-2013 obiettivo 2 asse IV, project EPHODS. The financial support of the Cassa di Risparmio di Firenze is also gratefully acknowledged.

REFERENCES

- Wittenberg, J. B.; Bolognesi, M.; Wittenberg, B. A.; Guertin, M. *J. Biol. Chem.* **2002**, *277* (2), 871–874.
- Wu, G.; Wainwright, L. M.; Poole, R. K., Microbial globins. In *Advances in Microbial Physiology*, Academic Press: 2003; Vol. 47, pp 255–310.
- Feis, A.; Lapini, A.; Catacchio, B.; Brogioni, S.; Foggi, P.; Chiancone, E.; Boffi, A.; Smulevich, G. *Biochemistry* **2007**, *47* (3), 902–910.
- Guallar, V.; Lu, C.; Borrelli, K.; Egawa, T.; Yeh, S.-R. *J. Biol. Chem.* **2009**, *284* (5), 3106–3116.
- Ouellet, H.; Milani, M.; LaBarre, M.; Bolognesi, M.; Couture, M.; Guertin, M. *Biochemistry* **2007**, *46* (41), 11440–11450.
- Milani, M.; Pesce, A.; Nardini, M.; Ouellet, H.; Oudlet, Y.; Devilde, S.; Bocedi, A.; Ascenzi, P.; Guertin, M.; Moens, L.; Friedman, J. M.; Wittenberg, J. B.; Bolognesi, M. *J. Inorg. Biochem.* **2005**, *99* (1), 97–109.
- Pesce, A.; Nardini, M.; Milani, M.; Bolognesi, M. *IUBMB Life* **2007**, *59* (8–9), 535–541.

- (8) Bonamore, A.; Ilari, A.; Giangiacomo, L.; Bellelli, A.; Morea, V.; Boffi, A. *FEBS J.* **2005**, *272* (16), 4189–4201.
- (9) Giangiacomo, L.; Ilari, A.; Boffi, A.; Morea, V.; Chiancone, E. *J. Biol. Chem.* **2005**, *280* (10), 9192–9202.
- (10) Droghe, E.; Nicoletti, F. P.; Bonamore, A.; Boechi, L.; Arroyo Manfrez, P.; Estrin, D. A.; Boffi, A.; Smulevich, G.; Feis, A. *Biochemistry* **2010**, *49* (49), 10394–10402.
- (11) Yoshimura, H.; Yoshioka, S.; Kobayashi, K.; Ohta, T.; Uchida, T.; Kubo, M.; Kitagawa, T.; Aono, S. *Biochemistry* **2006**, *45* (27), 8301–8307.
- (12) Frauenfelder, H.; McMahon, B. H.; Fenimore, P. W. *Proc. Natl. Acad. Sci.* **2003**, *100* (15), 8615–8617.
- (13) Lim, M.; Jackson, T. A.; Anfinrud, P. A. *J. Chem. Phys.* **1995**, *102*, 4355–4366.
- (14) Nuernberger, P.; Lee, K. F.; Bonvalet, A.; Bouzahir-Sima, L.; Lambry, J.-C.; Liebl, U.; Joffre, M.; Vos, M. H. *J. Am. Chem. Soc.* **2011**, *133* (43), 17110–17113.
- (15) van Wilderen, L. J. G. W.; Key, J. M.; Van Stokkum, I. H. M.; van Grondelle, R.; Groot, M. L. *J. Phys. Chem. B* **2008**, *113* (11), 3292–3297.
- (16) Kim, S.; Lim, M. *J. Am. Chem. Soc.* **2005**, *127* (16), 5786–5787.
- (17) Lim, M.; Jackson, T. A.; Anfinrud, P. A. *Nat. Struct. Mol. Biol.* **1997**, *4* (3), 209–214.
- (18) Nienhaus, K.; Dominici, P.; Astegno, A.; Abbruzzetti, S.; Viappiani, C.; Nienhaus, G. U. *Biochemistry* **2010**, *49* (35), 7448–7458.
- (19) Polack, T.; Ogilvie, J. P.; Franzen, S.; Vos, M. H.; Joffre, M.; Martin, J. L.; Alexandrou, A. *Phys. Rev. Lett.* **2004**, *93* (1), 018102.
- (20) Touron Touceda, P.; Mosquera Vázquez, S.; Lima, M.; Lapini, A.; Foggi, P.; Dei, A.; Righini, R. *Phys. Chem. Chem. Phys.* **14** (2), 1038–1047.
- (21) Afrawal, G. P.; Baldeck, P. L.; Alfano, R. R. *Phys. Rev. A* **1989**, *40*, 5063–5072.
- (22) Hamm, P. *Chem. Phys.* **1995**, *200* (3), 415–429.
- (23) Wynne, K.; Hochstrasser, R. M. *Chem. Phys.* **1995**, *193* (3), 211–236.
- (24) Lian, T.; Kholodenko, Y.; Locke, B.; Hochstrasser, R. M. *J. Phys. Chem.* **1995**, *99* (19), 7272–7280.
- (25) Lapini, A.; Mosquera Vázquez, S.; Touron Touceda, P.; Lima, M. *J. Mol. Struct.* **2011**, *993* (1–3), 470–473.
- (26) Hendler, R. W.; Shrager, R. I. *J. Biochem. Biophys. Methods* **1994**, *28* (1), 1–33.
- (27) Henry, E. R. *Biophys. J.* **1997**, *72* (2), 652–673.
- (28) Henry, E. R.; Hofrichter, J.; Ludwig Brand, M. L. J. Singular value decomposition: Application to analysis of experimental data. In *Methods Enzymology*; Academic Press: San Diego, CA, 1992; Vol. 210, pp 129–192.
- (29) Dioumaev, A. K. *Biophys. Chem.* **1997**, *67*, 1–25.
- (30) Bonneau, R.; Wirz, J.; Zuberbühler, A. D. *Pure Appl. Chem.* **1997**, *69*, 979–992.
- (31) Henry, E. R. *Biophys. J.* **1997**, *72*, 652–673.
- (32) Franzen, S.; Kiger, L.; Poyart, C.; Martin, J. L. *Biophys. J.* **2001**, *80*, 2372–2385.
- (33) van Stokkum, I. H. M.; Scherer, T.; Brouwer, A. M.; Verhoeven, J. W. *J. Phys. Chem.* **1994**, *98* (3), 852–866.
- (34) van Stokkum, I. H. M.; Larsen, D. S.; van Grondelle, R. *Biochim. Biophys. Acta* **2004**, *1657*, 82.
- (35) Satzger, H.; Zinth, W. *Chem. Phys.* **2003**, *295* (3), 287–295.
- (36) Neumann, K.; Verhoeven, M.-K.; Weber, I.; Glaubitz, C.; Wachtveitl, J. *Biophys. J.* **2008**, *94* (12), 4796–4807.
- (37) Mullen, K. M.; van Stokkum, I. H. M. *J. Stat. Software* **2007**, *18* (1), 1–5.
- (38) Mullen, K. M.; van Stokkum, I. H. M. *J. Stat. Software* **2007**, *18* (3), 1–46.
- (39) Cador, O.; Chabre, F.; Dei, A.; Sangregorio, C.; Slagere, J. V.; Vaz, M. G. F. *Inorg. Chem.* **2003**, *42* (20), 6432–6440.
- (40) Snellenburg, J. J.; Liptonok, S. P.; Seger, R.; Mullen, K. M.; van Stokkum, I. H. M. Glotaran: A Java-Based Graphical User Interface for the R Package TIMP; *Journal of Statistical Software*, **49** (3), 1–22, <http://www.jstatsoft.org/v49/i03/>.
- (41) Lim, M.; Jackson, T. A.; Anfinrud, P. A. *J. Am. Chem. Soc.* **2004**, *126* (25), 7946–7957.
- (42) Moore, J. N.; Hansen, P. A.; Hochstrasser, R. M. *Proc. Natl. Acad. Sci.* **1988**, *85* (14), 5062–5066.
- (43) Anfinrud, P. A.; Han, C.; Hochstrasser, R. M. *Proc. Natl. Acad. Sci.* **1989**, *86* (21), 8387–8391.
- (44) Lim, M.; Jackson, T. A.; Anfinrud, P. A. *J. Phys. Chem.* **1996**, *100* (29), 12043–12051.
- (45) Hush, N. S.; Williams, M. L. *J. Mol. Spectrosc.* **1974**, *50*, 349–368.
- (46) Sagnella, D. E.; Straub, J. E.; Jackson, T. A.; Lim, M.; Anfinrud, P. A. *Proc. Natl. Acad. Sci.* **1999**, *96* (25), 14324–14329.
- (47) Nuernberger, P.; Lee, K. F.; Bonvalet, A.; Vos, M. H.; Joffre, M. *J. Phys. Chem. Lett.* **2010**, *1* (14), 2077–2081.
- (48) Jasaitis, A.; Hola, K.; Bouzahir-Sima, L.; Lambry, J.-C.; Balland, V.; Vos, M. H.; Liebl, U. *Biochemistry* **2006**, *45* (19), 6018–6026.
- (49) Boechi, L.; Mañez, P. A.; Luque, F. J.; Marti, M. A.; Estrin, D. A. *Proteins: Struct., Funct., Bioinform.* **2010**, *78* (4), 962–970.
- (50) Grogan, T. G.; Bag, N.; Traylor, T. G.; Magde, D. *J. Phys. Chem.* **1994**, *98* (51), 13791–13796.
- (51) Jasaitis, A.; Ouellet, H.; Lambry, J.-C.; Martin, J.-L.; Friedman, J. M.; Guertin, M.; Vos, M. H. *Chem. Phys.* **2012**, *396*, 10–16.
- (52) Kim, J.; Park, J.; Lee, T.; Lim, M. *J. Phys. Chem. B* **2008**, *113* (1), 260–266.
- (53) Lim, M.; Jackson, T. A.; Anfinrud, P. A. *J. Biol. Inorg. Chem.* **1997**, *2*, 531–536.
- (54) Silkstone, G.; Jasaitis, A.; Vos, M. H.; Wilson, M. T. *Dalton Trans.* **2005**, *21*, 3489–3494.
- (55) Wand, A.; Rozin, R.; Eliash, T.; Jung, K.-H.; Sheves, M.; Ruhman, S. *J. Am. Chem. Soc.* **2011**, *133* (51), 20922–20932.



H-bonding networks of the distal residues and water molecules in the active site of *Thermobifida fusca* hemoglobin[☆]

Francesco P. Nicoletti^a, Enrica Droghetti^a, Barry D. Howes^a, Juan P. Bustamante^b,
Alessandra Bonamore^c, Nataschia Sciamanna^c, Dario A. Estrin^b, Alessandro Feis^a,
Alberto Boffi^c, Giulietta Smulevich^{a,*}

^a Dipartimento di Chimica "Ugo Schiff", Università di Firenze, Via della Lastruccia 3-73, I-50019 Sesto Fiorentino (FI), Italy

^b Departamento de Química Inorgánica, Analítica y Química Física, INQUIMAE-CONICET, Facultad de Ciencias Exactas y Naturales, Universidad de Buenos Aires, Ciudad Universitaria, Pabellón II, Buenos Aires C1428EHA, Argentina

^c Institute Pasteur, Fondazione Conci Bonagatti, Department of Biochemical Sciences and CNR, Institute of Molecular Biology and Pathology, University of Rome "La Sapienza", Piazzale Aldo Moro 5, I-00185 Rome, Italy

ARTICLE INFO

Article history:

Received 10 January 2013

Received in revised form 19 February 2013

Accepted 22 February 2013

Available online 5 March 2013

Keywords:

Hydroxyl ligand

Cyanide ligand

Hydrogen-bond

Resonance Raman

Truncated hemoglobin

ABSTRACT

The ferric form of truncated hemoglobin II from *Thermobifida fusca* (Tf-trHb) and its triple mutant WGBF-YB10F-YCD1F at neutral and alkaline pH, and in the presence of CN⁻ have been characterized by resonance Raman spectroscopy, electron paramagnetic resonance spectroscopy, and molecular dynamics simulations. Tf-trHb contains three polar residues in the distal site, namely TrpG8, TyrCD1 and TyrB10. Whereas TrpG8 can act as a potential hydrogen-bond donor, the tyrosines can act as donors or acceptors. Ligand binding in heme-containing proteins is determined by a number of factors, including the nature and conformation of the distal residues and their capability to stabilize the heme-bound ligand via hydrogen-bonding and electrostatic interactions. Since both the RR Fe–OH⁺ and Fe–CN⁻ frequencies are very sensitive to the distal environment, detailed information on structural variations has been obtained. The hydroxyl ligand binds on the WT protein giving rise to two different conformers. In form 1 the anion is stabilized by H-bonds with TrpG8, TyrCD1 and a water molecule, in turn H-bonded to TyrB10. In form 2, H-bonding with TyrCD1 is mediated by a water molecule. Unlike the OH⁻ ligand, CN⁻ binds both WT and the triple mutant giving rise to two forms with similar spectroscopic characteristics. The overall results clearly indicate that H-bonding interactions both with distal residues and water molecules are important structural determinants in the active site of Tf-trHb. This article is part of a Special Issue entitled: Oxygen Binding and Sensing Proteins.

© 2013 Elsevier B.V. All rights reserved.

1. Introduction

Ligand binding in heme-containing proteins is determined by a number of factors, including the nature and conformation of the distal residues and their capability to stabilize the heme-bound ligand via hydrogen-bonding and electrostatic interactions. The truncated hemoglobin II from *Thermobifida fusca* (Tf-trHb) contains three polar residues in the distal site: TrpG8, TyrCD1 and TyrB10. Whereas TrpG8 can act as

a potential hydrogen-bond donor, the tyrosines can act as donors or acceptors.

The ferric and ferrous derivatives of truncated hemoglobins, analogous to mammalian globins, bind a variety of small molecules, such as H₂O, NO, CN⁻, F⁻, and CO. Previous studies carried out on the CO [1], F⁻ [2,3] and HS⁻ [4] adducts formed with the native Tf-trHb and a combinatorial set of mutants, in which the three distal amino acids have been singly, doubly, or triply replaced by a Phe residue, revealed that all the ligands are stabilized by TrpG8 via a strong H-bond. TyrCD1 is able to interact with CO and fluoride, whereas TyrB10 is not directly involved in ligand stabilization and plays only a minor role.

In the present work we have extended the analysis to the ferric form, studying the behavior of the ferric native protein and its triple mutant WGBF-YB10F-YCD1F at neutral and alkaline pH, and in the presence of CN⁻. Since both the RR Fe–OH⁺ and Fe–CN⁻ frequencies are very sensitive to the distal environment, detailed information on structural variations can be obtained. In particular, the comparison of the spectroscopic signature of the OH⁻ ligated proteins at alkaline pH with those of the cyanide adducts is expected to provide information

Abbreviations: trHb, truncated hemoglobin; Tf, *Thermobifida fusca*; Hb, hemoglobin; WT, wild type; ASV, acidic surface variant of Tf-trHb containing two single-site mutations Phe107Glu and Arg31Glu; Mb, myoglobin; MES, 2-(N-morpholino)ethanesulfonic acid; MD, molecular dynamics; EPR, electron paramagnetic resonance; RR, resonance Raman; 5c, five-coordinate; 6c, six-coordinate; HS⁻, high spin; LS, low spin.

[☆] This article is part of a Special Issue entitled: Oxygen Binding and Sensing Proteins.

* Corresponding author. Tel.: +39 055 457 3083; fax: +39 055 457 3077.

E-mail address: giulietta.smulevich@unifi.it (G. Smulevich).

on the effects of H-bond interactions between the ligand and the distal residues as well on the Fe–CN geometry.

2. Material and methods

2.1. Sample preparation

Wild type (WT) Tf-trHb was expressed as a recombinant protein in *Escherichia coli* cells and purified as described previously [5]. As previously reported [1] the acidic surface variant (ASV) of Tf-trHb differs from the WT protein by mutation of both Phe107 and Arg91 to glutamic acid, which increases protein solubility during recombinant expression, without affecting thermostability or ligand binding properties [1–3]. Therefore, ASV was taken as an engineered scaffold of the WT protein for subsequent site-directed mutagenesis studies on the relevant residues of the distal heme pocket.

Phosphate salts and glycine were obtained from Merck AG (Darmstadt, Germany). 2-[N-morpholino]ethanesulfonic acid (MES) was bought from Sigma-Aldrich (Steinheim, Germany). All chemicals were of analytical or reagent grade and were used without further purification. The cyanide complexes were prepared by adding a few microliters of a diluted solution of potassium cyanide to the ferric proteins (ASV and triple mutant). Buffered solutions (0.1 M) were used for experiments at pH 9.8–10.1 (glycine), 7.0 (phosphate), and 6.1 (MES).

Protein concentrations in the range 10–70 μM were used for the electronic absorption and RR samples. Sample concentration for low-temperature RR was between 30 and 100 μM . Sample concentrations for electron paramagnetic resonance (EPR) experiments were in the range 130–600 μM .

The protein concentration was determined on the CO derivative in the presence of 10–20 mM sodium dithionite by using an extinction coefficient of $174000 \text{ M}^{-1} \text{ cm}^{-1}$ for Tf-trHb.

2.2. Spectroscopic characterization

Electronic absorption spectra, measured with a double-beam spectrophotometer (Varian Cary 5), were recorded using a 1 cm quartz cuvette and a 600 nm/min scan rate. Absorption spectra (using a 5-mm NMR tube) were measured both prior to and after RR measurements to ensure that no degradation had taken place under the experimental conditions used. RR spectra were measured with excitation at 413.1 nm (Kr⁺ laser, Coherent, Innova 300C) using a triple spectrometer (consisting of two Acton Research SpectraPro 2300i working in the subtractive mode, and a SpectraPro 2500i in the final stage with a 3600 grooves/mm grating), equipped with a liquid-nitrogen cooled CCD detector (Roper Scientific Princeton Instruments). RR spectra were calibrated with indene, n-pentane, and carbon tetrachloride as standards to an accuracy of 1 cm^{-1} for intense isolated bands.

The low-temperature experiments were carried out using an Air Products Displex closed-cycle He refrigerator with automatic temperature control. For the low-temperature RR measurements, 20 μl of the protein solution was deposited on the copper cold finger of the refrigerator at 90 K under a nitrogen flow. The temperature was then slowly decreased to 12 K under vacuum, and RR spectra were obtained at this temperature.

All RR measurements were repeated several times under the same conditions to ensure reproducibility. To improve the signal-to-noise ratio, a number of spectra were accumulated and summed only if no spectral differences were noted. All spectra were baseline corrected. To determine peak bandwidth and positions, a curve-fitting program (Lab Calc; Galactic) was used to simulate the spectra using a Lorentzian line shape. The frequencies of the bands were optimized with an accuracy of 1 cm^{-1} , and the bandwidths with an accuracy of 0.5 cm^{-1} . Bandwidths (full width at half-maximum) varied as follows: 12–14 cm^{-1} in the high frequency region; 9–12 cm^{-1} for the low frequency region.

EPR spectra were recorded as reported previously [6] and the g-values were determined by careful visual inspection of the spectra.

2.3. Molecular dynamics simulations

The simulations were performed starting from the crystal structure of WT Tf-trHb determined at 2.48 Å resolution, Protein Data Bank (PDB) entry 2BMM [5]. Two different systems of protein-ligand complexes, with a water or hydroxide ligand bound to the heme group, were built and simulated. The water molecule was added in the distal site bound to Fe(III) according to the equilibrium structure in an isolated model system QM calculation at the DFT level (with the PBE functional and 6–31 G** basis sets), taking into account the distal site environment. The charges and parameters for Fe(III) heme – water molecule were determined by a standard procedure: partial charges were computed using the restricted electrostatic potential (RESP) recipe and DFT electronic structure calculations with the PBE functional and 6–31 G** basis sets. The calculation has been performed in the high spin (HS) state. Equilibrium distances and angles, as well as force constants, were computed using the same methods and basis set used for computed charges. The same procedure was used for the hydroxide ligand. The parm99 force field implemented in AMBER was used to describe the protein [7]. The system was then immersed in a pre-equilibrated octahedral box of 4909 TIP3P water molecules using the tLEaP module of the AMBER package [7]. We used periodic boundary conditions with a 9 Å cutoff and Ewald sums for treating long-range electrostatic interactions. The SHAKE algorithm [8] was used to keep bonds involving H atoms at their equilibrium length, allowing us to use a 2 fs time step for the integration of Newton's equations. The histidine tautomeric state and protonation (Ne-H, N δ -H, His⁺) were carefully analyzed for each of the three His residues (namely His99, His122, and His135) and set to favor the hydrogen bond network suggested by the experimental crystal structure. Equilibration protocol consisted of (i) slowly heating the whole system from 0 to 300 K for 20 ps at constant volume, with harmonic restraints of 80 Kcal per mol Å² for all C α atoms; (ii) pressure equilibration of the entire system simulated for 1 ns at 300 K with the same restrained atoms. After these two steps unconstrained 30 ns of molecular dynamics (MD) simulations at constant temperature (300 K) were performed. To simulate the triple mutant (YB10F-YCD1F-WG8F) protein, we introduced *in silico* mutations by changing the corresponding amino acid in the original structure and allowing the system to equilibrate as mentioned earlier. All structures were found to be stable during the timescale of the simulations, as evidenced by the root mean square displacements (RMSD), depicted in Fig. S1, Supplementary data.

3. Results

3.1. Hydroxyl ligand

Fig. 1 shows the UV-vis titration and the RR spectra in the high frequency region of Tf-trHb between pH 6.1 and 10.1, together with the corresponding spectra of the triple mutant at neutral pH. In this pH range Tf-trHb undergoes coordination and spin state changes. At acidic pH the absorption spectrum shows a Soret band at 407 nm (409 nm at neutral pH), Q bands at 498, 541 and 577 nm, and a broad CT band centered at 634 nm. The corresponding RR spectrum clearly indicates that at low pH the protein is a mixture of three species, an aquo 6cHS (ν_2 at 1480 cm^{-1} , ν_2 at 1563 cm^{-1}), a 6dLS (ν_2 at 1503 cm^{-1} , ν_2 at 1579 cm^{-1} , ν_{10} at 1638 cm^{-1}) and a small amount of 5cHS form (ν_2 at 1489 cm^{-1} and ν_2 at 1570 cm^{-1}). At alkaline pH the 5cHS species disappears, and, similar to Hb and Mb [9], the absorption spectrum becomes typical of a hydroxo complex characterized by a mixture of 6cHS and 6dLS species with the Soret band at 413 nm, Q bands at 545 and 577 nm, and a shoulder at about 609 nm due to the CT1 band. Accordingly, at alkaline pH, in the high frequency RR region two sets of core size marker bands are found, corresponding to a

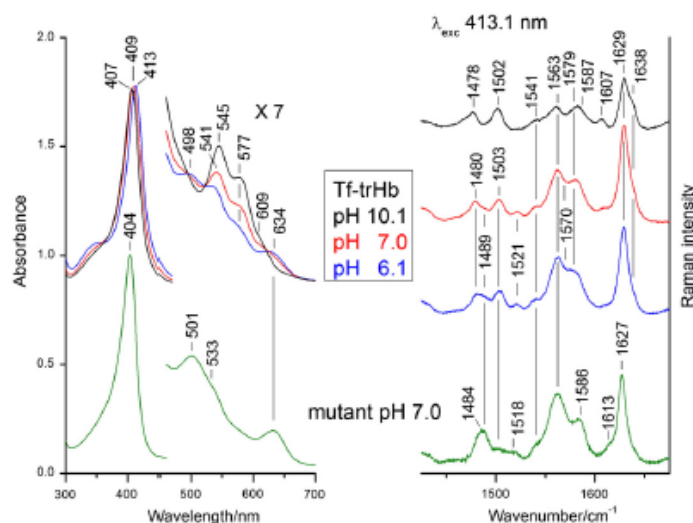


Fig. 1. UV-Vis titration (left) and RR spectra (right) in the high frequency region of Tf-trHb at pH 6.1, 7.0, and 10.1, together with the corresponding spectra of the triple Y810F-YCD IF-WGRF mutant at neutral pH. Left: the region between 400 nm and 700 nm has been expanded seven-fold. Right: 413.1 nm laser excitation; 1 cm^{-1} spectral resolution. Experimental conditions: Tf-trHb: 10 mW laser power at the sample; average of 3 spectra (pH 6.1 and 7.0) and 2 spectra (pH 10.1) with 240 s integration time; Triple mutant: 15 mW laser power at the sample; average of 3 spectra with 360 s integration time. A baseline has been subtracted from all spectra. Spectra have been shifted along the ordinate axis to allow better visualization.

hydroxo 6cHS (ν_1 at 1478 cm^{-1} , ν_2 at 1563 cm^{-1} , ν_{17} at 1587 cm^{-1}) and 6cLS (ν_1 at 1502 cm^{-1} , ν_2 at 1579 cm^{-1} , ν_{17} at 1607 cm^{-1} , ν_{10} at 1638 cm^{-1}). The two forms, existing in a thermal spin-state equilibrium at room temperature, convert to almost a pure 6cLS heme at 15 K (ν_1 at 1506 cm^{-1} , ν_2 at 1588 cm^{-1} , ν_{10} at 1642 cm^{-1}) (Fig. S2, Supplementary data). The triple mutant behaves quite differently. Between pH 6.1 and 7.0 the absorption spectrum does not change (data not shown) and it is mainly characteristic of an HS form with the Soret band at 404 nm, Q bands at 501 and 533 nm, and CT at 634 nm; the corresponding RR spectrum clearly indicates the presence of a predominant 6cHS species (ν_1 at 1484 cm^{-1} , ν_2 at 1563 cm^{-1} , ν_{17} at 1586 cm^{-1} , ν_{10} at 1613 cm^{-1}). The broadness of the ν_2 band suggests also the presence of a 5cHS, which has been confirmed by a band fitting analysis which clearly shows ν_2 at 1489 cm^{-1} , and ν_2 at 1567 cm^{-1} (data not shown). In addition, a weak ν_3 at 1503 cm^{-1} is observed due to a 6cLS species. At alkaline pH the protein becomes unstable.

Fig. 2 (left) shows the low frequency region RR spectra of Tf-trHb at alkaline pH in H_2O , D_2O , and H_2^{18}O buffered solutions, at 298 and 15 K, together with the corresponding band fitting analysis. Table 1 reports the band fitting parameters together with the band assignments. Whereas the hydroxide 6cHS complex is present at room temperature and undetectable at 15 K, at both temperatures the band at 485 cm^{-1} is affected by the isotopic substitution. It up-shifts by 4 cm^{-1} in D_2O (489 cm^{-1}), and downshifts to 471 cm^{-1} (-14 cm^{-1}) in H_2^{18}O , as also confirmed by the difference spectra (Fig. 2, right). Therefore, the band at 485 cm^{-1} is assigned to the $\nu(\text{Fe}-\text{OH})$ stretching mode of the 6cLS form. Hence, in Tf-trHb the low-spin $\nu(\text{Fe}-\text{OH})$ stretching mode is about 65 cm^{-1} lower than the corresponding bands observed for metMb and metHb [9]. This anomalous very low frequency indicates unusually strong hydrogen bonding between the OH^- ligand and distal residues. In fact, with an increase of the H-bond strength, a decrease of the force constant of the Fe–OH bond together with a loss of its biatomic

oscillator character (via vibrational coupling with the Fe–OH bending and torsion and the O–HX stretch modes) is expected. In addition, the strength of the H-bond is predicted to weaken upon deuterium substitution; in particular, for O–O distances $> 2.6 \text{ \AA}$ [10]. As a consequence, the Fe–OD stretch can experience a smaller downshift, or even an upshift, compared with the corresponding Fe–OH stretch despite the increased mass.

Fig. 3 shows the EPR spectra (at 5 K) at alkaline and neutral pH of the Tf-trHb and its triple mutant. On the basis of previously reported hydroxo complexes (Table 2), the LS species with g_{\parallel} values in the range $g = 2.7\text{--}2.8$ are assigned to HS/OH coordination, where the OH group is strongly H-bonded. The weak species with $g_{\parallel} = 2.66$ is similar to cases of HS/OH coordination where the OH group is not strongly H-bonded. The g_{\perp} values and assignments of the various Tf-trHb LS species are reported in Table 2.

At pH 6, the HS signal for both samples becomes considerably more intense than that observed for WT at alkaline pH, whereas the LS signals are approximately 10-fold weaker compared to the LS species of WT at alkaline pH. The inset (Fig. 3) shows the relative intensities of the LS signals of the three spectra (without expansion), clearly demonstrating the marked intensification of the LS signals at alkaline pH. At pH 6 all the high spin bands show a variable degree of rhombicity. This suggests that the HS state is a 5c species or, alternatively, there is a mixture of 6cHS and 5cHS species present. The apparently lower g_{\perp} value in the case of the WT HS signal (5.71) compared to that of the mutant (5.85) is probably simply due to the superposition of a more rhombic 5cHS and a 6cHS species. The extremely weak HS signal at alkaline pH is characterized by a rhombic g tensor (6.31, 5.85, 1.99) (data not shown), and likely results from free heme dissociated from the protein due to structural instability at alkaline pH.

Classical MD simulations of Fe(III) Tf-trHb with coordinated water were performed to shed light on the nature of the H-bond network

Table 2
EPR spectral parameters of WT Tf-trHb, its triple mutant and various low-spin hydroxide bound (His-Fe-OH⁻) heme proteins.

Protein	LS signals				Coordination	HS signals		REF
	g ₁	g ₂	g ₃	Intensity ^a		g ₁	g ₂	
WT Tf-trHb pH 9.8	2.73	2.19	1.76	s	His/OH ^b			This work
	2.66	2.19	1.81	vw	His/OH ^b			This work
WT Tf-trHb pH 6.0	2.82	2.32	1.60	vw	His/OH ^b	5.71	1.99	This work
	2.73	2.19	1.76	vw	His/OH ^b			This work
Mutant of Tf-trHb pH 6.0	2.66	2.19	1.81	vw	His/OH ^b			This work
	2.82	2.32	1.60	vw	His/OH ^b	5.85	1.99	This work
HRPA2 ^c	2.71	–	1.71	vw	His/OH ^b			
	2.96	2.13	1.66		His/OH ^b			[25]
Mb	2.55	2.17	1.85		His/OH ^b			[26]
Lacilin pectinatus Hb II	2.61	2.20	1.82		His/OH ^b			[26]

^a s, strong; w, weak; vw, extremely weak.
^b OH⁻ strongly H-bonded.
^c HRPA2, Hirsradish peroxidase isoenzyme A2.

At alkaline pH, two different conformers were found for the WT protein during the timescale of the MD simulation. Fig. 5 displays the change of the H-bonding distance between OH⁻ and O_{YCD1} as a function of time, showing the interconversion of conformers, as well as a representation of the distal side in both conformations. The optimized Fe–OH bond distance was found to be about 1.8 Å. In both forms the hydroxide ligand is strongly stabilized by three H-bonds involving the distal polar residues. In one form, TrpG8 and TyrCD1 directly interact with the ligand (OH⁻–N_{WCA} = 3.1 Å; OH⁻–O_{YCD1} = 3.2 Å), whereas TyrB10 is H-bonded to a water molecule which, in turn, is H-bonded with the distal ligand (OH⁻–H₂O(W1) = 2.7 Å; H₂O(W1)–O_{YB10} = 2.6 Å) (Fig. 5A). In the second conformer only the TrpG8 is directly H-bonded with the hydroxide (OH⁻–N_{WCA} = 3.1 Å), whereas both the tyrosines interact with the ligand via a water molecule (OH⁻–H₂O(W2)–O_{YCD1} = both 2.6 Å; OH⁻–H₂O(W1)–O_{YB10} = 2.7 and 2.6 Å) (Fig. 5B).

3.2. Cyanide ligand

Upon addition of cyanide to both WT and the triple mutant, their sixth ligand is replaced by the exogenous ligand to form a cyanide 6C1S complex. Both UV–vis (419, 543, 578 nm) and RR spectra in the high frequency region (ν_3 at 1503 cm⁻¹, ν_2 at 1582 cm⁻¹, ν_{10} at 1637 cm⁻¹) are identical to each other and similar to other cyanide complexes (data not shown).

Figs. 6 and 7 show the low-frequency RR spectra of the cyanide adducts of ferric Tf-trHb and its triple variant, respectively, along with those of the ¹³C¹⁴N, ¹²C¹⁵N, and ¹³C¹³N analogs to effectively identify those modes associated with the Fe(III)–CN linkage. It is immediately apparent that for the Tf-trHb the band at 439 cm⁻¹ exhibits a monotonic downshift as the mass of cyanide increases from ¹²C¹⁴N (439 cm⁻¹), through ¹³C¹⁴N and ¹²C¹⁵N (436 cm⁻¹), to ¹³C¹³N (432 cm⁻¹). Therefore, this band is assigned to the $\nu(\text{FeCN})$ mode. The isotope-sensitive mode at 380 cm⁻¹ exhibits a zigzag isotopeshift pattern. The difference spectra show features at about 383 and 378 cm⁻¹. Since the zigzag pattern is characteristic of a bending mode [11], we assign the band at 380 cm⁻¹ to the $\delta(\text{Fe–C–N})$ mode. Accordingly, this band disappears in the difference spectra obtained by subtraction of pairs of the spectra of adducts in which the mass of the carbon atoms is equal but the total mass of the cyanide isotopomers is different (¹²C¹⁴N, ¹²C¹⁵N and ¹³C¹⁴N-¹³C¹⁵N). In fact, in these two cases, the bending vibrations should occur at the same frequency and thus cancel out, whereas features associated with the stretching modes should appear in the difference spectra.

Inspection of Fig. 6 reveals the presence of several weak isotope-sensitive bands which are not readily discernible in the RR spectra owing to their weak intensity, but clearly appear in the difference spectra. In the region near 420 cm⁻¹ another band shows a zigzag pattern, with difference maxima appearing at 415–419 cm⁻¹ and minima at 405–407 cm⁻¹. Simulated difference spectra (Fig. S3, Supplementary data) indicate that this corresponds to a band with

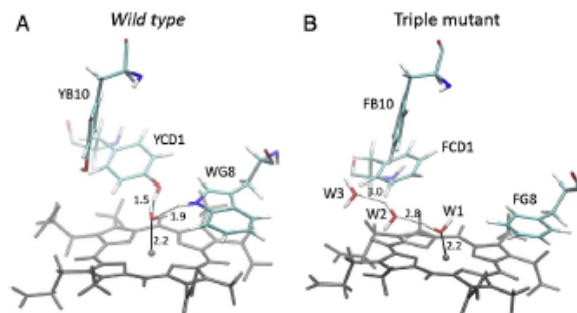


Fig. 4. Schematic representation of the distal side of WT Tf-trHb (A) and its TrpG8-TyrB10-FYCD1F triple mutant (B), showing the hydrogen-bond network (dotted lines) stabilizing the iron-bound H₂O on the basis of MD simulations. Distances are in angstroms.

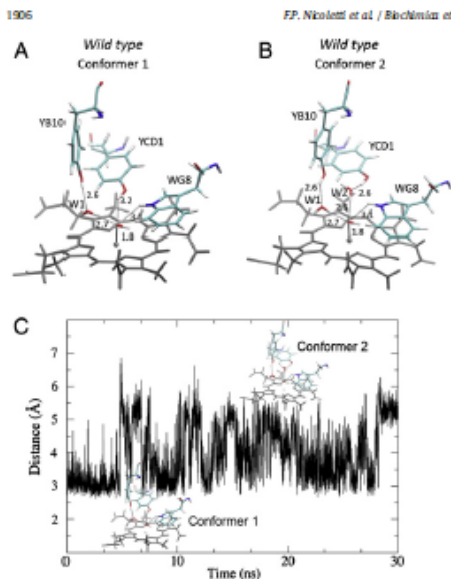


Fig. 5. (A and B): Schematic representation of the distal side of the two conformers of the WT Tf-trHb at alkaline pH showing the hydrogen-bond network (dotted lines) stabilizing the iron-bound OH^- on the basis of MD simulations. Distances are in angstroms. (C): Time evolution of OH^- -Fe distance showing swapping configurations between two conformers during the timescale of simulation.

maximum at 414 cm^{-1} in the natural isotopomer spectrum and full width at half maximum 20 cm^{-1} .

The intensity pattern in the difference spectra is closely related to that of the 380 cm^{-1} band. In addition, as for the band at 380 cm^{-1} , this band disappears in the difference spectra obtained by subtraction of pairs of the spectra of adducts in which the mass of the carbon atoms is equal but the total mass of the cyanide isotopomers is different ($^{13}\text{C}^{14}\text{N}$, $^{13}\text{C}^{15}\text{N}$) and ($^{12}\text{C}^{14}\text{N}$, $^{12}\text{C}^{15}\text{N}$) and is observed, together with the band at 380 cm^{-1} , in the difference spectra ($^{12}\text{C}^{15}\text{N}$, $^{13}\text{C}^{14}\text{N}$) where only the bending modes are present. Therefore, we assign this band as another $\delta[\text{Fe}-\text{C}-\text{N}]$ mode, similar to the RR spectra of cyanide adducts of horseradish peroxidase at pH 12 [12], which displayed a secondary $\delta[\text{Fe}-\text{C}-\text{N}]$ band at 420 cm^{-1} with a $\nu[\text{Fe}-\text{CN}]$ band at 355 cm^{-1} . The corresponding $\nu[\text{Fe}-\text{CN}]$ cannot be identified in our spectra, however, we cannot rule out that it is obscured by the intense porphyrin ν_8 band at 347 cm^{-1} . However, the RR results provide unambiguous evidence that a main CN conformer has been found, exhibiting $\nu[\text{Fe}-\text{CN}]$ and $\delta[\text{Fe}-\text{C}-\text{N}]$ modes at 439 and 380 cm^{-1} .

The effect of the distal residue mutations is small (Fig. 7). The main change in the RR spectra of the CN^- adduct of the Trp8Phe-TyrCD1Phe-TyrB10Phe triple mutant is a shift of the $\delta[\text{Fe}-\text{C}-\text{N}]$ band from 380 to 370 cm^{-1} , together with a 7 cm^{-1} shift of the secondary $\delta[\text{Fe}-\text{C}-\text{N}]$ band. The intensity changes in the difference spectra follow a pattern which is similar to that of the native protein.

4. Discussion

Extensive work on heme proteins has demonstrated that the frequency of the $\nu[\text{Fe}-\text{OH}]$ RR mode depends on the Fe ion spin state, the distal environment, and especially on the number and strength

of H-bonding interactions between the hydroxide and the distal polar residues [9,13–15]. Typical $\nu[\text{Fe}-\text{OH}]$ wavenumbers are around 490 and 550 cm^{-1} for 6c1S and 6d1S species, respectively. H-bonding can lower the stretching frequency by decreasing the Fe–O electron density and, as a consequence, the Fe–OH force constant. For example, in horseradish peroxidase only a 6d1S form has been found at 503 cm^{-1} , as the hydroxide is stabilized by accepting H-bonds from the distal His and the distal Arg. Similarly for Tf-trHb, only the 6d1S species has been identified. It is characterized by an extremely low $\nu[\text{Fe}-\text{OH}]$ frequency, about 65 cm^{-1} lower than the corresponding vibration in Mb. This frequency strongly supports the presence of numerous H-bonds formed by the bound hydroxyl with distal residues and water molecules. Based on MD simulations, the OH^- anion builds three H-bonds in an alkaline Tf-trHb form 1 with Trp8 and TyrCD1 (which is fully consistent with the results obtained with other ligands, see below), and with a water molecule H-bonded to TyrB10. In form 2, H-bonding with TyrCD1 is mediated by a water molecule.

Previous studies carried out on the CD [1], F^- [23], and HS^- [4] adducts formed with the WT protein and a combinatorial set of mutants, in which these three amino acids have been singly, doubly, or triply replaced by a Phe residue, revealed that all the ligands are stabilized by Trp8 via a strong H-bond. TyrCD1 is able to interact with CO and fluoride, whereas TyrB10 is not directly involved in the ligand stabilization and plays only a minor role. Therefore, the present case is the first example of involvement of TyrB10 – albeit an indirect one – in the stabilization of the exogenous ligand. In fact, previously we found that in the presence of the fluoride anionic ligand, which can only accept H-bonds, Trp8 and TyrCD1 form strong H-bonds with fluoride since the WT protein is characterized by a $\nu[\text{Fe}-\text{F}]$ stretch at 385 cm^{-1} . In contrast, the YB10F-YCD1F-WG8F mutant displayed the highest $\nu[\text{Fe}-\text{F}]$ stretch (471 cm^{-1}). These results clearly highlight that the heme environment, where fluoride is surrounded by three Phe residues, does not appear to be apolar as would be expected. Accordingly, MD simulations indicated that two water molecules, interacting with the coordinated fluoride ion, are accommodated in the active site. Unlike fluoride, hydroxide can act as an H-bond donor or acceptor. In addition, whereas Trp8 can act as a potential hydrogen-bond donor only, the tyrosines can act as donor or acceptor. Therefore, we suggest that in the present case whereas Trp8 and TyrCD1 stabilize the hydroxide by donating a proton, similar to the fluoride case, TyrB10 acts as an H-bond acceptor. In fact, crystallographic data indicate that the TyrCD1 phenol hydroxide is directed toward the hydrogen bond coordination sphere of the iron bound ligand, whereas the TyrB10 phenol hydroxide is clearly directed “off axis” in the direction of the heme propionate, with respect to the ligand. It is thus envisaged that the phenolic oxygen atom of TyrB10 may assume a conformation that is favorable for a hydrogen bond acceptor.

Whereas the $\nu[\text{Fe}-\text{OH}]$ mode is very sensitive to the nature of the distal residues, its frequency being markedly affected by the presence of H-bonds between the oxygen and polar residues, the RR frequencies of the CN conformers may be interpreted in terms of steric hindrance within the distal cavity. A CN^- anion in the absence of any steric hindrance should bind to a ferric heme with a linear (upright) geometry. In this case the $\delta[\text{Fe}-\text{C}-\text{N}]$ mode should be RR-inactive. However, deviations from linearity are possible and, in fact, are occasionally observed in the X-ray structures of cyanide complexes of heme proteins. Accordingly, the observed $\nu[\text{Fe}-\text{CN}]$ and $\delta[\text{Fe}-\text{C}-\text{N}]$ Raman frequencies are significantly scattered since sterically encumbering groups in close contact with the bound CN^- cause a bent Fe–CN unit and a decrease of the Fe–CN stretching frequency [16].

The Fe–CN stretching frequency in various hemoproteins typically falls in the $400\text{--}460\text{ cm}^{-1}$ range. For instance, the $\nu[\text{Fe}-\text{CN}]$ RR bands of MbCN and HbCN were observed around 452 cm^{-1} [17], which corresponds to a slightly bent FeCN moiety [18]. In fact, the $\nu[\text{Fe}-\text{CN}]$ of an unhindered CN-bound heme complex was observed at 456 cm^{-1} , whereas analogous “strapped hemes”, in which the ligand binding is

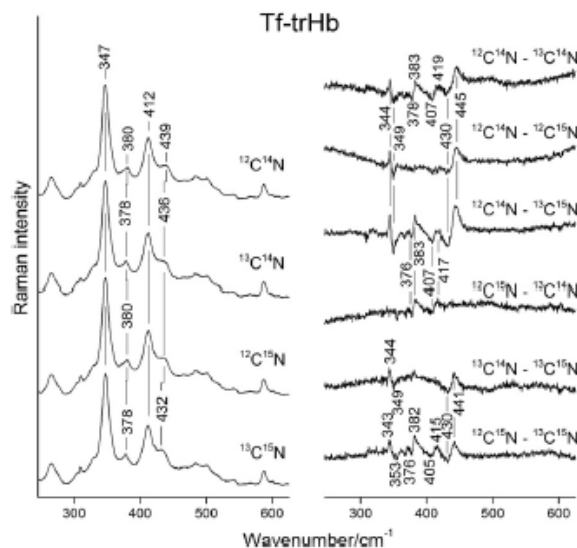


Fig. 6. Left: low-frequency region RR spectra of the cyanide complexes of ferrous Tf-trHb for the four isotopes at pH 7.0; right: difference spectra. Experimental conditions: 1 cm^{-1} spectral resolution; 10 mW laser power at the sample. $^{12}\text{C}^{14}\text{N}$, average of 11 spectra; $^{12}\text{C}^{15}\text{N}$, average of 6 spectra; $^{13}\text{C}^{14}\text{N}$, average of 6 spectra; $^{13}\text{C}^{15}\text{N}$, average of 5 spectra. Integration time for each spectrum was 1200 s.

sterically hindered by a $(\text{GH}_2)_n$ -chain strap over the iron at the CN^- binding site, displayed downshifted $\nu(\text{Fe}-\text{CN})$ frequencies, i.e. between 447 and 445 cm^{-1} for n between 15 and 13 [16].

In the present case, for both proteins we observe a main conformer characterized by $\nu(\text{Fe}-\text{CN})$ at about 440 cm^{-1} , more than 10 cm^{-1} lower than that of mammalian globins, with a smaller isotopic shift (7 cm^{-1}) than the expected value for a linear $\text{Fe}-\text{CN}$ oscillator, and a $\delta(\text{Fe}-\text{C}-\text{N})$ at 380 cm^{-1} (370 cm^{-1} in the mutated protein). Therefore, we propose that the $\text{Fe}-\text{C}-\text{N}$ moiety adopts a bent structure similar to other truncated hemoglobins [19–21] which is maintained in the triple mutant, where the polar residues are replaced by the non-polar Phe. A second, less abundant conformer, is characterized by a $\delta(\text{Fe}-\text{C}-\text{N})$ band frequency at 414 cm^{-1} (407 cm^{-1} in the mutant) whose corresponding $\nu(\text{Fe}-\text{CN})$ has not been clearly observed, and likely has an even less linear $\text{Fe}-\text{CN}$ moiety. In fact, on the basis of normal-mode calculations [12,22] it has been proposed that for the linear or slightly bent conformers the $\text{Fe}-\text{CN}$ stretching mode has a frequency higher than the bending mode, whereas the strongly bent conformer exhibits a reverse pattern in which the frequency of the bending mode is higher than that of the stretching mode.

Similar results have been obtained for the CN^- adduct of the single domain Hb from *Campylobacter jejuni*. The two conformers have been assigned to a “linear” $\text{Fe}-\text{C}-\text{N}$ moiety ($\nu(\text{Fe}-\text{CN})$ at 440 cm^{-1} and $\delta(\text{Fe}-\text{C}-\text{N})$ at 403 cm^{-1}) and a “bent” form ($\nu(\text{Fe}-\text{CN})$ at 353 cm^{-1} and $\delta(\text{Fe}-\text{C}-\text{N})$ at 417 cm^{-1}) [23]. The corresponding X-ray structure (ZWY4) indeed shows an almost linear $\text{Fe}-\text{CN}$ unit (176°) with a strong H-bond between the cyanide ion and the TyrB10 residue.

A combination of RR and X-ray data of cyanide complexes of truncated bacterial heme proteins is available only for *Chlamydomonas eugametos* trHb. In the wild-type protein, the highly constrained structure of the $\text{Fe}-\text{C}-\text{N}$ moiety is a result of distal interactions. In fact, the $\nu(\text{Fe}-\text{CN})$ at 440 cm^{-1} in the native protein shifts up to 452 cm^{-1} in

the GlnE7Gly mutant, consistent with a more relaxed structure in the mutant. Conversely, when the TyrB10 is mutated to Leu, the $\nu(\text{Fe}-\text{CN})$ frequency shifts down to 435 cm^{-1} , indicating an even more constrained structure [19]. We found a somewhat related situation in a mutated plant hemoglobin from *Arabidopsis thaliana*. In that case, the $\nu(\text{Fe}-\text{CN})$ frequency for the complex of the native protein was at 454 cm^{-1} . Mutation of the distal Phe residue to Leu induced a downshift to 439 cm^{-1} , possibly due to an increased steric hindrance, whereas the distal His to Leu mutation lead to a $\nu(\text{Fe}-\text{CN})$ at 457 cm^{-1} , corresponding to an unhindered FeCN moiety [24].

We finally note that the similarity of the RR results obtained for native Tf-trHb and the triple mutant suggests that H-bonding interactions with the cyanide ligand have negligible effects. However, distal H-bonding with water molecules may be present in the mutant as well, similar to the case of the fluoride adduct [3]. Preliminary MD simulations on the WT and the triple mutant indicate that in both cases the CN^- ligand is strongly H-bonded. In the native protein the H-bonds are donated by the TrpG8 and TyrCD1 residues, whereas in the triple mutant, two water molecules interacting with the coordinated cyanide ion are accommodated into the active site (data not shown).

5. Conclusions and perspectives

In conclusion, we have demonstrated how complementary structural information can be obtained by a combination of RR spectra, EPR spectra and MD simulations of the cyanide and hydroxide complexes of Tf-trHb. Whereas the effect of distal H-bonding on the $\nu(\text{Fe}-\text{OH})$ band has been rationalized, further studies are necessary to highlight the correlation between RR $\text{Fe}-\text{CN}$ frequencies, X-ray structures, and MD simulations, taking into account the effect of both steric effects and H-bonding interactions.

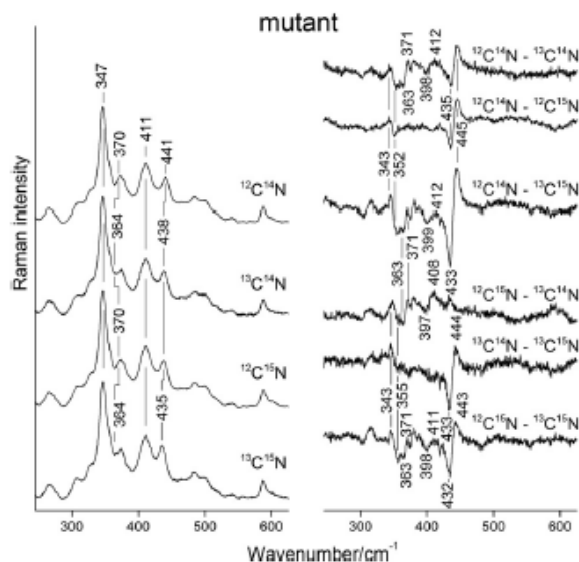


Fig. 7. Left: low-frequency region RR spectra of the cyanide complexes of the ferric triple variant for the four isotopes at pH 7.0; right: difference spectra. Experimental conditions: 1 cm^{-1} spectral resolution; 10 mW laser power at the sample. $^{12}\text{C}^{14}\text{N}$, average of 17 spectra; $^{13}\text{C}^{14}\text{N}$, average of 19 spectra; $^{12}\text{C}^{15}\text{N}$, average of 3 spectra; $^{13}\text{C}^{15}\text{N}$, average of 8 spectra. Integration time for each spectrum was 1200 s.

Acknowledgments

This work was supported by the Institute Pasteur Fondazione Cenci Bolognietti (A. Boffi), MIUR FIRB RBF08F4IU_002 (A. Bonamore), MIUR PRIN 2008BFJ34 (A. Feis and A. Boffi), University of Buenos Aires (grant X074), CONICET and European Union FP7 project NOSTRESS (D. Estrin), and the Italian Ministero dell'Istruzione, dell'Università e della Ricerca (MIUR), Direzione Generale per l'Internazionalizzazione della Ricerca, Progetti di Grande Rilevanza Italia-Argentina. We thank Dr Maria Fitipaddi for provision of EPR facilities and assistance in recording the spectra.

Appendix A. Supplementary data

Supplementary data to this article can be found online at <http://dx.doi.org/10.1016/j.bbapap.2013.02.033>.

References

- [1] E. Drogheiti, F.P. Nicolletti, A. Bonamore, L. Boechi, P. Arroyo Manez, D.A. Estrin, A. Boffi, G. Smulevich, A. Feis, Heme-pocket structural properties of a bacterial truncated hemoglobin from *Thermobifida fusca*, *Biochemistry* 49 (2010) 10394–10402.
- [2] E. Drogheiti, F.P. Nicolletti, A. Bonamore, N. Sciamanna, A. Boffi, A. Feis, G. Smulevich, The optical spectra of fluoride complexes can effectively probe H-bonding interactions in the distal cavity of heme proteins, *J. Inorg. Biochem.* 105 (2011) 1328–1343.
- [3] F.P. Nicolletti, E. Drogheiti, L. Boechi, A. Bonamore, N. Sciamanna, D.A. Estrin, A. Feis, A. Boffi, G. Smulevich, Fluoride as a probe for H-bonding interactions in the active site of heme proteins: the case of *Thermobifida fusca* Hemoglobin, *J. Am. Chem. Soc.* 133 (2011) 20970–20980.
- [4] F.P. Nicolletti, A. Comandini, A. Bonamore, L. Boechi, F.M. Boubeta, A. Feis, G. Smulevich, A. Boffi, Sulfide binding properties of truncated hemoglobins, *Biochemistry* 49 (2010) 2269–2278.

- [5] A. Bonamore, A. Iaffi, L. Giangiacomo, A. Bellelli, V. Morea, A. Boffi, A novel thermostable hemoglobin from the actinobacterium *Thermobifida fusca*, *FEBS J.* 272 (2005) 4189–4201.
- [6] F.P. Nicolletti, M. Thompson, B.D. Howes, S. Franzen, G. Smulevich, New insights into the role of distal histidine flexibility in ligand stabilization of dehaloperoxidase-hemoglobin from *Amphibacillus oryzae*, *Biochemistry* 49 (2010) 1903–1912.
- [7] D.A. Pearlman, D.A. Case, J.W. Caldwell, W.S. Ross, T.E. Cheatham III, S. DeBolt, D. Ferguson, G. Seibel, P. Kollman, AMBER, a package of computer programs for applying molecular mechanics, normal mode analysis, molecular dynamics and free energy calculations to simulate the structural and energetic properties of molecules, *Comput. Phys. Commun.* 91 (1995) 1–41.
- [8] J.-P. Ryckaert, G. Cicotti, H.J.C. Berendsen, Numerical integration of the cartesian equations of motion of a system with constraints: molecular dynamics of n-alkanes, *J. Comput. Phys.* 23 (1977) 327–341.
- [9] A. Feis, M.P. Mazzocchi, M. Paoli, G. Smulevich, Spin state and axial ligand bonding in the hydroxide complexes of metmyoglobin, methemoglobin, and horseradish peroxidase at room and low temperatures, *Biochemistry* 33 (1994) 4577–4583.
- [10] T. Saftoiu, K. Mori, R. Itob, Two-dimensional vibrational analysis of the Lippincott-Schröder potential for OH–O, NH–O and NH–N hydrogen bonds and the deuterium isotope effect, *Chem. Phys.* 60 (1982) 161–180.
- [11] N.-T. Yu, B. Benko, E.A. Kerr, K. Gensoudi, Iron-carbon bond lengths in carbonmonoxy and cyanomet complexes of the monomeric hemoglobin III from *Chironomus thummi thummi*: a critical comparison between x-ray Raman and X-ray diffraction studies, *Proc. Natl. Acad. Sci. U. S. A.* 81 (1984) 5106–5110.
- [12] J.-M. Mustafa, J.R. Kincaid, Resonance Raman study of cyanide-ligated horseradish peroxidase. Detection of two binding geometries and direct evidence for the “push-pull” effect, *Biochemistry* 33 (1994) 2191–2197.
- [13] B.D. Howes, J.N. Rodríguez-Lopez, A.T. Smith, G. Smulevich, Mutation of distal residues of horseradish peroxidase: influence on substrate binding and cavity properties, *Biochemistry* 36 (1997) 1532–1543.
- [14] C.S. Lukat-Rodgers, K.R. Rodgers, Spin-state equilibria and axial ligand bonding in Fx1 hydroxide: a resonance Raman study, *J. Biol. Inorg. Chem.* 3 (1998) 274–281.
- [15] T. Egawa, S.-R. Yeh, Structural and functional properties of hemoglobins from unicellular organisms as revealed by resonance Raman spectroscopy, *J. Inorg. Biochem.* 99 (2005) 72–96.
- [16] T. Tanaka, N.T. Yu, C.K. Chang, Resonance Raman studies of sterically hindered cyanomet “strapped” hemes. Effects of ligand distortion and low tension on iron-carbon bond, *Biophys. J.* 52 (1987) 801–805.

- [17] S. Hirota, T. Ogura, K. Shinzawa-Itoh, S. Yoshikawa, T. Kitagawa, Observation of multiple CN-isotope-sensitive Raman bands for CN⁻ adducts of hemoglobin, myoglobin, and cytochrome c oxidase: evidence for vibrational coupling between the Fe-C-N bending and porphyrin in-plane modes, *J. Phys. Chem.* 100 (1996) 15274–15279.
- [18] M. Bolognesi, C. Rosano, R. Loto, A. Bossa, M. Rizzi, J.B. Wittenberg, A. Boffi, P. Ascenzi, Cyanide binding to *Lactuca pectinatus* hemoglobin I and to sperm whale myoglobin: an X-Ray crystallographic study, *Biophys. J.* 77 (1999) 1093–1099.
- [19] T.K. Das, M. Courton, M. Guerin, D.J. Rausosa, Distal interactions in the cyanide complex of ferrous *Chlamydomonas* haemoglobin, *J. Phys. Chem. B* 104 (2000) 10750–10756.
- [20] M. Milani, A. Pece, Y. Ouellet, P. Ascenzi, M. Guerin, M. Bolognesi, Mycobacterium tuberculosis haemoglobin N displays a protein tunnel suited for O₂ diffusion to the heme, *EMBO J.* 20 (2001) 3902–3909.
- [21] M. Milani, Y. Ouellet, H. Ouellet, M. Guerin, A. Boffi, G. Antonini, A. Bredini, M. Matsu, M. Bolognesi, P. Ascenzi, Cyanide binding to truncated hemoglobins: a crystallographic and kinetic study, *Biochemistry* 43 (2004) 5213–5221.
- [22] J. Al-Mustafa, M. Sykora, J.R. Kincaid, Resonance Raman investigation of cyanide ligated beef liver and *Aspergillus niger* catalases, *J. Biol. Chem.* 270 (1995) 10449–10460.
- [23] C. Liu, M. Mukai, Y. Liu, G. Wu, R.K. Poole, S.-R. Yeh, Structural and functional properties of a single domain hemoglobin from the food-borne pathogen *Campylobacter jejuni*, *J. Biol. Chem.* 282 (2007) 25917–25928.
- [24] F. Spyrakis, S. Faggiano, S. Abbotazzi, P. Dominici, E. Cacciamari, A. Astegno, E. Droghezz, A. Feis, G. Smulevich, S. Bruno, A. Mazzeoli, P. Cazzini, C. Viappiani, A. Bodon-Chanal, F.J. Lacque, Heterodine E7 dynamics modulates ligand exchange between distal pocket and solvent in AHB1 from *Arabidopsis thaliana*, *J. Phys. Chem. B* 115 (2011) 4138–4146.
- [25] B.D. Howes, A. Feis, C. Indiani, M.P. Marzocchi, G. Smulevich, Formation of two types of low-spin heme in homodimeric peroxidase isoenzyme A2 at low temperature, *J. Biol. Inorg. Chem.* 5 (2000) 227–235.
- [26] D.W. Kraus, J.B. Wittenberg, J.F. Lu, J. Peisach, Hemoglobins of the *Lactuca pectinatus*/Bacteria Symbiosis, *J. Biol. Chem.* 265 (1990) 16054–16059.

Molecular Basis of Thermal Stability in Two Members of the Truncated Hemoglobins Subfamily

J.P. Bustamante¹, A. Bonamore², L. Boechi³, A.D. Nadra⁴, N. Sciamanna², A. Boffi² and D.A. Estrin¹

¹*Departamento de Química Inorgánica, Analítica y Química Física, INQUIMAE-CONICET, Facultad de Ciencias Exactas y Naturales, Universidad de Buenos Aires, Buenos Aires, Argentina*

²*Instituto Pasteur, Fondazione Cenci Bolognetti, Department of Biochemical Sciences, University of Rome "La Sapienza", Italy*

³*Instituto de Cálculo, Facultad de Ciencias Exactas y Naturales, Universidad de Buenos Aires, Buenos Aires, Argentina*

⁴*Departamento de Química Biológica, IQUBICEN-CONICET, Facultad de Ciencias Exactas y Naturales, Universidad de Buenos Aires, Buenos Aires, Argentina*

Abstract

Much interest has been generated in the field of organisms adapted to extreme temperature conditions, both from a biophysical or biotechnological point of view. Understanding the molecular mechanism that allows proteins to be functional at extreme high and low temperatures is one of the key issues in structural biology. Although the global structure of homologous proteins belonging to extreme temperature conditions adapted and non-adapted organisms barely differs between them, their thermal stability characteristic is quite different. We perform Molecular Dynamics (MD) simulations at 300K and 360K and thermal melting profiles measurements of two member of the truncated hemoglobin subfamily belonging to the thermophile *Thermobifida fusca* (Tf-trHbO) and the mesophile *Mycobacterium tuberculosis* (Mt-trHbO) microorganisms. In this work, several analyses are considering in order to understand molecular basis of thermal stability of these proteins. Particularly, regarding polar interactions, no clear differences are observed taking into account the total number of H-bonds interactions comparing both proteins. However, significant number increase of salt-bridges was measured upon increasing the temperature for Tf-trHbO, gaining interactions that account for the folded state. Our results over *wild type* and mutant proteins analyses also provide theoretical and experimental evidence of a singular proline role that make possible a significant thermal stability shift. We found that the presence/absence of a key proline causes a tertiary distortion on the native fold favoring CD loop high local flexibility. This proline residue not only gives more flexibility to the CD loop, also allows forming new intramolecular interactions that stabilize the protein native state. On this basement, melting temperature measurements confirm that this specific residue is able to increases (by 8 degrees) or decreases (by 4 degrees) T_m in Mt-trHbO and Tf-trHbO, respectively. We present a clear thermal stability shift by changing only this single residue, suggesting that structural and dynamical involved behaviors are responsible for protein thermal stability.

Keywords: truncated hemoglobin, thermostability, *Thermobifida fusca*, *Mycobacterium tuberculosis*, molecular dynamics, folding.

Introduction

In nature there are many examples of organisms adapted to high temperatures. They can be classified as thermophiles with optimal growth temperatures between 333K and 353K, and hyperthermophiles with optimal growth temperatures between 353K and 383K, compared to the non-adapted mesophiles with optimal growth between 298K and 323K. Generally, enzymes belonging to these adapted organisms are also thermostable enzymes with T_m , the temperature at which 50% of the proteins are folded, close to the organism's optimal growth temperature[1]. The thermostable protein most studied is the rubredoxin, from *Pyrococcus furiosus*, which presents a global unfolding rate of 10^{-6} s^{-1} at 373K[2].

Homologous enzymes from adapted and non-adapted organisms present the same catalytic mechanisms, high sequence identity and also share a highly similar global structure[3–5]. Due to this structural similarity between the thermostable and non-thermostable enzymes, it is not trivial to rationalize the differential adaptation to a high temperature at the molecular level. Indeed, an understanding of the physicochemical features that determine thermal stability still remains as one of the key issues in protein biophysics. Moreover, there is an increasing interest in the use of modified proteins/enzymes with enhanced thermal stability for solving different tasks in biotechnology[6–8].

It has been proposed that thermostability is strictly related to the flexibility of the protein. Assuming that both thermostable and non-thermostable homologues enzymes perform the same function at different temperatures, and that the protein function is related to a certain degree of flexibility, the thermostable protein may have less flexibility at the same temperature. Increased rigidity of the folded state at room temperature would thus be related to an increased thermal stability. The lack of flexibility would also explain why thermophiles and hyperthermophiles are inactive at low temperatures. Many theoretical and experimental approaches support that thermophiles are more rigid at normal temperatures compared to their homologous non-thermostable proteins[9–13], although new results coming from amide exchange experiments contradict the proposed hypothesis[14] thus opening the discussion about the relationship between flexibility and thermal stability.

According to the folding theory, the melting temperature (T_m) is related to the gap between the effective or free energy (averaged over the solvent degrees of freedom) of the folded state vs all the possible unfolded states[15]. Therefore, a large amount of hydrophilic as well as hydrophobic (related to the water entropic gain) contacts in the folded state compared to the ones observed in the unfolded state would favor a larger T_m . The number of hydrogen bonds (H-Bonds), mainly through internal residues themselves, and also salt-bridges were additionally found to correlate with thermal stability[16].

On the other hand, proteins have to loose configurational entropy to reach the folded state, since their configurational space is enormous in the unfolded state, but very narrow in the folded state. So, any process that helps to decrease the configurational entropy in the unfolded state, allows the system to stabilize the folded state at higher temperatures, thus increasing T_m [17]. This is observed, for example, in membrane proteins where the membrane restricts the conformations of the protein thus increasing the temperature at which the system reaches the unique conformation that characterizes the folded state[18]. Considering that each backbone residue is able to explore different configurational space depending on the residue, it was proposed that the presence of more rigid backbone residues, such as prolines, are responsible for an increase thermostability through reducing the configurational entropy[17]. Minor trends have been observed where all the residues, including prolines, from mesophilic and hyperthermophilic proteins are compared[19]. In this context, although many hypotheses were proposed, none of them are conclusive neither absolute to explain the thermostability from a rational view.

Regarding temperature perturbation, we can consider the thermostability issue as how temperature affects protein conformational sampling, and how this affects protein function. In this article we focused only on the first part of the problem, which is how the temperature affects conformational sampling, specifically considering differences between the thermostable and non-thermostable proteins. We also addressed on how the thermostable proteins handle the temperature increase and avoid being unfolded.

Two members of the subfamily of truncated hemoglobins (trHb) were studied: the trHb belonging to the thermophilic microorganism *Thermobifida fusca* (Tf-trHbO), with an optimal growth temperature of 333K[21], and the trHb from the mesophilic microorganism *Mycobacterium tuberculosis* (Mt-trHbO)[22], having the optimal growth temperature at 298K. Both proteins have 58% sequence identity and a highly similar tertiary structure[21]. By performing Molecular Dynamics (MD) simulations and thermal unfolding measurements of the *wild type* (wt) and crossed mutants of these trHbs members, we were able to understand the responsible differences for the thermostable and non-thermostable proteins dealing with temperature perturbation. Particularly, we propose a mechanism by which the thermostable protein is able to avoid the unfolding process at high temperatures. The Tf-trHbO has a flexible loop through which it can concentrate most of its fluctuations, thus avoiding the unfolding process. We found that the flexibility of the loop is controlled by the presence or absence of a proline residue. The lack of a flexible loop in the non-thermostable protein spreads the fluctuations over the entire protein, especially the termini, thus beginning the protein unfolding process at high temperatures.

Methods

Computer simulations. Crystal structures of both wt trHbs, Tf-trHbO (PDB ID 2BMM [21]) and Mt-trHbO (PDB ID 1NGK [22]) were used as starting points for all the MD simulations. Although Tf-trHbO crystal structure lacks around 30 amino acids from each protein extremes, there are several previous works where structural and functional properties had been reproduced by simulations and validated by experimental methods[23–26]. Mutant proteins, i.e. ProE3Gly Tf-trHbO and GlyE3Pro Mt-trHbO, were built *in-silico* by changing the corresponding amino acid in the original structure and allowing the system to equilibrate in order to avoid any possible crashes of the system. Amino acids protonation states were assumed to correspond to those at physiological pH, all solvent exposed His were protonated at the N- δ delta atom, as well as HisF8, which is coordinated to the heme iron. The systems were immersed in a pre-equilibrated octahedral box of 10 Å of radius with ~4910 TIP3P water molecules using the tLEaP module of the AMBER11 package[27]. Residue parameters correspond to parm99 AMBER11 force field[28] except for the heme which correspond to those developed[29] and widely used in several heme-proteins studies[30–36]. All simulations were performed using periodic boundary conditions with a 9 Å cutoff and particle mesh Ewald (PME) summation method for treating the electrostatic interactions. The bond lengths involving hydrogen atoms were kept at their equilibrium distance by using the SHAKE algorithm, while temperature and pressure were kept constant with Langevin thermostat and barostat, respectively, as implemented in the AMBER11 program[27]. A minimization of the crystal structures was performed to optimize any possible structural clashes using Sander module of AMBER11 package carrying out 1000 cycles of Steepest Descent algorithm. Equilibration protocol was performed as follows: the systems were heated slowly from 0 to 300K for 20ps at constant pressure (1 atm), with harmonic restraints of 80 Kcal per mol Å² for all C_α atoms and then a pressure equilibration of the entire system simulated for 2ns at 300K with the same restrained atoms. In the case of the systems simulated at high temperature (360K), after the equilibration at 300K, the systems were heated from 300K to 360K for 20ps and equilibrated for 2ns. These equilibrated structures were the starting points for the MD simulations productions. We performed 100ns of MD of deoxy forms of wt and *in-silico* mutants of both proteins using the AMBER11-99 force field[28], all of them at 300K and 360K. All simulations productions were performed with pmemd module of AMBER11 package[27].

Genetic Engineering Procedures. ProE3Gly Tf-trHbO and GlyE3Pro Mt-trHbO mutants were obtained by PCR on plasmid pET28b-trfHb and pET28b-MthbO respectively as a DNA template. Site-directed mutagenesis was conducted with the Quickchange mutagenesis kit (Stratagene) according to the manufacturer's instructions, using complementary oligonucleotide pairs introducing the amino acid substitutions. The mutants were transformed into *E. coli* XL1 Blue competent cells, selected on kanamycin plates, and screened by DNA sequencing. Plasmid DNA bearing the gene with the desired mutation was then transformed into *E. coli* BL21(DE3) cells (Novagen) for expression.

Protein expression and purification. *E. coli* cells expressing the wt trHbs and their mutants were grown in Luria-Bertani medium containing 30 mg/L kanamycin at 37 °C. When $OD_{600}=0.6$ protein expression was induced overnight with 1 mM IPTG at 37 °C for wt Tf-trHbO and ProE3Gly Tf-trHbO and at 25 °C for wt Mt-trHbO and GlyE3Pro Mt-trHbO. Cells were recovered by centrifugation at 13000 rpm, resuspended in a minimum volume of lysis buffer (20mM phosphate buffer pH 7 supplemented with complete one Roche protease inhibitor cocktail) and sonicated until the supernatant was reddish and clear. After centrifugation at 12000 rpm for 40 min at 4 °C, the pellet was resuspended in 20 mM phosphate buffer pH 7 containing 6M urea under stirring for 1h and centrifuged again in the same condition. The supernatant was loaded on a DEAE-cellulose column (Whatman International Ltd, Maidstone, UK) equilibrated with 20 mM phosphate buffer pH 7 (buffer A) and extensively washed with the same buffer. Protein was eluted with a linear gradient of NaCl in buffer A, dialyzed versus 100 mM phosphate buffer pH 7 and titered with hemin while monitored by an UV-Vis spectrophotometer. Purified reconstituted proteins were dialyzed versus buffer A and loaded again on DEAE-cellulose column in order to eliminate the excess of hemin. The protein purity was confirmed by a single band at about 15.000 Da on a SDS-PAGE.

Thermal unfolding analysis. Thermal unfolding experiments in the far-UV region were carried out by measuring circular dichroism spectra on a JascoJ-715 spectropolarimeter as reported in [XX]. Melting profiles were measured on the cyano-met derivatives of all proteins in a 0.1 cm quartz cell at protein concentrations of 10-20 μ M heme by following the circular dichroism signal at 225 nm. Denaturation free energies were determined in temperature-melting experiments at different GdmCl (Sigma-Aldrich, St. Louis, MO) concentrations, assuming a two-state model, in the framework of the Gibbs-Helmoltz equation:

$$\Delta G_{unf} = \Delta H_{T_m} - \frac{T\Delta H_{T_m}}{T_m} + \Delta C_p [T - T_m - T \ln(T/T_m)]$$

Accordingly, the fitting of the melting profiles as a function of T yielded the unfolding enthalpy, ΔH_{T_m} , the melting temperature, T_m , and the heat capacity change associated to the unfolding process, ΔC_p . Two sloped baselines were also fitted to take into account temperature-dependent effects uncorrelated with the cooperative folding process[37].

GdmCl denaturation experiments were carried out in 50 mM phosphate buffer containing 2 mM KCN at pH 7.0 and 25 °C. Experiments were carried out by monitoring the far-UV circular dichroism spectra. The circular dichroism signal at 225 nm as a function of GdmCl concentration was followed with a slit aperture of 4 nm. In the experiments ($T = 25$ °C) samples were equilibrated for 4 h in GdmCl before measurement. Full reversibility of the denaturation process was observed under these conditions. Solvent denaturation curves were fitted to the simple two state model according to the formalism described by Clarke et al.[38]:

$$\Delta G_{unf}^{GdmCl} = \Delta G_{unf}^{water} - m[GdmCl]$$

where $\Delta G_{\text{unf}}^{\text{GdmCl}}$ is the solvent-dependent denaturation free energy, ΔG_{unf} is the unfolding free energy in water and m is a fitting constant representing the differential binding of GdmCl between the folded and unfolded state. Least squares minimizations were carried out by the MATLAB 6.0 program (South Natick, MA).

Results and discussion

Protein dynamics on temperature shift. In order to address the differences of thermal stability between both Tf-trHbO and Mt-trHbO, 100ns of unconstrained MD simulations for each protein at room (300K) and high temperature (360K) were performed. Analysis of the Root Mean Square Deviation and Fluctuations (RMSD and RMSF), as well as a close monitoring of MD simulations show that no difference between both thermostable and the non-thermostable proteins at room temperature are observed in terms of protein structural motions, giving a ΔRMSF average value of 0.08 ± 0.22 Å, in disagreement with the hypothesis about the decrease of flexibility of the thermostable one. Furthermore, these results reveal that wt Tf-trHbO concentrates a high fluctuations degree in a flexible loop between C and E helices, called CD loop, and conserves the overall fold even at high temperature (see Table 1 and Figures 1.A, 2.A). On the other hand, wt Mt-trHbO presents a very rigid CD loop and concentrates many fluctuations at both amino and carboxyl-terminal regions of the protein (Figure 1.B, 2.B). This increased flexibility at the terminal residues of the protein causes what seems to be an onset of the unfolding process.

		Tf-trHbO		Mt-trHbO	
		300K	360K	300K	360K
<i>Wild type</i>	Complete	1.10 ± 0.13	1.98 ± 0.33	1.08 ± 0.14	3.03 ± 0.62
	No terminal	1.00 ± 0.11	1.48 ± 0.24	0.87 ± 0.14	1.35 ± 0.23
	Only terminal	1.25 ± 0.19	2.18 ± 0.44	1.37 ± 0.24	5.21 ± 1.30
	Terminal and CD loop	1.31 ± 0.20	2.58 ± 0.47	1.35 ± 0.22	4.87 ± 1.17
<i>Mutant</i>	Complete	-	1.91 ± 0.41	-	2.03 ± 0.37
	No terminal	-	1.35 ± 0.18	-	1.46 ± 0.22
	Only terminal	-	2.65 ± 0.90	-	2.84 ± 0.76
	Terminal and CD loop	-	2.46 ± 0.75	-	2.69 ± 0.65

Table 1. RMSD and standard deviation values (Å) for wt and mutant proteins, i.e. ProE3GlyTf-trHbO and GlyE3Pro Mt-trHbO at different temperatures, 300K and 360K. RMSD values considering the complete protein, with no terminal residues (first and last 12 residues), with only terminal residues and terminal and CD loop residues were calculated.

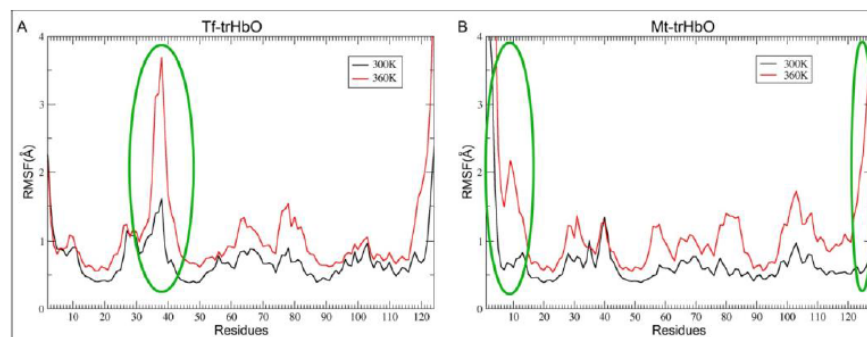


Figure 1. RMSF analysis for wt Tf-trHbO (A) and Mt-trHbO (B) proteins at different temperatures, 300K (black lines) and 360K (red lines). Differential and significant behaviors between both proteins are highlighted in green. Region between residues 35 to 42 in Tf-trHbO (A) corresponds to CD loop secondary structure, instead of for Mt-trHbO (B) it is between residues 37 to 44.

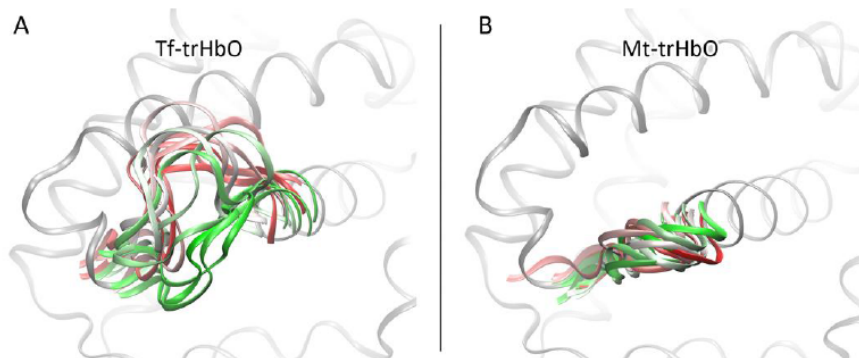


Figure 2. CD loop conformations during MD simulations for wt Tf-trHbO (A) and Mt-trHbO (B) at 360K. Snapshots are colored according to timestep, on a green-white-red color scale.

A microscopic observation evidences an incipient breakage of a nine residues long α -helix, called E α -helix, contiguous to the CD loop and towards the C-terminal that is broken during MD simulations of wt Tf-trHbO (Figure 2.A, 3.A). Although both proteins share most of the identity of these nine residues (Figure 3, on the bottom), an incipient E α -helix formation is observed in wt Mt-trHbO (Figure 3.B). As is well known, due to side chain constraints and sterics, the prolines are unable to satisfy the Ramachandran angles requisite for the α -helix formation. In this sense, on one hand, their side chain is cramped into the α -helix backbone space and, on the other, the methyl group is in the space that would normally be occupied by an H-bonding amide proton, thus disrupting the H-bond network of the helix. In wt Tf-trHbO, a proline at E3 position (ProE3) was observed to destabilize the E α -helix formation, causing the breakage of the H-bond interaction between AspCD5 and AlaE4 residues (Figure 3). Mt-trHbO has a glycine at E3 (GlyE3) that keeps the H-bond between AspCD5 and AlaE4, thus stabilizing the E α -helix complex formation is observed.

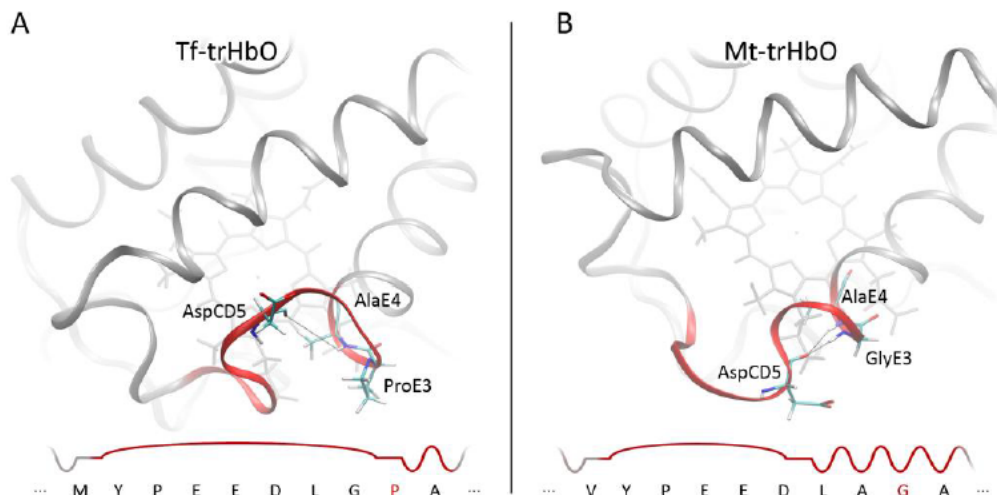


Figure 3. At the top: incipient breakage (A) / formation (B) of E α -helix complex close by to CD loop secondary structure (in red) since the presence of different residues at E3 position, ProE3 in wt Tf-trHbO and GlyE3 in wt Mt-trHbO. The incipient beginning of the E α -helix complex in Mt-trHbO due to the H-bond interaction between AspCD5 and AlaE4 reducing the loop length could be observed. On the bottom: amino acids sequence on the one letter code for CD loop and nearby residues in studied proteins. Information about secondary structure is also shown. Pro and Gly residues at E3 position are highlighted in red.

In-silico mutant protein dynamics. Taking into account that the residue at E3 position seems to be responsible of the CD loop flexibility at high temperatures, and thus to be involved in thermal stability, we performed MD simulations of the two crossed mutants: a Tf-trHbO where ProE3 was replaced by Gly (ProE3Gly Tf-trHbO), and a Mt-trHbO where GlyE3 was replaced by Pro (GlyE3Pro Mt-trHbO). The results show that the mutation in ProE3Gly Tf-trHbO makes a subtle increase of their N-terminal flexibility and restricts in a very significant way the CD loop flexibility (Figure 4.A), also disposing a reasonable local structural accommodation for the incipient formation of E α -helix complex. On the other hand, a marked decrease of C-terminal flexibility degree in GlyE3Pro Mt-trHbO was observed. As expected, a little flexibility gain of its CD loop (Figure 4.B) together with an abatement of incipient E α -helix complex interactions were displayed. In the latest case, no clear breakage of E α -helix complex was detected, maybe due to the simulation timescale and/or force field limitations.

These results revealed by *in-silico* mutant simulations support the fact of the relevance of E3 residue in the dynamics of the CD loop and suggest an interesting role on the global fold thermal stability.

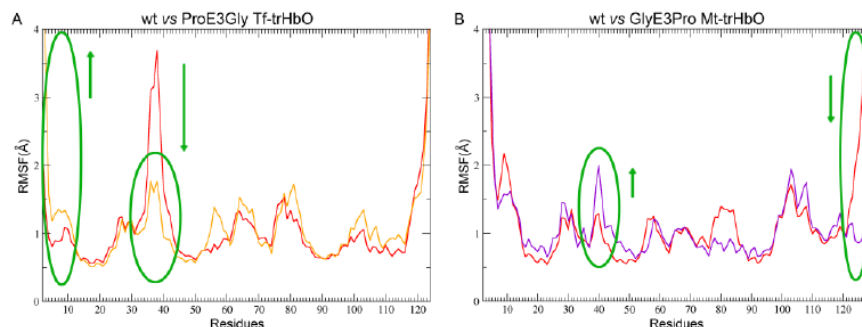


Figure 4. RMSF analysis for wt vs ProE3Gly Tf-trHbO (A) and wt vs GlyE3Pro Mt-trHbO proteins (B), all at 360K. Wt proteins are shown in red. Significant differences on both CD loops and extremes fluctuations are highlighted in green. Arrows show fluctuations changes upon *in-silico* mutation.

Polar interactions of wt and mutants Mt-trHbO and Tf-trHbO proteins. Sequence analysis of both proteins evidences that the thermostable protein has an overall enrichment in charged residues Arg, Lys, Asp or Glu over the mesophilic (54 vs 41). Despite the observed differences in the total amount of charged residues, the number of polar interactions (H-bonds and salt-bridges) observed through MD simulations is similar at room temperature (Table 2). Upon increasing the temperature until 360K both proteins undergo a loss of polar interactions, mainly the protein-solvent ones (Table 2). However, regarding to salt-bridges interactions, the observed trend is quite different. Wt Tf-trHbO show an increment of ~6 salt-bridges interactions at 360K due to the gained CD loop high flexibility, which facilitates salt-bridges interactions between CD loop and B α -helix complex charged residues as shown in Figure S3. Regarding the latest phenomenon, comparing obtained values at high temperature for wt and GlyE3Pro Mt-trHbO on Table 2, the same trend is observed, where a single residue mutation promote the greater CD loop flexibility and consequent new salt-bridges interactions. In summary, both proteins offer comparable amounts of polar interactions in the folded state, and H-bonds interactions seems to be affected similarly by the temperature increasing shift. On the other hand, a clear difference considering only salt-bridges interactions was detected, where the number of it was raised on ProE3 presence upon increasing the temperature, gaining interactions in the folded state.

		Tf-trHbO		Mt-trHbO	
		300K	360K	300K	360K
<i>Wild type</i>	Salt-bridges	17 \pm 1	23 \pm 2	17 \pm 2	16 \pm 2
	H-bonds-Intra	53 \pm 5	50 \pm 5	57 \pm 5	46 \pm 4
	H-bonds-Total	230 \pm 12	189 \pm 11	241 \pm 13	201 \pm 12
<i>Mutant</i>	Salt-bridges	-	18 \pm 2	-	23 \pm 1
	H-bonds-Intra	-	47 \pm 5	-	52 \pm 5
	H-bonds-Total	-	190 \pm 12	4	201 \pm 12

Table 2. Number of polar interactions (salt-bridges and H-bonds) calculated for wt and mutant proteins at 300K and 360K during 100ns of unconstrained MD simulations are shown. Salt-bridges and H-bonds are defined considering a cut-off distance less than 3.3 Å between the two charged or electronegative atoms respectively.

Thermal melting measurement of wt and mutant proteins. For the purpose of determining and

characterizing possible thermodynamic properties that could be modified by changing only the E3 residue, temperature dependence of the circular dichroism signal at 225 nm has been examined for wt and mutant Tf-trHbO and Mt-trHbO cyano-met holoproteins, respectively, as a function of GdmCl concentration. The observed profiles, fitted to a single, two-state unfolding process under the assumption of temperature independent ΔC_p (see supporting information, Figure S1), bring about a clear picture on the thermodynamic determinants of thermostability on both proteins and their mutants. As expected, analysis of the thermal melting profiles data indicate that Tf-trHbO is indeed significantly more thermostable than Mt-trHbO under all conditions examined, showing a T_m of 348K compared to 330K. It is also noteworthy that both Tf-trHbO, Mt-trHbO and their mutants are characterized by similar ΔC_p values (see Table 3) and comparable solvent stabilities, as indicated by isothermal GdmCl denaturation experiments (see supporting information, Figure S2). The thermal behavior of Tf-trHbO with respect to the ProE3Gly mutant is intriguing in that a sizeable decrease in T_m and ΔC_p values is observed in the mutated protein (see Figure 5). In particular, the T_m values of wt and mutated proteins, 348K and 344K respectively, are strongly divergent in buffer but merge by increasing GdmCl concentration (see Figure 5). In other words, GdmCl appears to “quench” the effect of the mutation on the thermal melting profile, such that, at GdmCl concentrations higher than 2 M, the unfolding line shapes are almost superimposable in the native protein and in the mutant. In structural terms, the CD loop region appears to be destabilized by the presence of a highly polar cosolvent much in the same way as it is destabilized by the ProE3Gly mutation. This is expected because H-bond network that allow the stabilization of other conformations on this loop seems to be disrupted by guanidine molecules due to the fact that relevant charged residues are on the protein surface, where solvent molecules have a complete access (Figure S3). As shown in Figure S3, the thermodynamic interpretation is consistent with the role of the H-bonded network within the CD loop, which is most likely destabilized in the presence of GdmCl or by substitution of the rotamerically rigid proline with the flexible glycine residues. The energetic balance, *i.e.* the $\Delta\Delta G_{\text{unf}}$ (wt *minus* mutant) accounts for about 1 kcal/mol, a figure that is also consistent with a balance in which several H-bonds are formed and disrupted, *i. e.* H-bonds that stabilize CD loop conformations are broken and those involved on α -helix complex are formed. Thermal and chemical unfolding data for Mt-trHbO and its GlyE3Pro mutant indicate a reverse, though not specular, picture with respect to Tf-trHbO and its ProE3Gly mutant. Actually, the substitution of GlyE3 into proline, in a topologically analogous position with respect to Tf-trHb, brings about a clear increase in the T_m , from 330K to 338K, and ΔH_{unf} values and a $\Delta\Delta G_{\text{unf}}$ (wt *minus* mutant) increase of 0.5 kcal/mol. At variance with Tf-trHbO (see Figure 5.B), however, the quenching effect of GdmCl is observed to a lesser extent with respect to Tf-trHbO. On this basement, the structural basis for increase in thermostability upon GlyE3Pro mutation in Mt-trHbO is most likely explained in terms of additional structure stabilizing interactions in the former protein, combined with the contribution of the new polar interactions established on overall fold. The topological positions within the CD loop and closest regions (ten residues in length, see Figure 3, on the bottom) thus appear to play a pivotal role within the unfolding process and confirm that in the thermostable protein, the ProE3 imposes a structural constraint by impairing the α -helix formation towards the C-terminal, whereas in the non-thermostable protein the GlyE3 residue take its place without any possible structural hindrance, allowing the formation of the α -helix complex.

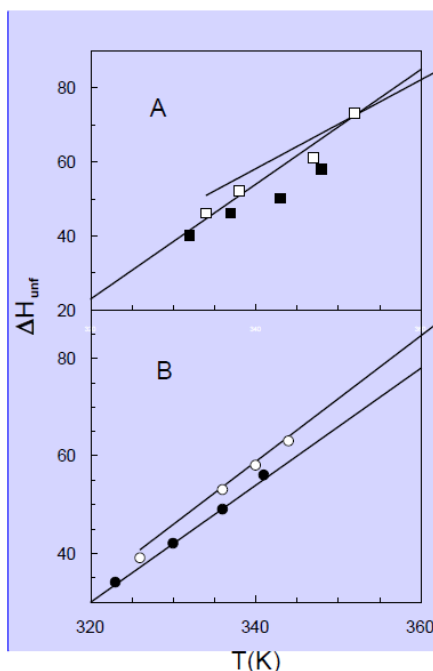


Figure 5. Temperature dependence of ΔH_{T_m} for wt and ProE3Gly Tf-trHbO (A) and GlyE3Pro Mt-trHbO (B) trHbs. The thermodynamic parameters ΔH_{T_m} and T_m , obtained from the fitting procedure of the melting profiles of Figure 1S are shown as a function of GdmCl concentration (0.5, 1, 1.5 and 2 M, respectively). The slopes yielded values of ΔC_p ($\text{kcal}\cdot\text{mol}^{-1}\cdot\text{K}^{-1}$) of 1.55 ± 0.09 for wt Tf-trHbO (\square), 1.22 ± 0.07 for ProE3Gly Tf-trHbO (\blacksquare) and 1.20 ± 0.04 for wt Mt-trHbO (\bullet), 1.29 ± 0.03 for GlyE3Pro Mt-trHbO (\circ), respectively.

		m ($\text{kcal}\cdot\text{mol}^{-1}$) M^{-1}	ΔG_{unf} $\text{kcal}\cdot\text{mol}^{-1}$	ΔC_p $\text{kcal}\cdot\text{mol}^{-1}\cdot\text{K}^{-1}$	T_m K
Tf-trHbO	wt	2.7 ± 0.07	9.1 ± 0.02	1.55 ± 0.08	348
	ProE3Gly	2.3 ± 0.05	8.2 ± 0.02	1.22 ± 0.09	344
Mt-trHbO	wt	2.1 ± 0.04	7.4 ± 0.01	1.20 ± 0.05	330
	GlyE3Pro	2.4 ± 0.05	7.9 ± 0.01	1.29 ± 0.07	338

Table 3. Thermodynamic parameters obtained from the curve fitting of guanidine denaturation experiments shown in Fig. S2 (m and ΔG_{unf}) and from linear fitting of Fig. 1 (ΔC_p). Curve fitting for GdmCl experiments were carried out according to the formalism used by Clarke *et. al.*[38]. Experimental conditions: $T = 25$ °C, 50 mM phosphate buffer at pH 7.0 containing 2 mM KCN.

Discussion

Flexibility at the temperature shift. The aim of this study was to shed light on the molecular mechanism of thermal stability in truncated hemoglobins. Our theoretical and experimental results

demonstrated that besides of some variations at sequence level, there are important dynamical and structural differences between thermostable and non-thermostable trHbs under high temperature perturbation. MD simulations allowed us to inquire if thermostability correlates with rigidity/flexibility of protein structure. Comparing wt trHbs belonging to thermophilic and mesophilic microorganisms, no significant differences on residue flexibilities were observed at room temperature. Similar results were observed previously by performing amide exchange experiments[14], although other theoretical and experimental evidence had showed differential degree of flexibility for thermostable and non-thermostable proteins[9–13].

Polar interactions at room temperature. No substantial differences were observed in the number of polar interactions (H-bonds and salt-bridges) between thermostable and non-thermostable trHbs. It was mentioned that T_m is related to the difference between the energy of the folded state vs the unfolded but collapsed states. Despite of no data about the polar interactions in the unfolded (but collapsed) state were given, it is known that Tf-trHbO presents 7 more charged residues than Mt-trHbO. This excess of charged residues may contribute to the unfolded state stabilization of Tf-trHbO compared to Mt-trHbO because of the interaction with solvent molecules, and thus compensates the higher stabilization of the folded Tf-trHbO compared to Mt-trHbO.

Polar interactions at high temperature. When the temperature is increased from 300K to 360K both proteins loose several H-bonds, mainly residue-water interactions. It means that both proteins are affected in a similar way by the temperature perturbation shift considering H-bonds interactions. Interestingly, wt Tf-trHbO increases their number of salt-bridges interactions upon temperature increase, whereas Mt-trHbO does not. This fact may be related to a previous observation about the lack of first solvation shells at high temperatures[39], [40], and this is possible in Tf-trHbO due to structural accommodations where surface charged residues are now able to form salt-bridges interactions, such as shown in Figure S3. This phenomenon involves a decrease in magnitude of the solvation free energy of a charged residue at high temperatures, which is in energetic balance with increased Coulombic and electrostatic interactions of side-chains of surface charged residues, enhancing the global fold stability against temperature perturbation. However, the number of salt-bridges interactions does not increase in wt Mt-trHbO case, due to a structural inability to form those salt-bridges interactions because of a short CD loop. Since in GlyE3Pro Mt-trHbO protein the environment of the CD loop is almost the same as in wt Tf-trHbO, with a longer loop, the same increase of salt-bridges amount was observed, gaining interactions that account for the folded state. Interestingly, a single residue, a proline, not only gives more flexibility to the CD loop, also allows forming new interactions that stabilize the protein native state.

Configurational entropy. It was proposed that prolines increase T_m by reducing the configurational entropy of the proteins for having more rigid backbones[17]. This interesting hypothesis considers only the primary structure of the protein, and does not consider the secondary and tertiary structure changes that these residues cause. By performing MD simulations of wt and mutant trHbs, we found that the presence of a specific proline, ProE3, allows the CD loop to gain flexibility in the native state. The fact that these fluctuations are concentrated in a flexible loop seems stabilize the folded state. Melting temperature measurements of Mt-trHbO and Tf-trHbO and the crossed mutants GlyE3Pro Mt-trHbO and ProE3Gly Tf-trHbO confirm that a specific residue is able to increase (by 8 degrees) or decrease (by 4 degrees) T_m in the corresponding protein. Therefore, we propose that the increase of the measured melting temperature is related to a tertiary distortion produced only by the ProE3. Specifically, ProE3 unlocks the CD loop which can now fluctuates more actively and interacts with B α -helix complex residues, thus stabilizing the folded state.

This study elucidated the importance of loop flexibility in truncated hemoglobin thermal stability, and our structural/dynamical approach can be applied as a thermostabilization strategy at least for this subfamily of proteins.

Acknowledgments

This work was supported by CONICET and UBA, Argentina-Italia grant Progetti di grande Rilevanza, Ministero degli Affari Esteri, CoMIUR FIRB RBF08F41U_002 (A. Bonamore), and by Institute Pasteur, Fondazione Cenci Bolognetti (A. Boffi). J.P.B. holds a CONICET PhD fellowship. L.B. is a Pew Latin American Fellow. D.A.E. and A.D.N. are members of CONICET. J.P.B. thanks to Marcelo A. Marti for revealing and very helpful discussions.

References

- [1] and R. M. K. Hicks, P. M., M. W. W. Adams, "Enzymes, extremely thermostable," *M. C. Flickinger and S. W. Drew (ed.), Encyclopedia of bioprocess technology: fermentation, biocatalysis, and bioseparation. John Wiley & Sons, Inc., New York*, pp. 987–1004, 1999.
- [2] M. W. Day, B. T. Hsu, L. Joshua-Tor, J.-B. Park, Z. H. Zhou, M. W. W. Adams, and D. C. Rees, "X-ray crystal structures of the oxidized and reduced forms of the rubredoxin from the marine hyperthermophilic archaeobacterium *Pyrococcus furiosus*," *Protein Science*, vol. 1, no. 11, pp. 1494–1507, 1992.
- [3] G. Auerbach, R. Ostendorp, L. Prade, I. Korndörfer, T. Dams, R. Huber, and R. Jaenicke, "Lactate dehydrogenase from the hyperthermophilic bacterium *Thermotoga maritima*: The crystal structure at 2.1 Å resolution reveals strategies for intrinsic protein stabilization," *Structure*, vol. 6, no. 6, pp. 769–781, 1998.
- [4] C. Vieille, J. Hess, R. Kelly, and J. Zeikus, "xylA cloning and sequencing and biochemical characterization of xylose isomerase from *Thermotoga neapolitana*," *Applied and Environmental Microbiology*, vol. 61, no. 5, pp. 1867–1875, 1995.
- [5] L. Chen and M. F. Roberts, "Characterization of a tetrameric inositol monophosphatase from the hyperthermophilic bacterium *Thermotoga maritima*," *Applied and Environmental Microbiology*, vol. 65, no. 10, pp. 4559–4567, 1999.
- [6] R. Jaenicke, "Protein stability and molecular adaptation to extreme conditions," *European Journal of Biochemistry*, vol. 202, no. 3, pp. 715–728, 1991.
- [7] M. W. W. Adams and R. M. Kelly, "Enzymes from microorganisms in extreme environments," *Chemical and Engineering News*, vol. 73, no. 51, pp. 32–42, 1995.
- [8] R. Jaenicke and G. Böhm, "The stability of proteins in extreme environments," *Current Opinion in Structural Biology*, vol. 8, no. 6, pp. 738–748, 1998.
- [9] T. Lazaridis, I. Lee, and M. Karplus, "Dynamics and unfolding pathways of a hyperthermophilic and a mesophilic rubredoxin," *Protein Science*, vol. 6, no. 12, pp. 2589–2605, 1997.
- [10] G. Manco, E. Giosuè, S. D'Auria, P. Herman, G. Carrea, and M. Rossi, "Cloning, overexpression, and properties of a new thermophilic and thermostable esterase with sequence similarity to hormone-sensitive lipase subfamily from the archaeon *Archaeoglobus fulgidus*," *Archives of Biochemistry and Biophysics*, vol. 373, no. 1, pp. 182–192, 2000.

- [11] A. Gershenson, J. A. Schauerte, L. Giver, and F. H. Arnold, "Tryptophan phosphorescence study of enzyme flexibility and unfolding in laboratory-evolved thermostable esterases," *Biochemistry*, vol. 39, no. 16, pp. 4658–4665, 2000.
- [12] P. Závodszy, J. Kardos, Svingor, and G. A. Petsko, "Adjustment of conformational flexibility is a key event in the thermal adaptation of proteins," *Proceedings of the National Academy of Sciences of the United States of America*, vol. 95, no. 13, pp. 7406–7411, 1998.
- [13] T. Mamonova, A. Glyakina, O. Galzitskaya, and M. Kurnikova, "Stability and rigidity/flexibility - two sides of the same coin?," *Biochimica et biophysica acta*, vol. 1834, no. 5, pp. 854–866, 2013.
- [14] G. Hernández, F. E. Jenney Jr., M. W. W. Adams, and D. M. LeMaster, "Millisecond time scale conformational flexibility in a hyperthermophile protein at ambient temperature," *Proceedings of the National Academy of Sciences of the United States of America*, vol. 97, no. 7, pp. 3166–3170, 2000.
- [15] J. D. Bryngelson, J. N. Onuchic, N. D. Socci, and P. G. Wolynes, "Funnels, pathways, and the energy landscape of protein folding: A synthesis," *Proteins: Structure, Function and Genetics*, vol. 21, no. 3, pp. 167–195, 1995.
- [16] G. Vogt, S. Woell, and P. Argos, "Protein thermal stability, hydrogen bonds, and ion pairs," *Journal of Molecular Biology*, vol. 269, no. 4, pp. 631–643, 1997.
- [17] B. W. Matthews, H. Nicholson, and W. J. Becktel, "Enhanced protein thermostability from site-directed mutations that decrease the entropy of unfolding.," *Proceedings of the National Academy of Sciences of the United States of America*, vol. 84, no. 19, pp. 6663–6667, 1987.
- [18] L. Boechi and P. Wolynes, "Manuscript in preparation."
- [19] G. Bohm and R. Jaenicke, "Relevance of sequence statistics for the properties of extremophilic proteins," *International Journal of Peptide and Protein Research*, vol. 43, no. 1, pp. 97–106, 1994.
- [20] A.-K. Bock, J. Glasemacher, R. Schmidt, and P. Schönheit, "Purification and characterization of two extremely thermostable enzymes, phosphate acetyltransferase and acetate kinase, from the hyperthermophilic eubacterium *Thermotoga maritima*," *Journal of Bacteriology*, vol. 181, no. 6, pp. 1861–1867, 1999.
- [21] A. Bonamore, A. Ilari, L. Giangiacomo, A. Bellelli, V. Morea, and A. Boffi, "A novel thermostable hemoglobin from the actinobacterium *Thermobifida fusca*," *FEBS journal*, vol. 272, no. 16, pp. 4189–201, Aug. 2005.
- [22] M. Milani, P.-Y. Savard, H. Ouellet, P. Ascenzi, M. Guertin, and M. Bolognesi, "A TyrCD1/TrpG8 hydrogen bond network and a TyrB10TyrCD1 covalent link shape the heme distal site of *Mycobacterium tuberculosis* hemoglobin O," *Proceedings of the National Academy of Sciences of the United States of America*, vol. 100, no. 10, pp. 5766–71, May 2003.
- [23] F. P. Nicoletti, E. Droghetti, L. Boechi, A. Bonamore, N. Sciamanna, D. a Estrin, A. Feis, A. Boffi, and G. Smulevich, "Fluoride as a probe for H-bonding interactions in the active site of heme proteins: the case of *Thermobifida fusca* hemoglobin," *Journal of the American Chemical Society*, vol. 133, no. 51, pp. 20970–80, Dec. 2011.

- [24] F. P. Nicoletti, E. Droghetti, B. D. Howes, J. P. Bustamante, A. Bonamore, N. Sciamanna, D. A. Estrin, A. Feis, A. Boffi, and G. Smulevich, "H-bonding networks of the distal residues and water molecules in the active site of *Thermobifida fusca* hemoglobin," *Biochimica et Biophysica Acta - Proteins and Proteomics*. Dipartimento di Chimica Ugo Schiff, Università di Firenze, Via della Lastruccia 3-13, I-50019 Sesto Fiorentino (FI), Italy, 2013.
- [25] E. Droghetti, F. P. Nicoletti, A. Bonamore, L. Boechi, P. Arroyo Mañez, D. a Estrin, A. Boffi, G. Smulevich, and A. Feis, "Heme pocket structural properties of a bacterial truncated hemoglobin from *Thermobifida fusca*," *Biochemistry*, vol. 49, no. 49, pp. 10394–402, Dec. 2010.
- [26] A. Marcelli, S. Abbruzzetti, J. P. Bustamante, A. Feis, A. Bonamore, A. Boffi, C. Gellini, P. R. Salvi, D. a Estrin, S. Bruno, C. Viappiani, and P. Foggi, "Following Ligand Migration Pathways from Picoseconds to Milliseconds in Type II Truncated Hemoglobin from *Thermobifida fusca*," *PLoS one*, vol. 7, no. 7, p. e39884, Jan. 2012.
- [27] D. A. Pearlman, D. A. Case, J. W. Caldwell, W. S. Ross, T. E. Cheatham III, S. DeBolt, D. Ferguson, G. Seibel, and P. Kollman, "AMBER, a package of computer programs for applying molecular mechanics, normal mode analysis, molecular dynamics and free energy calculations to simulate the structural and energetic properties of molecules," *Computer Physics Communications*, vol. 91, no. 1–3, pp. 1–41, 1995.
- [28] J. Wang, P. Cieplak, and P. A. Kollman, "How Well Does a Restrained Electrostatic Potential (RESP) Model Perform in Calculating Conformational Energies of Organic and Biological Molecules?," *Journal of Computational Chemistry*, vol. 21, no. 12, pp. 1049–1074, 2000.
- [29] M. A. Martí, L. Capece, A. Bidon-Chanal, A. Crespo, V. Guallar, F. J. Luque, and D. A. Estrin, "Nitric Oxide Reactivity with Globins as Investigated Through Computer Simulation," *Methods in Enzymology*, vol. 437, pp. 477–498, 2008.
- [30] M. A. Martí, A. Crespo, L. Capece, L. Boechi, D. E. Bikiel, D. A. Scherlis, and D. A. Estrin, "Dioxygen Affinity in Heme Proteins Investigated by Computer Simulation.," *Journal of Inorganic Biochemistry*, vol. 100, no. 4, pp. 761–770, 2006.
- [31] D. E. Bikiel, L. Boechi, L. Capece, A. Crespo, P. M. De Biase, S. Di Lella, M. C. González Lebrero, M. A. Martí, A. D. Nadra, L. L. Perissinotti, D. A. Scherlis, and D. A. Estrin, "Modeling heme proteins using atomistic simulations," *Physical Chemistry Chemical Physics*, vol. 8, no. 48, pp. 5611–5628, 2006.
- [32] F. Forti, L. Boechi, D. Bikiel, M. A. Martí, M. Nardini, M. Bolognesi, C. Viappiani, D. Estrin, and F. J. Luque, "Ligand migration in *methanosarcina acetivorans* protoglobin: Effects of ligand binding and dimeric assembly," *Journal of Physical Chemistry B*, vol. 115, no. 46, pp. 13771–13780, 2011.
- [33] L. Capece, A. Lewis-ballester, M. A. Martí, D. A. Estrin, and S. Yeh, "Molecular Basis for the Substrate Stereoselectivity in Tryptophan Dioxygenase," *Biochemistry*, vol. 50, pp. 10910–10918, 2011.
- [34] P. Arroyo Mañez, C. Lu, L. Boechi, M. A. Martí, M. Shepherd, J. L. Wilson, R. K. Poole, F. J. Luque, S.-R. Yeh, and D. A. Estrin, "Role of the distal hydrogen-bonding network in regulating oxygen affinity in the truncated hemoglobin III from *campylobacter jejuni*," *Biochemistry*, vol. 50, no. 19, pp. 3946–3956, 2011.

- [35] D. Giordano, L. Boechi, U. Samuni, A. Vergara, M. A. Marti, A. Estrin, J. M. Friedman, L. Mazzarella, G. Prisco, and L. Grassi, "The Hemoglobins of the Sub-Antarctic Fish *Cottoperca gobio*, a Phyletically Basal Species – Oxygen-Binding Equilibria, Kinetics and Molecular Dynamics," *FEBS Journal*, vol. 276, pp. 2266–2277, 2009.
- [36] L. L. Perissinotti, M. A. Marti, F. Doctorovich, F. J. Luque, and D. A. Estrin, "A Microscopic Study of the Deoxyhemoglobin-Catalyzed Generation of Nitric Oxide from Nitrite Anion," *Biochemistry*, vol. 47, no. 37, pp. 9793–9802, 2008.
- [37] A. Matouschelt, J. M. Matthews, C. M. Johnson, and A. R. Fersht, "Extrapolation to water of kinetic and equilibrium data for the unfolding of barnase in urea solutions," *Protein Engineering*, vol. 7, no. 9, pp. 1089–1095, 1994.
- [38] J. Clarke and A. R. Fersht, "Engineered disulfide bonds as probes of the folding pathway of barnase: Increasing the stability of proteins against the rate of denaturation," *Biochemistry*, vol. 32, no. 16, pp. 4322–4329, 1993.
- [39] P. I. W. De Bakker, P. H. Hünenberger, and J. A. McCammon, "Molecular dynamics simulations of the hyperthermophilic protein Sac7d from *Sulfolobus acidocaldarius*: Contribution of salt bridges to thermostability," *Journal of Molecular Biology*, vol. 285, no. 4, pp. 1811–1830, 1999.
- [40] G. I. Makhatadze, V. V. Loladze, D. N. Ermolenko, X. Chen, and S. T. Thomas, "Contribution of surface salt bridges to protein stability: Guidelines for protein engineering," *Journal of Molecular Biology*, vol. 327, no. 5, pp. 1135–1148, 2003.